GEM TN-93-287

GEM Muon Group Meeting - Duncanville, Tx.

February 3, 1993

Abstract:

Agenda, attendees, and presentations of the GEM Muon Group Meeting held at the Holiday Inn in Duncanville, Tx. on February 3, 1993.

Agenda of 2/3/93 Muon Meeting

TO: GEM Muon Group
FROM: Mike Marx and Frank Taylor
SUBJECT: Short Term Tasks and 2/3/93 Meeting
DATE: 1/22/93

Now that we have recommended that the CSCs be our baseline technology we have to concentrate our efforts for R&D and writing the TDR. The following is a list of key issues which we should address at the next Muon Group Meeting 2/3/93.

(1) Presentation of the Recommendation Report:
- why CSCs are better than RDT/RPC(PWC) [Polychronakos, Taylor]

(2) Organization of urgent short term R&D:
[Mitselmakher - coordinator]
- demonstrate all operating parameters of the CSC (T0, efficiency, and resol'n) in one chamber.
- study chamber performance vs strip width. Will 1 cm (0.8 cm) strips yield our baseline resolution? Can chambers at the TTR or RD5 be used to make measurements?
- develop L-angle correction strategy. Do we want to rotate chambers in the endcaps? [Vorobyov, Tchernetin]
- hole in chamber for alignment really works? other solution ?

(3) Develop a procedure to fix the baseline CSC chamber design.
The makers of the existent chamber designs should meet before 2/3/93 to formulate a plan. [Dubna, PNPI, UH, BU, BNL, ...]
[coordinator to be determined]

(4) Decide on the baseline chamber configuration - driven by resolution requirements and chamber characteristics and layout.
[Nimblett, McNeil, Whitaker, Taylor]

Suggested configuration - [all chambers with projective strips]
Barrel: 6-6-6
Endcaps: 8-6-6 in outer angle region [SW conf. h]
8-8-6 in inner region

Compute the angle coverage with/without hole in chamber.

(5) Organization of urgent simulations work for design decisions:
[McNeil, Golutvin, Wenus, et al.]
- pattern recognition
- momentum reconstruction
- trigger simulation

(6) TDR progress and organization:
[Marx]

3-Feb-1993.
muon meeting
@SSCL - Holiday Inn

NAME	ORGANIZATION	TEL #	E-MAIL #
Michael Marx	SSC	6188	SSCVX1 . MARX
Howard Baker	Draper	617-258-3411	hbaker@draper.com
Igor Golutvin	Dubna JINR	(214)-708-3084	IGOLUTVIN @ SSCVX1
Yuri Kiryushin	JINR	(214)-708-6303	YUKIR @ SSCVX1
Carl Bromberg	MSU	(517) 353-1809	BROMBERG@ MSUPA
Yuri Fisyak	SSCL	(214) 708-6322	FISYAK@SSCVX1
Andrey Golutvin	ITEP/SSCL	(214) 708-6385	Golutvin@SSCVX1
VLADIMIR GLEBOV	SSCL	(214)-708-6321	GLEBOV@SSCVX1
JIM SHANK	BOSTON U.	617-353-6028	shank@BUPHYC
Pe. Ter Dingus	SSCL	214-708-6260	DINGUS@SSCVX1
Andrey Ostapchuk	SSCL/ITEP	(214) 708-3007	SSCVX1::OSTAPCH
Yuri Bonushkin	SSCL/JINR	(214) 708-3078	SSCVX1::BONUSHKI
Rick Shypit	SSCL	(214) 708-4465	SSCVX1:: SHYPIT
Rick Sawicki	LLNL	(510) 423-0463	SAWICKI1@LLNL.GOV
Frank Nimblett	Draper	(617) 258-1393	Nimblett@DRAPER.COM
PAUL MURAT	ITEP/SSCL	(214) 708-3066	MURAT@SSCVX1
Dmitry Onoprienko	ORNL	(615) 576-6914	ONOPRIENKO@ORPHO1
Tom Ferguson	CMU	(412) 268-2744	FERGUSON@CMPHYS
TORRE WENAUS	LLNL	(510) 423-1813	WENAUS@POSF.SSC.GOV
Xiaorong Shi	Caltech	(818) 356-6696	SHI@SSCVX1
Yanan GUO	SSCL	(214)-708-4457	GUO@SSCVX1
COLEMAN JOHNSON	SSCL	214 708 1188	JOHNCOLE@SSCVX1
KARL VAN BIBBER	LLNL	510 423 8949	KVB@SLACESA
Gary Liu	Caltech	818-356-6681	CITHEX:: GL
Joe Paradiso	Draper	617-258-2413	neuromancer@draper.com
Yuri Efremenko	ORNL	(615)-576-6914	EFREMENKO@ORPHO1
Roger McNeil	LSU	(504)-388-6857	LSUHEP:: MCNEIL
Bill Metcalf	LSU	(504) -388-8312	LSUHEP:: METCALF
Bill W. Mayes II	Houston	(713)-743-3548	Mayes@UH.EDU
Jörg Pyrlik	Houston	(713) 743-3603	PYRLIK@UHIBIO.PHYS.UH.EDU
KWONG LAU	Houston	(713) 743-3600	LAU@UH.EDU
Roy Weinstein	Houston	(713) "	Weinstein@UH.EDU
Gena Mitselmakher	SSCL	(214)-708-6001	MITSELMAKHER@SSCVX1
Craig Wuest	LLNL	(510) 423-2909	Wuest@LLNL.GOV
Chiaki Yanagisawa	Stony Brook	(516) 632-8105	SBHEP:: CHIAKI
Andrey Korytov	MIT	617-253-7587	KORYTOV@MITLNS
HANS KOBRAK	UCSD	(619) 534-2291	SDPH:: KOBRAK
VINNIE POLYCHRONAKOS	BNL	516-282-3982	BNLDAG:: POLYCHRON
Andrei Varobyov	BNL/ITEP	[illegible]	[illegible]

gem

γeμ

Presentation by:

V. Polychronakos

BROOKHAVEN NATIONAL LABORATORY

February 4, 1993 GEM/CSC 2-93

DRAFT
February 4, 1993

The Interpolating Cathode Strip Chambers of the GEM Muon System

Prototype Development and Performance

V.A. Polychronakos
for the CSC Group

1 Introduction

A series of interpolating Cathode Strip Chamber(CSC) prototypes have been constructed in our effort to develop the CSC technology for application to the Muon System for GEM. These prototypes include a "full scale" (1.8x1.2m^2) four-layer module (at BNL), a large (1.5x1m^2) module at Dubna, three $\approx$0.5x0.5m^2, four-gap chambers, one with radial strips (Boston U.), one with parallel strips (BNL), and a similar one at PNPI but using a construction technique more suitable for mass production. A number of small, specialized chambers to study a variety of parameters relevant to the CSC operation were also built at BNL, PNPI, and Boston University. In addition a 1x0.5m^2 prototype using Iarocci-type tubes with a cathode strip readout has been constructed by the Houston University group.

The emphasis, throughout this R&D program, has been on developing and understanding all aspects of this technology. An appropriate, nonflammable gas has been identified meeting all requirements of the full detector. Single layer spatial resolution better than the 75μm required by the baseline design has been achieved in both small and large prototypes. Efficient bunch crossing timing was demonstrated by identifying the earliest signal arrival from 4 or 6 layers using a simple OR circuit. The tagging efficiency ranges from 92% (with 6 layers and simple time- over-threshold discriminators) to 100% (four layers with constant fraction discriminators). Chamber efficiency better than 99% with either anode or cathode signals has been achieved.

The importance of a relatively simple, robust, low cost electronic readout system in achieving 1% measurements with a detector with $\approx 10^6$ channels was recognized. An aggressive, two-prong approach has been followed:

- A compact, low cost, highly multiplexed readout system for the prototypes was developed utilizing existing monolithic amplifiers augmented by custom hybrid preamplifiers. Most of the prototypes are tested fully instrumented. The "small" BNL four layer module, for example, has 288 cathode and 32 anode channels. The large four layer module will have a total of 704 cathode channels (only two layers have been tested todate, the other two are nearing completion and are expected to be delivered at the SSC at the end of February). It should be noted that the largest Barrel module will have no more than about 1000 channels.

- In parallel, an effort to develop a custom monolithic front end suitable for the GEM muon detector subsystem was launched. Prototype circuits featuring a low noise preamplifier, shaper, and sample and hold have already been fabricated and tested.

Alignment is another crucial factor in achieving the baseline performance. A novel alignment system is being developed utilizing collimated high energy (36 keV) X-rays which are directly detected by the CSCs providing relative alignment of all layers of a superlayer and, possibly, between superlayers. Promising results were recently achieved by the PNPI group.

2 Prototype Development

2.1 Mechanical construction

Almost all CSC prototypes are built as two-gap modules. The two gaps are formed by three flat, rigid panels made of a 23 mm thick sheet of nomex honeycomb and two 1.25 mm thick copper-clad FR4 laminates. The 0.5 oz/ft^2 copper (17 μm thick) forms the cathodes of the two proportional chambers. The panel frames were made of machined zelux (fiberglass reinforced lexan). They provide the 2.5 mm step for the anode plane of gold-plated tungsten wires 30 μm in diameter with a 2.5mm pitch. The frames of the outer panels have a milled cavity with enough room for the epoxy beads for the wire attachment as well as the anode blocking capacitors. A rubber gasket just outside this cavity provides the gas seal for the assembly. In this manner no components under high voltage are outside the seal thus minimizing the risk of high voltage breakdowns. This technique has been successfully used in several chamber designs by the MPS group at BNL. A mechanical drawing of one of these panels is shown in Figure 1 with a more detailed view of the frame cross sections in Figure 2. The sensitive area of this prototype is 45x37 cm^2. A drawing of the two-gap assembly (for the large trapezoidal prototype) is shown in Figure 3.

The position sensing cathode strips are lithographically etched on either side of the central panel. These cathodes are precisely positioned with respect to each other with the aid of locating pins. The strips are oriented at 90° with respect to the anode wires providing the precision position measurement in a direction along the wires.

On one of the continuous cathodes four windows of approximately 4x3 cm^2 were cut out. Four collimators made of 0.025″ half hard brass shim stock were placed in these windows. Each collimator has 25 slits 100 μm wide, 1.5 cm long cut every 1 mm. A drawing of one of these is shown in Figure 4. A thin layer of mylar glued on the back side of the collimators guarantees the integrity of the gas volume. Corresponding windows were opened on the outside skin of this panel to allow penetration of the soft X-rays from an ^{55}Fe source.

2.2 Position sensing cathode geometry

Seen as gaseous detectors the CSCs are Multiwire Proportional Chambers with a symmetric cell in which the anode-cathode spacing, h, is equal to the wire pitch, s, which equals 2.5 mm. The readout pitch, w_r, is 5 mm.[1] Thus the ratio of the readout pitch to anode-cathode spacing is $w_r/h = 2$. Such a high ratio results in significant (>50%) position encoding differential non-linearity since the FWHM of the cathode induced charge is about 1.5h. It has been shown [1],[2],[3] that the condition for negligible (≈1%) differential non-linearity is $w_r/h \leq 0.8$. This condition would dictate a readout pitch of 2 mm resulting in an unacceptably large number of channels. E. Mathieson and G. C. Smith have shown that linearity of response can be restored to near optimum with the use of intermediate strips between readout nodes which provide increased charge sampling frequency and are capacitively coupled to the adjacent readout strips.[4] We used an arrangement with two intermediate strips which is shown in Figure 5 along with the equivalent electrical circuit. For this capacitive interpolation to work the interstrip capacitance, C_1, must be much larger than that of a strip to ground, C_0, ($C_1/C_0 \geq 10$). For the present design of the CSCs, $C_1/C_0 \approx 10$–12. Further optimization results in intermediate strips of a slightly larger width than the readout strips.[5] In Figure 6 the expected differential nonlinearity is shown as a function of the readout strip width (expressed as fraction of the width this strip would have for the case of equal strip widths) and for several ratios C_1/C_0. For the prototypes the gap between strips is 0.250 mm, the readout strip width is 1.1 mm and that of the two intermediate strips 1.57 mm. It is necessary to provide a high resistance path to ground to avoid charge buildup on the intermediate strips. A thin strip of resistive epoxy (conductivity 6 MOhm per square) was silk screened on the tips of the strips at the end of the cathode opposite to the amplifiers.

3 Electronic Readout

The fine granularity of the CSC detectors results in a large number of channels (of order 10^6 for the entire system). In addition, the 1% charge measurement required in order to achieve the single layer resolution of the baseline design makes the readout system the most critical component of a CSC based muon detector system. Development of a credible readout system has always been a high priority item within the CSC group We adopted an aggressive, two pronged approach with the following goals:

- To fully equip the prototype modules with an electronic readout chain that closely resembles the architecture to be eventually used for the detector.
- To immediately start the development of a custom monolithic front end integrated circuit which will be the basis for a highly multiplexed, compact readout system that could be tested at the earliest possible time.

The following subsections describe the progress on these two fronts.

[1] This is true for 3/4 of the area of the detectors. For the remaining the pitch was increased to 7 mm.

3.1 Cathode Strip Readout

The spatial resolution of the CSCs depends linearly on the signal to noise ratio. For a given gas gain the lowest possible electronic noise results in optimum resolution. Note that one can not arbitrarily increase the gas amplification in order to compensate for poor noise performance. It has been shown[6] that for most gases the resolution degrades rapidly for anode charge larger than $\approx$1 pC due, primarily, to photon mediated avalanche fluctuations.

We have designed a readout system which features a high performance, low noise, hybrid, charge integrating preamplifier followed by a 16-channel monolithic shaping amplifier with multiplexed output. This CMOS integrated circuit (AMPLEX) [7]was designed at CERN for silicon detector applications and hence the need for a different front end.A block diagram of the cathode readout is shown in Figure 7 and a schematic diagram of the preamplifier is given in Figure 8. It has a JFET front end (Interfet NJ132L) optimized for an input electrode capacitance range of 50–150 pf corresponding to cathode strip lengths of 1–3 m. The feedback capacitor is 5 pf and the feedback resistor 50 MOhm so that it contributes negligible parallel noise even for long shaping times. A single transistor inverter matches the polarities of the two amplifiers and provides an additional gain of 3–4. This compensates for a gain loss of about the same factor when the AMPLEX amplifier is coupled to the hybrid with a 1.35 pf capacitor. This coupling mode allows the AMPLEX amplifier to operate with an effective input capacitive load of only 1.35 pf, close to its optimum. Although the monolithic AMPLEX still dominates the amplifier noise ($\approx$1200 equivalent rms electrons) the noise slope as a function of input capacitance is now determined by the hybrid and is only 7 electrons/pf for the shaping time of 550 ns. Had the AMPLEX amplifier been the front end this slope would have been 40–80 electrons/pf (depending on the amplifier bias current).

The multiplexed outputs from all amplex chips are buffered and sent to an on-board unity gain summing node. Up to 512 multiplexed channels are output on a single cable. Two such groups for a total of 1024 channels are read by a single CAMAC module.[8] This module digitizes the analog signals with an 8-bit flash ADC, subtracts prestored pedestals for all channels, suppresses empty channels, and builds a list of the addresses of the strips with a signal above an individually adjustable threshold and its corresponding amplitude. It results in a compact, low cost readout system with a small number of cables (less than ten for our 800 channel prototype). This immensely facilitates the task of effectively shielding the modules against electromagnetic interference as well as controlling ground loops, the bane of precision measurements in large systems.

3.2 Calibration of the Cathode Readout System.

Knowledge of the relative electronic gains in neighboring channels at the $\leq$1% level is necessary to achieve the design spatial resolution of 75μm. Precision calibration capacitors were built into the multilayer readout printed circuit board. The value of these capacitors was 0.65 pf and their uniformity was measured with a precision bridge to be better than 0.5%. Every fourth capacitor was connected to the same calibration line which was terminated into 50 Ohms. The resulting four calibration lines were fed by the same precision pulser, one at a time via a computer controlled wide-band router. The amplitude of the precision pulser as

well as its trigger were also computer controlled. At regular intervals calibration data were taken by stepping the pulser amplitude through 30 values spanning the whole dynamic range in use. A few hundred events were accumulated for every pulser value and the mean values and rms deviations calculated for all channels. A third order polynomial was then fitted to these values. This was necessary because in order to gain as much dynamic range as possible we used the AMPLEX chip in a region well beyond its linear range. Figure 9a shows one such calibration curve and corresponds to the response of the AMPLEX. The fit coefficients were then recorded and used to correct the amplitudes during data analysis. In order to check this calibration procedure a known pulse was injected in all channels. The values read back were corrected and are plotted in Figure 9b. The distribution of their variations from the nominal is plotted in Figure 9c and has a sigma of 0.55%.

3.3 Anode Readout

The anode readout is far less demanding in spite of the fact that fast shaping is required (30 ns) in order to provide trigger information and bunch crossing tagging. No amplitude information is necessary. The anode wires are connected in groups of 20 providing 5 cm wide hodoscope elements. We used the bipolar, grounded-base amplifier shown in Figure 10 (BNL Instrumentation Division, IO-354-2) and a 30 ns shaping amplifier shown in Figure 11 (BNL Instrumentation Division, IO-638-01). These are implemented in thin film hybrid technology and are mounted on a printed circuit board on the detector. They are followed by on-board discriminators which provide a fast OR for self-triggering. Thus the module is self-sufficient not requiring any additional detectors in order to be tested with sources, cosmic rays, or particle beams. The discriminator outputs are available for input into TDCs to obtain additional information during the tests although they will not be used in the final detector.

3.4 Development of a Monolithic Front End

A custom monolithic front end has been designed and prototypes have already been fabricated and are currently undergoing tests at BNL. The prototype chips contain 8 channels each of which consists of a charge-sensitive, folded cascode preamplifier, a fourth order semi-gaussian shaper with 750 nsec integration time, and a track and hold circuit. The 2μm Orbit process was used . Details of the design of this chip can be found elsewhere[9]. Figure 11a shows the noise of the preamplifier as a function of the input capacitance (top), and the linearity of response (bottom). Notice that the noise slope is just about 7 equivalent rms electrons/pf, a performance that rivals the best discrete component hybrid preamplifiers.

Work on the anode readout is also in progress although it is not as advanced as the one described above. A design has already been completed, however, and is in the process of the circuit layout. The bibolar technology (Tektronix quick chip) has been chosen as more efficient for the short integration time ($\approx$30nsec) needed for the anode readout. Simulations of the circuit show that 7 nsec rise time can be achieved even for electrodes with input capacitance as high as 300pf (equivalent to the capacitance of approximately 40 wires).

4 Prototype Performance

4.1 Gas Amplification and Gain Uniformity

The chamber gas used for all the data discussed in this report was a mixture of 90%Ar + 10%CH_4. This gas is not only readily available in premixed form but also essential for meaningful resolution measurements using the 5.9 keV X-rays from an ^{55}Fe source as will be discussed later on. These soft X-rays can not penetrate the honeycomb panels. For studies of the gain uniformity we used the 60 keV X-rays from an ^{241}Am source. Such energetic X-rays, however, produce ionization over a large area of the detector making quantitative measurements difficult. An unexpected benefit of using copper cathodes is a 8 keV Cu fluorescence line quite distinctly visible in our chambers. Using this peak in the Am spectrum we were able to measure the gas gain in the entire chamber area. Figure 12a shows the percent gain variation from a mean gain at various positions of one of the planes. In Figure 12b a histogram of these deviations is shown. All gains are contained within $\pm 20\%$ indicating that the cathode flatness (peak to peak variation) was not more that $\approx 75\mu m$.

The absolute gas gain was measured using the ^{55}Fe source illuminating the chamber through one of the four collimators. Both the cathode strips and the anode wires were used in independent measurements. A QVT was attached to the output of the shaper of one of the wire channels since no analog measurement is built-in. For the cathodes the strip with the largest pulse height was identified and then the amplitudes of its four nearest neighbors were added to that to obtain the total charge. Consistent results were obtained with both methods. In both cases the fraction of the charge collected was taken into account in order to estimate the true gain. Figure 13 shows the gas amplification as a function of the anode voltage. Most of the data discussed here were obtained with a high voltage of 1575 V corresponding to a gas gain of $2\text{x}10^4$.

4.2 Single Layer Spatial Resolution

To determine the spatial resolution of the prototypes the ^{55}Fe source was placed at a distance of 25 cm from the window of one of the brass collimators to minimize the angular divergence of the photons entering the 100μm wide slits. An additional collimator was placed directly on the honeycomb panel restricting the overall illumination to about 1cm. The signal from the wire plane was used to trigger the data acquisition system. The precision coordinate of the photon absorption position was reconstructed using the following simple algorithm. The strip with the highest amplitude was identified and the induced charge centroid was calculated using this strip as well as its four nearest neighbors. The calibration constants were used to correct the amplitudes for gain variations as described earlier. No cuts were applied in energy or otherwise. A histogram of the reconstructed coordinate is shown in Figure 14a. The image of the collimator slits can be seen. Three of the histograms magnified are shown in Figure 14b. The standard deviations of the observed peaks are typically 50–60μm. They represent convolutions of a square distribution 100μm wide with a resolution function (presumed to be Gaussian). The following simple Monte Carlo method was used to unfold this resolution. A uniformly random distribution 100μm was generated. Each point was smeared by a gaussian distribution with a given σ. This was repeated with sigmas

ranging from 10 to 100 microns. In Figure 15 is shown the width of the composite distribution as a function of the width of the convolving gaussian. One notes that for infinitely good resolution the observed width would be $\approx 30\mu m(100/\sqrt{12})$. The resolution dominates the width for $\sigma > \approx 60$ μm. The observed widths of 50–60μm correspond to single layer spatial resolutions of 40–50 μm. It should be noted that the photoelectron range limits the resolution to about 40 microns. Fischer, Radeka, and Smith[6] in an extensive study using a chamber designed so that all other limitation to the resolution were small compared to the contribution of the photoelectron range, measured a resolution of about 40 microns using the same gas.

The total capacitive load on each readout node was measured to be 26 pf. Capacitors of 100 pf were added to all nodes to simulate 2.5 m long strips. The resolution (without increasing the gas gain) degraded to about 75μm.

4.3 Linearity of Response

The reconstructed versus true [2] positions of the slits are plotted in Figure 16a. The solid line is a least squares fit of the data to a straight line. It can be seen that the capacitive interpolation with the aid of the two floating strips restores the linearity of response in spite of the fact that the ratio of the readout pitch to the anode-cathode distance is 2.0. There is, however, a residual nonlinearity as can be seen from Figure 15b where the variation of the reconstructed positions of the slits from the straight line fit is plotted. The rms position error (or rms integral nonlinearity) is

$$\sigma = \frac{1}{N}\sqrt{\sum_{i=1}^{N}(y_i - x_i)^2} = 14.9\mu m$$

The differential nonlinearity as plotted in Figure 6 is defined in terms of the detector's response function $v(y)$ to uniform irradiation as follows.[10] Let $y = f(x)$ be the track's reconstructed position as a function of the true position x. If the detector is subjected to a uniform irradiation $u(x) = const.$ then

$$v(y) = \frac{1}{f'(x)}$$

is the normalized uniform irradiation response as a function of the reconstructed position y. $f'(x)$ is the derivative of the reconstructed position as a function of the true position. The differential nonlinearity, DFNL, is then defined as:

$$DFNL = \frac{v_{max} - v_{min}}{(v_{max} + v_{min})/2}$$

It can be shown that in terms of the rms position error the DFNL can be written as

$$DFNL = 4\sqrt{2}\pi\sigma/l_a$$

where l_a is the readout node spacing. Applying the above formula we find DFNL=4.8%.

[2]The slits of the collimator were measured to be accurately cut every millimeter with a precision of $\approx$30 microns.

4.4 Choice of the Operating Gas

Threre are three basic requirements that need to be met by a chamber gas suitable for a CSC-based Muon System . These are:

- High drift velocity ($> 60\mu m/nsec$)
- Low ($< 10°$) Lorentz angle
- Nonflammable

Such a gas has been identified and already used for all our tests at the TTR. The composition of the gas is 30% Ar, 50% CO_2, 20% CF_4. Figure 17 shows the drift velocity as a function of electric field for this and two more gases which also meet the requirements. The option of using xenon is being considered if the development of the x-ray alignment system proves to be viable. Figure 18 shows the Lorentz angle as a function of electric field for the same gases. We expect that the experiment will use one of these gases.

4.5 Tests with cosmic rays at the SSC TTR

Most of the prototypes have been installed at the TTR and have been undergoing tests over the past few months. Figure 19 shows schematically the arrangement of the four small BNL chambers with parallel strips and a two-layer large module. The TTR scintillators in coincidence with a local scintillator and the anode planes are used for triggering. Similar arrangements exist for the rest of the prototypes at the TTR. Figure 20(top) shows a typical Landau distribution from the cathode strips. At the bottom of Figure 20 is shown a spectrum of the highest amplitude of a cluster. The events overflowing the 8-bit FADC are not included in the analysis. Figure 21 shows a typical event as seen by the six cathode planes. The single layer spatial resolution of the small chambers is determined by using three layers to define a track and then histogram the residual of the fourth. Figure 22 shows the distributions of all four of these residuals. Figure 23 shows one of them magnified. Average resolutions over a $\pm 6°$ acceptance in phi are of the order of 68 microns. Figure 24 shows the dependence of the resolution as a function of phi. For normal incidence the resolution is of the order of 45–50 microns. It should be noted that multiple scattering(not subtracted) is estimated to contribute about 30 microns in quadrature. Figure 25 shows the resolution obtained by the 1x1.5 m^2 Dubna prototype. Figure 26 shows the resolutions obtained for nearly normal incidence at three different high voltage values by the Houston group and the 1x0.5 m^2 using Iarocci-type profiles with cathode strips.

The resolution of the full scale prototype is also consistent with <70 microns but is difficult to further quantify it until two more similar layers are available at the end of February. Figure 27 shows a distribution of the quantity $(x_5 - x_6 - h \tan \phi)$ The rms should be divided by $\sqrt{2}$ to get the single layer resolution. Further the fact that the transverse coordinate is not known to better than 5 cm contributes an error estimated at about 70 microns which should be subtracted in quadrature. More precise resolution values will be determined when all 4 modules become available. Figure 28 shows the efficiency of the PNPI prototypes. Essentially 100% efficiencies are measured by all the modules tested at the TTR. Figure 29shows the distribution of the earliest time of arrival from the four planes in the PNPI

test setup using 1.7 GeV/c protons from the Gatchina Synchrocyclotron. Constant fraction discriminators were used. It can be seen that all events can be contained in a 16 nsec window.

4.6 Summary

The tests with X-rays described in this report allow a thorough understanding of the cathode strip chambers as well as testing aspects of the technology and our particular design that could be difficult or impossible to be performed in a single layer setup either with cosmic rays or beam particles. The capacitive interpolation with the floating strips, its effects on resolution and differential nonlinearity are examples of the latter. We have demonstrated a compact, low cost, multiplexed readout suitable for systems with large numbers of channels. The 288 channels of this prototype represent nearly one third of the maximum number of channels anticipated for *any* GEM superlayer module. Noise levels of 1600 equivalent rms electrons for 550 nsec shaping time has been demonstrated. Intercalibration of the cathode strip channels to the 0.5% level has been achieved. Gas amplification stability and its implications to construction tolerances have been thoroughly studied. The capacitive interpolation with the floating strips has been found to perform as designed both in restoring linear response and in reducing the capacitive load of the preamplifiers. Finally the achieved resolution of $\approx 50\mu m$ is consistent with the limits imposed by the range of photoelectrons indicating no other fundamental limits due to excessive thermal noise etc. Tests with cosmic rays show single layer resolution consistent with the baseline design, demonstrate fully efficient bunch crossing tagging, and operation with a safe gas suitable for use in the GEM Detector. Noise and calibration issues were demonstrated with a large number of channels.

References

[1] E. Gatti, A. Longoni, H. Okuno, and P. Semenza, Nucl. Instr. and Meth. **163**, 83, (1979).

[2] V. Radeka, and R.A. Boie, Nucl. Instr. and Meth. **178**, 543, (1980).

[3] E. Gatti, A. Longoni, and V. Radeka, Nucl. Instr. and Meth. **220**, 445, (1984).

[4] E. Mathieson, and G.C. Smith, IEEE Transactions on Nuclear Science, Vol. 36, No. 1, February 1989.

[5] B. Yu, G.C. Smith, and V. Radeka, "Developments in interpolating cathode structures for high precision gas proportional detectors", to be presented at the 1992 IEEE Nuclear Science Symposium, Orlando, Florida, 1992.

[6] J. Fischer, V. Radeka, and G.C. Smith, Nucl. Instr. and Meth. **A252**, 239, (1986).

[7] "AMPLEX-A Low noise, Low power Analog CMOS Signal Processor for Multielement Silicon Particle Detectors", E. Beuville, K. Borer, E. Chesi, EHM Heijne, P. Jarron, B. Lisowski, S. Singh, CERN/EF89-9, Sept. 1989.

[8] E. Chesi, and P. Martinengo, "Digital Readout for Analog, Multiplexed Signals", CERN, Note PS 202, January 1988.

[9] "The GEM Muon System Based on Cathode Strip Chambers, GEM TN-92-199, October,1992.

[10] B. Yu,"Gas Proportional Detectors with Interpolating Cathode Pad Readout for High Track Multiplicities", Ph.D. Thesis, Pittsburgh 1991 (BNL 47055 Informal Report).

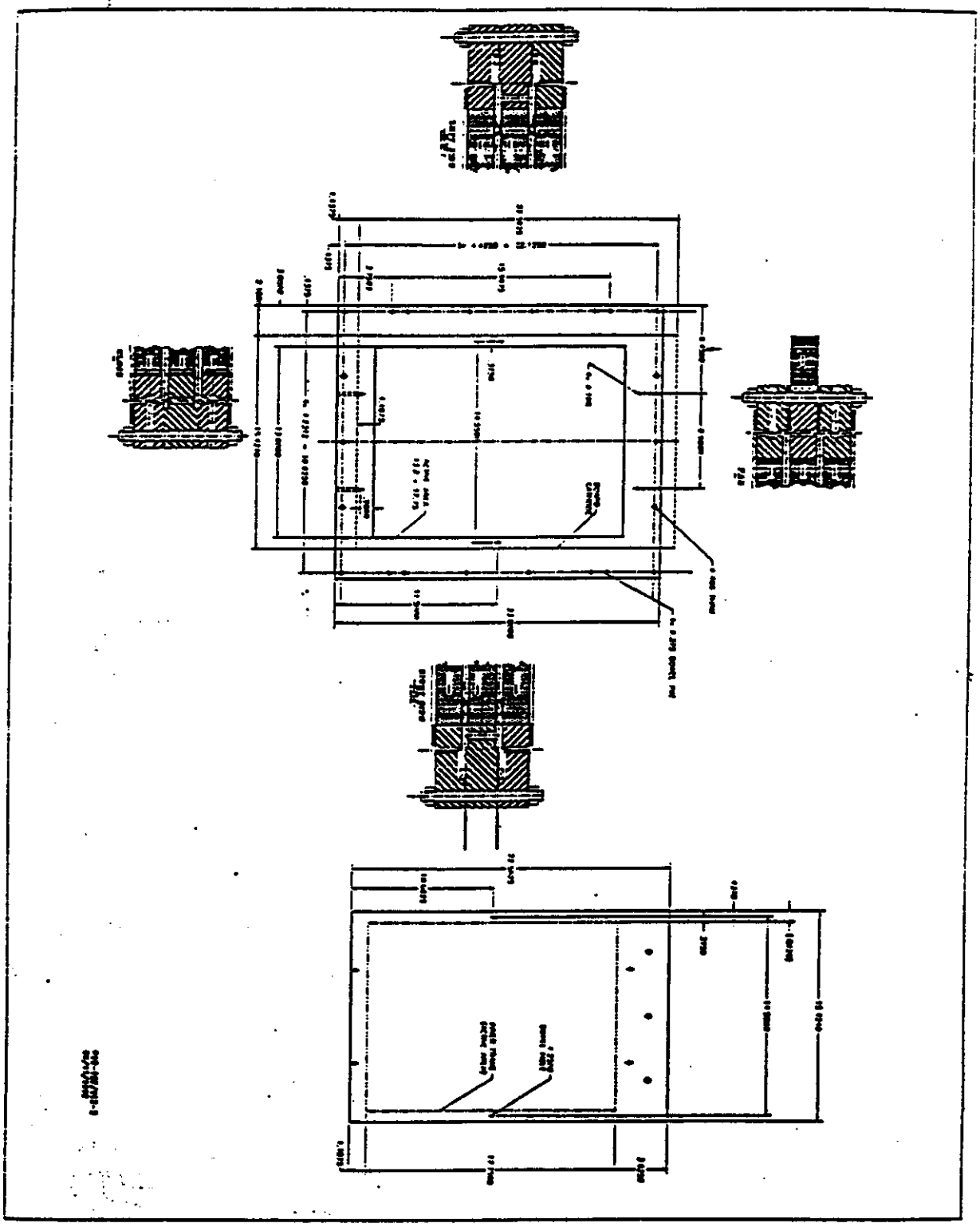

Figure 1

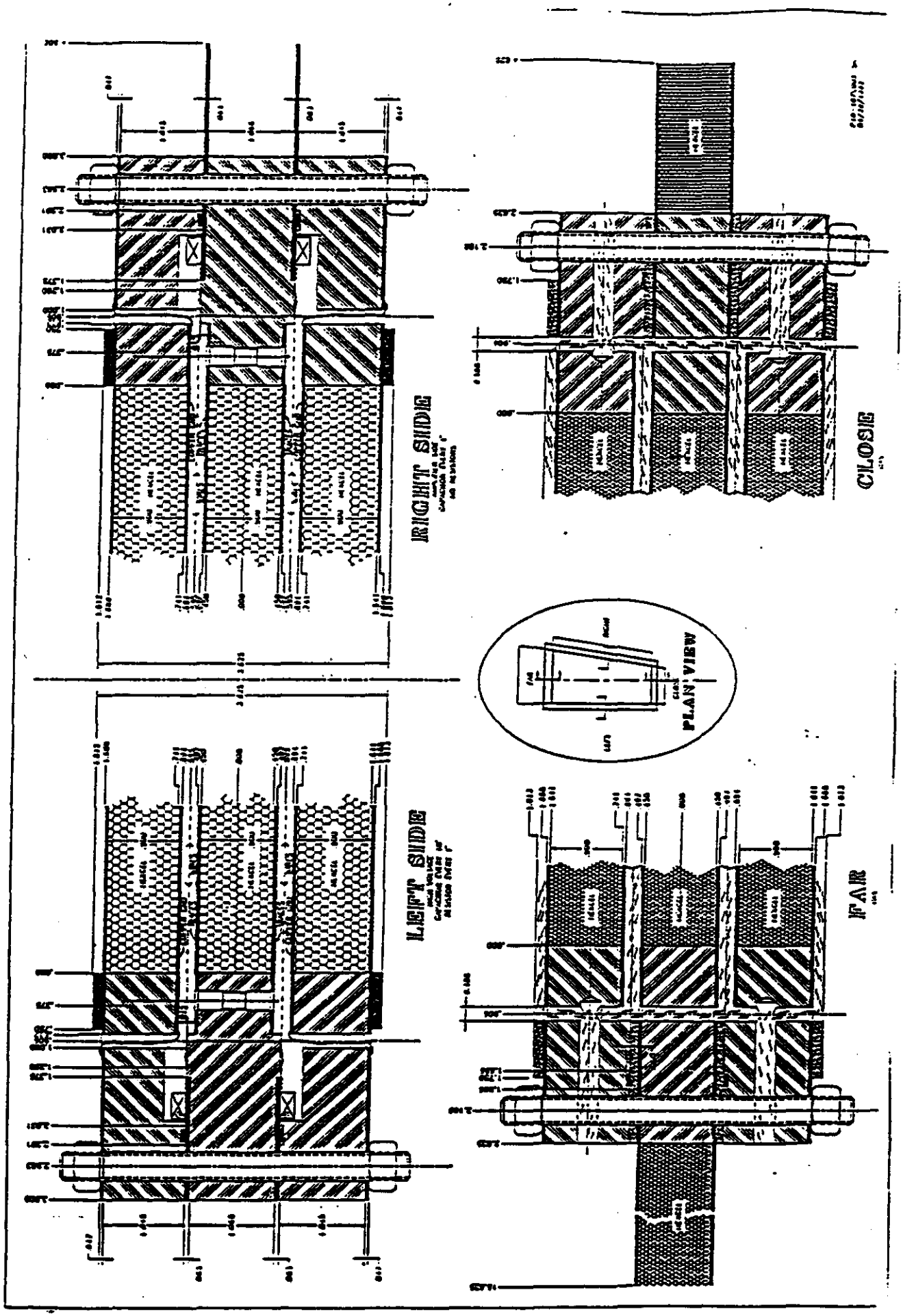

Figure 2

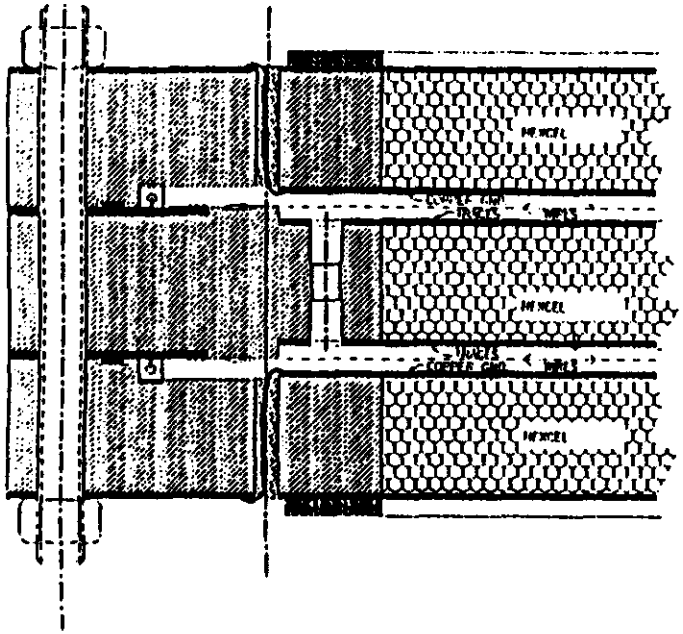

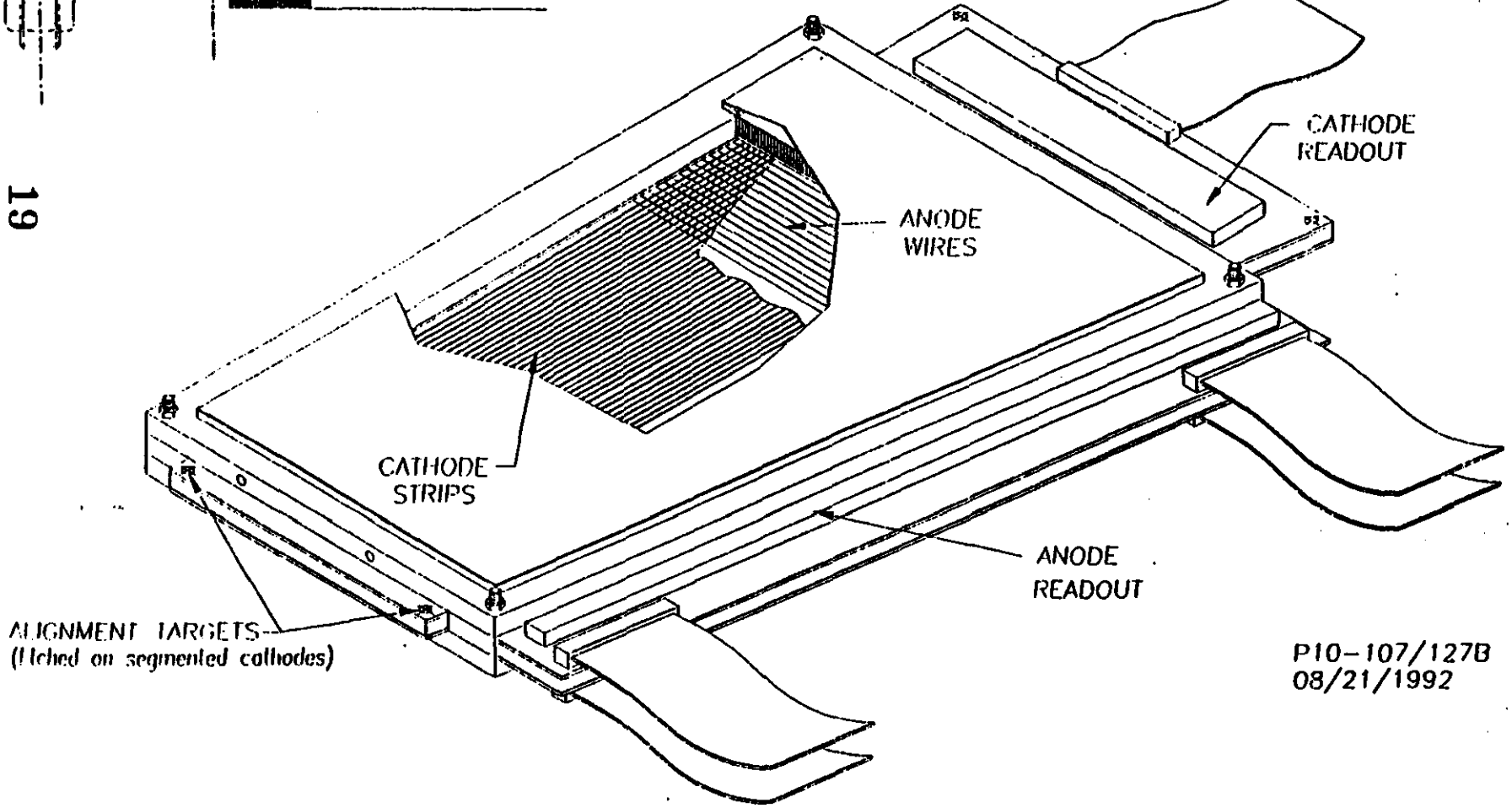
CATHODE READOUT
ANODE WIRES
CATHODE STRIPS
ANODE READOUT
ALIGNMENT TARGETS
(Etched on segmented cathodes)
P10-107/127B
08/21/1992

Figure 3

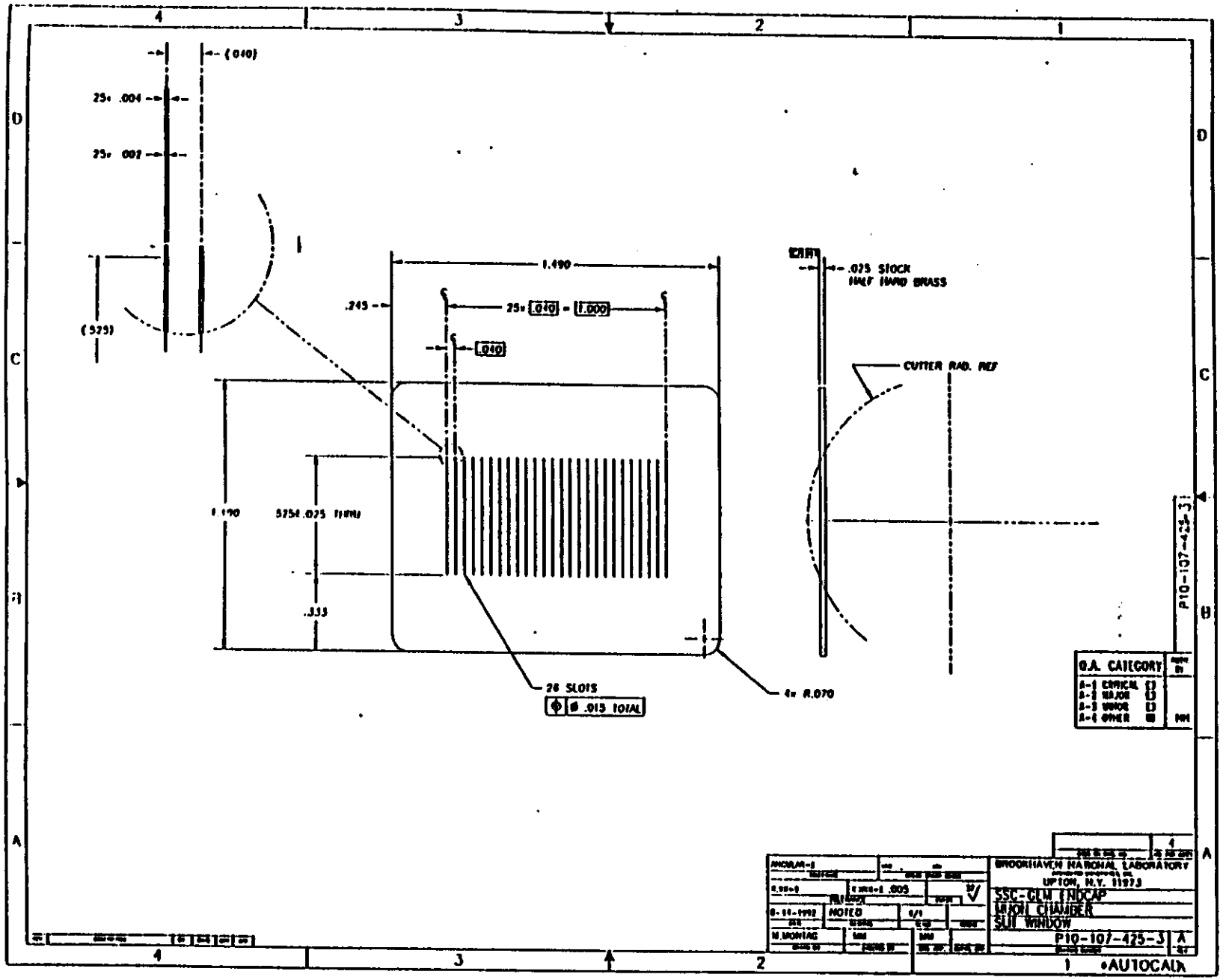
(.040)
25x .004
25x .002
(.575)
1.490
.245
25x .040 = 1.000
.040
.025 STOCK
HALF HARD BRASS
CUTTER RAD. REF
1.190
.575±.025 TYPU
.333
26 SLOTS
⌖ Ø .015 TOTAL
4x R.070
Q.A. CATEGORY
CRITICAL
MAJOR
MINOR
OTHER
P10-107-425-3
BROOKHAVEN NATIONAL LABORATORY
UPTON, N.Y. 11973
SSC-GLM ENDCAP
MAGN CHAMBER
SLIT WINDOW
P10-107-425-3
NOTED
AUTOCAD

Figure 4

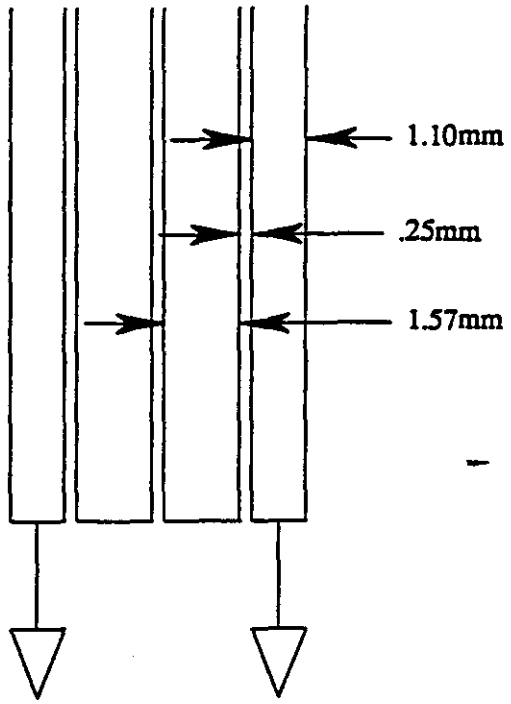

Figure 5a

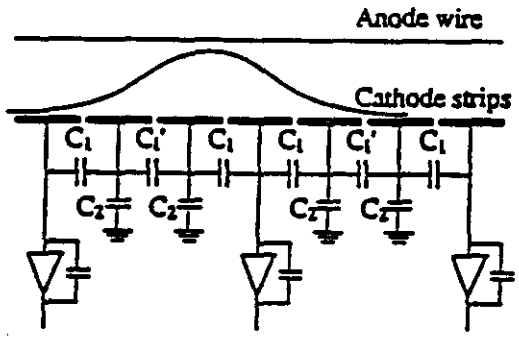

Figure 5b

op_varw1

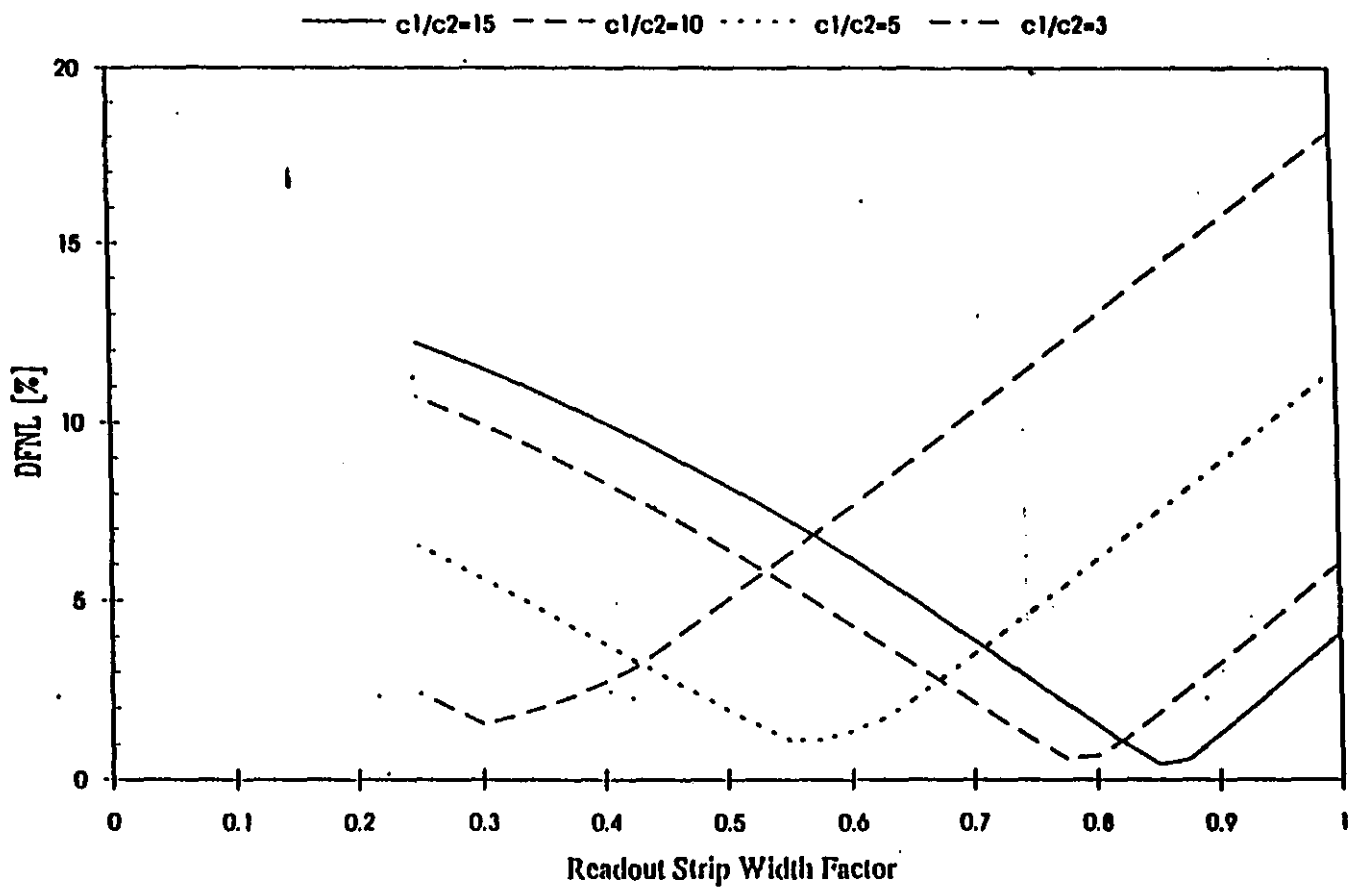

Figure 6

la=5, h=2.5, k3=.55, width factor is calculated with respect to la/3

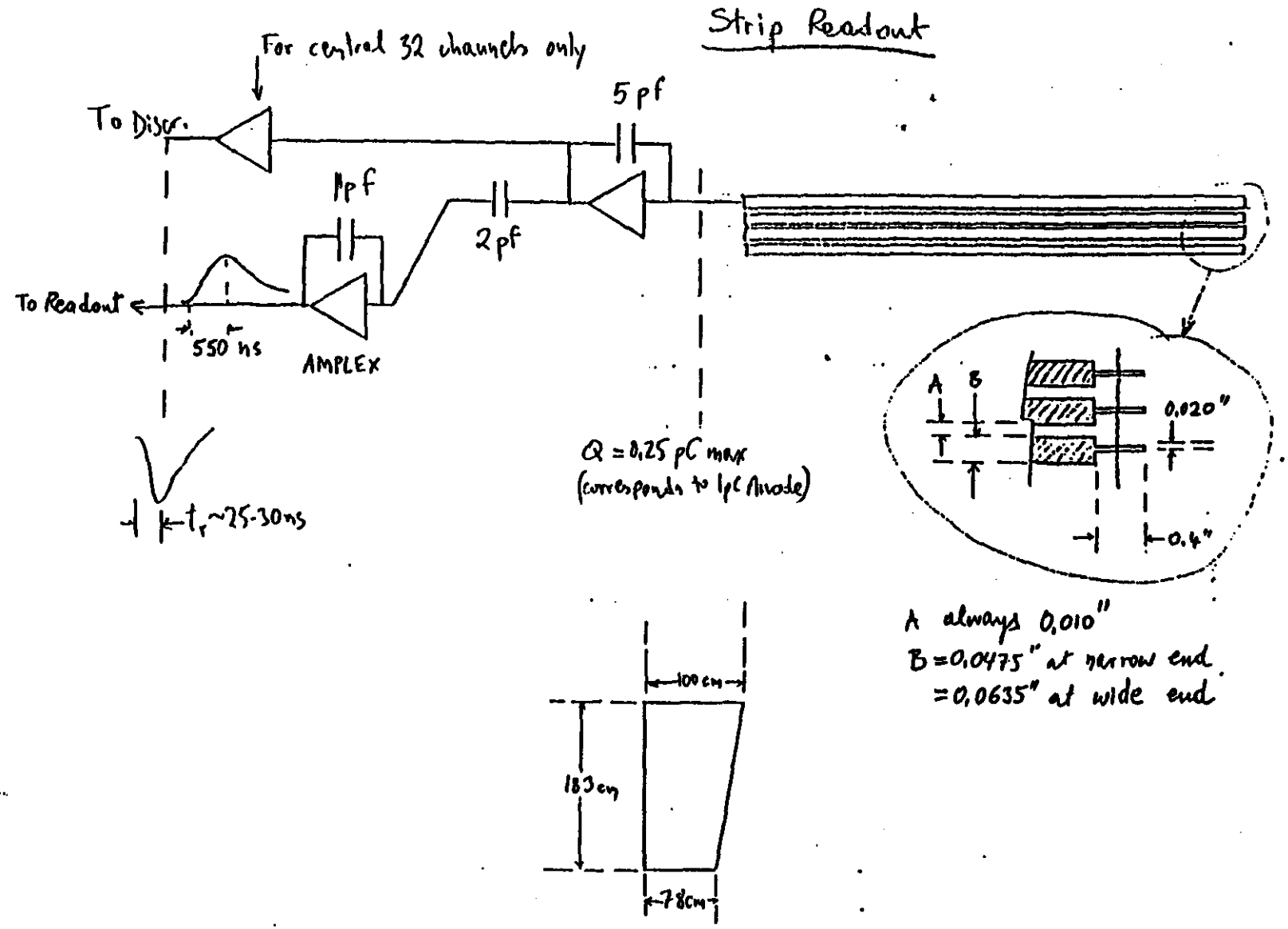
Strip Readout
For central 32 channels only
To Discr.
5 pf
1pf
2pf
To Readout
550 ns
AMPLEX
t_r ~25-30ns
Q = 0.25 pC max
(corresponds to 1pC Anode)
A
B
0.020"
0.4"
A always 0.010"
B = 0.0475" at narrow end
= 0.0635" at wide end
100 cm
183 cm
78 cm

Figure 7

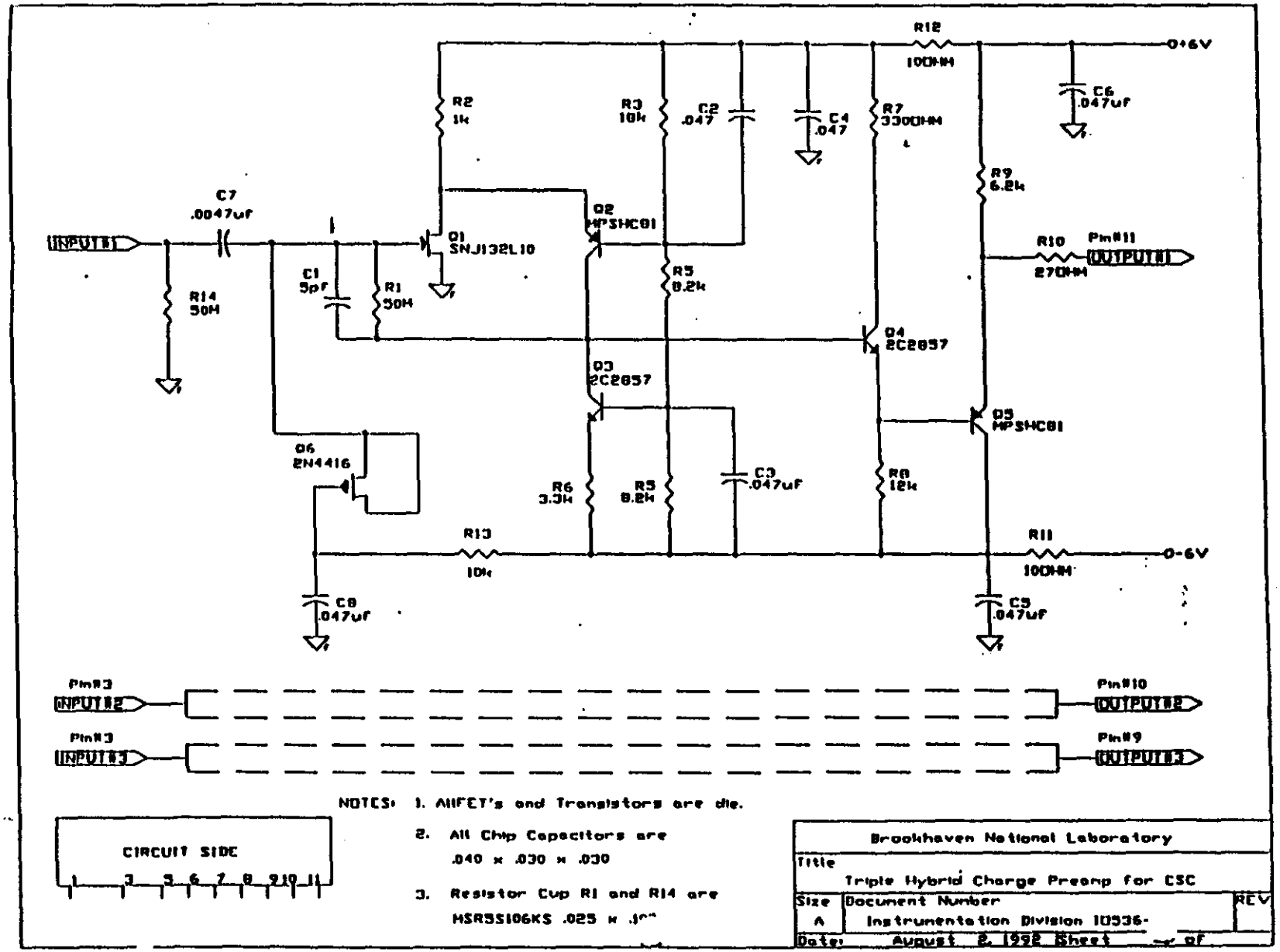
R12
100HM
0+6V
C6
.047uf
R2
1k
R3
10k
C2
.047
C4
.047
R7
330OHM
R9
6.2k
C7
.0047uf
INPUT#1
Q1
SNJ132L10
Q2
MPSHC01
R10
27OHM
Pin#11
OUTPUT#1
C1
5pf
R1
50H
R5
8.2k
R14
50H
Q4
2C2857
Q3
2C2857
Q5
MPSHC01
Q6
2N4416
R6
3.3k
R5
8.2k
C3
.047uF
R8
12k
R13
10k
R11
100HM
0-6V
C8
.047uf
C5
.047uf
Pin#3
INPUT#2
Pin#10
OUTPUT#2
Pin#3
INPUT#3
Pin#9
OUTPUT#3
NOTES: 1. All FET's and Transistors are die.
2. All Chip Capacitors are .040 x .030 x .030
3. Resistor Cup R1 and R14 are HSR5S106KS .025 x .1
CIRCUIT SIDE
1 3 5 6 7 8 9 10 11
Brookhaven National Laboratory
Title
Triple Hybrid Charge Preamp for CSC
Size
A
Document Number
Instrumentation Division 10536-
REV
Date: August 2, 1992 Sheet of

Figure 8

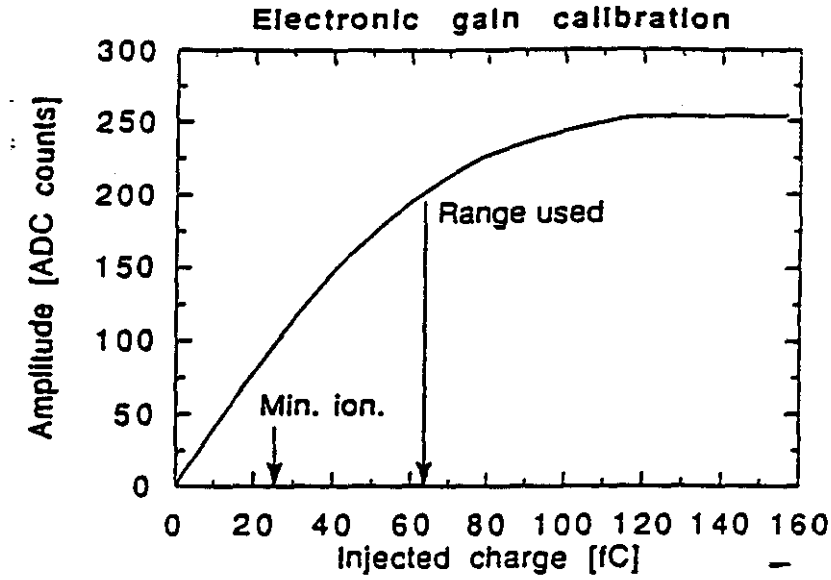

Figure 9a

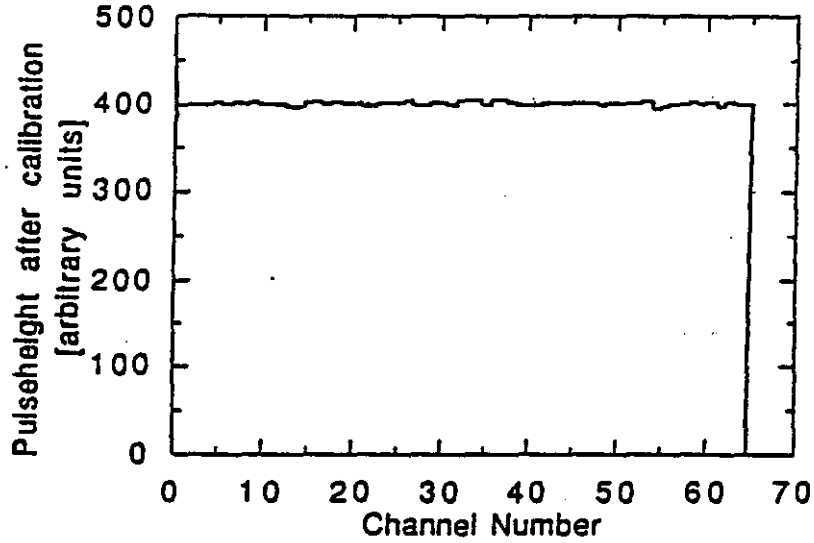

Figure 9b

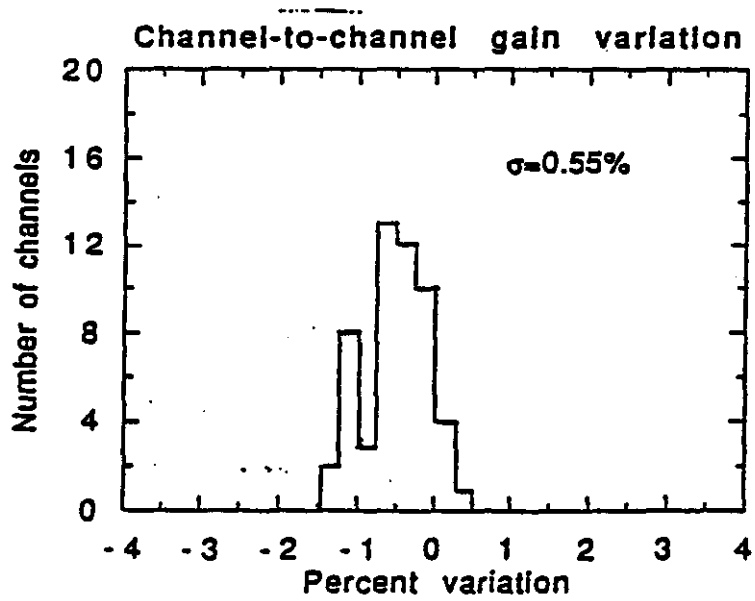

Figure 9c

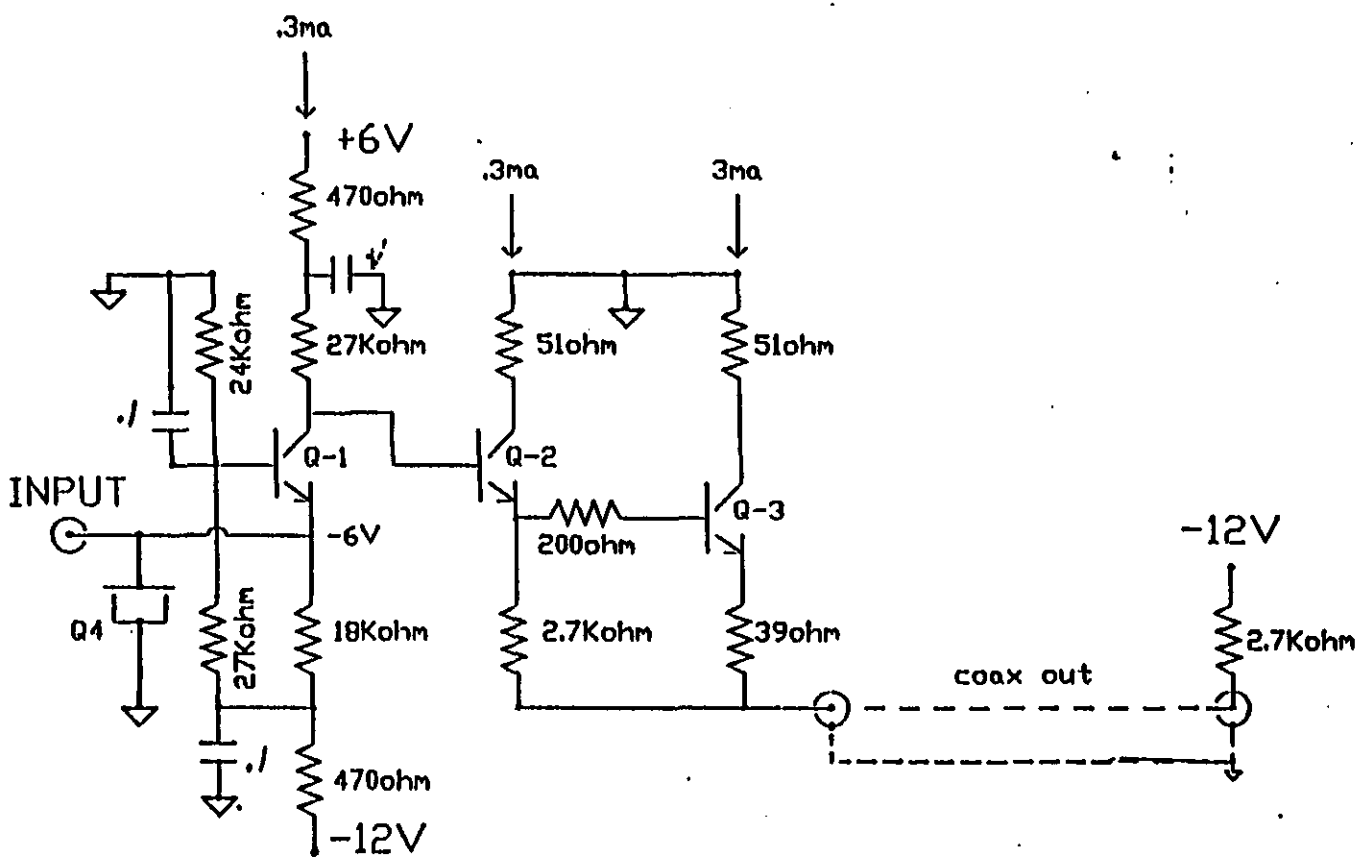

Q1-BFT-25
Q2-BFT-25
Q3-BFR-92
Q4-2N4416/FET

preamplifier Dim .700"x.400"
pins on .100" CC.
pin #1-•

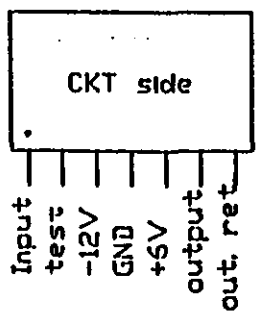

Figure 10

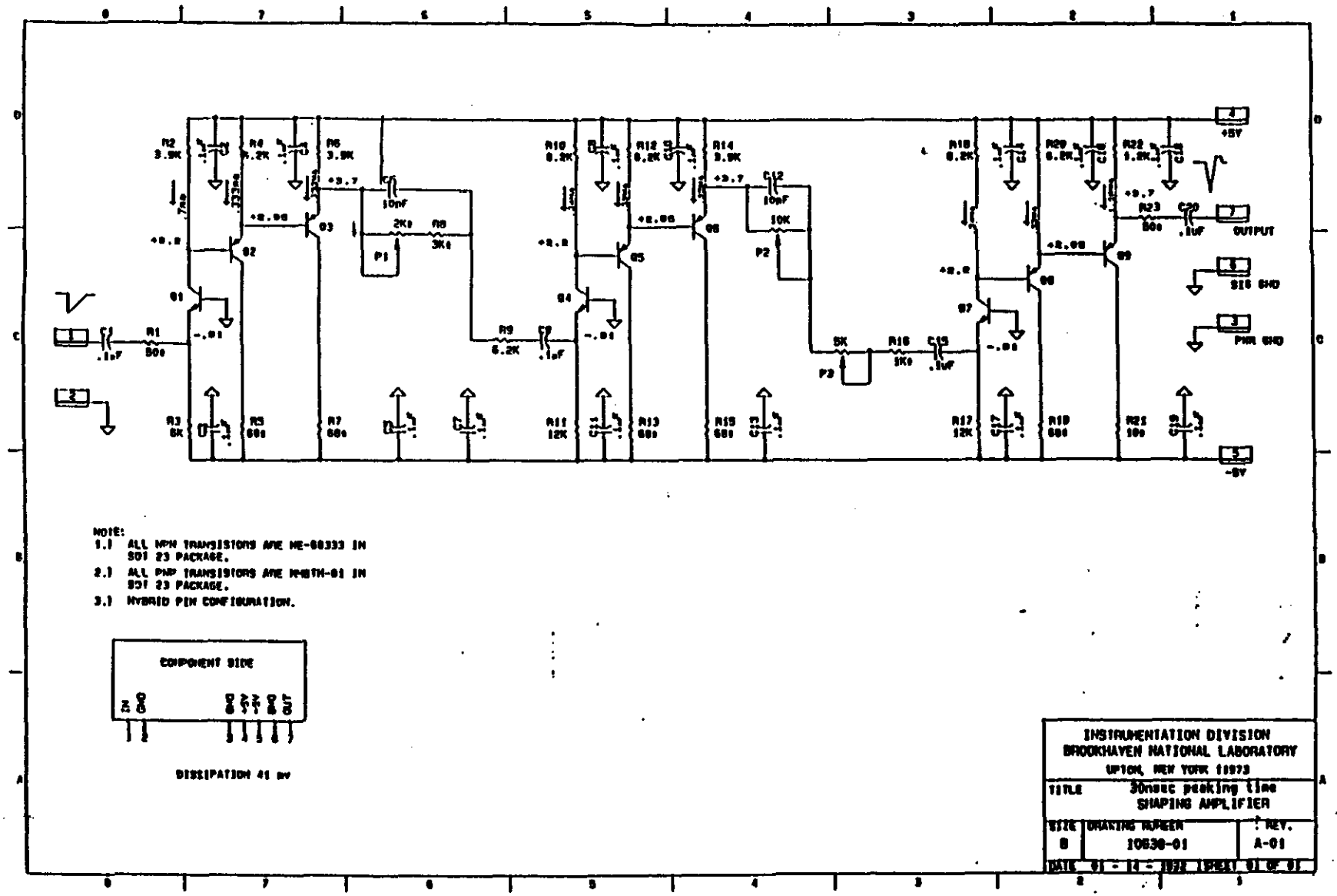
NOTE:
1.) ALL NPN TRANSISTORS ARE NE-68333 IN SOT 23 PACKAGE.
2.) ALL PNP TRANSISTORS ARE MMBTH-81 IN SOT 23 PACKAGE.
3.) HYBRID PIN CONFIGURATION.
COMPONENT SIDE
DISSIPATION 41 mw
INSTRUMENTATION DIVISION
BROOKHAVEN NATIONAL LABORATORY
UPTON, NEW YORK 11973
TITLE
30nsec peaking time
SHAPING AMPLIFIER
SIZE
B
DRAWING NUMBER
10630-01
REV.
A-01
+5V
OUTPUT
SIG GND
PWR GND
-5V

Figure 11

Preliminary

IC6A	Device #7		Qin:	5.00E-14					1/7/93
Cd	Vout	Vnoise	System	SNR	Gain	ENC	ENC	Slope	Intercept
0	1.839	6.18	0.65	299	36.78	1.67E-16	1043	6.85	1018.85
22	1.771	6.7	0.96	267	35.42	1.87E-16	1168		
47	1.697	7.13	0.64	239	33.94	2.09E-16	1306		
68	1.613	7.75	0.94	210	32.26	2.38E-16	1488		
100	1.485	8.13	0.74	183	29.70	2.73E-16	1701		
150	1.377	9.13	0.94	152	27.54	3.30E-16	2058		
pF	V p-p	mV rms	mV rms	-	mV/fC	C	e-	e-/pF	e-

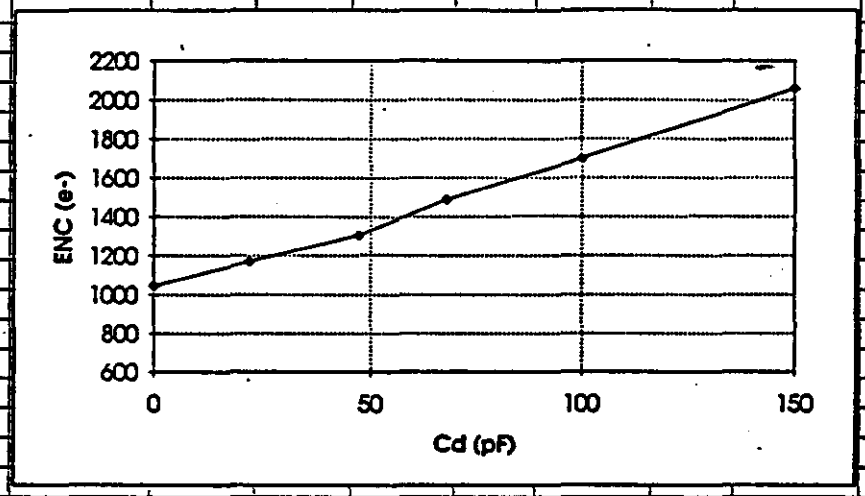

Linearity									
	Cd=100 pF			Tp=750 nsec					1/7/93
Vin	Vout								
0	0								
25	734								
50	1506								
100	2946								
140	3806								
150	4020								
160	4201								
170	4351								
180	4481								
200	4700								

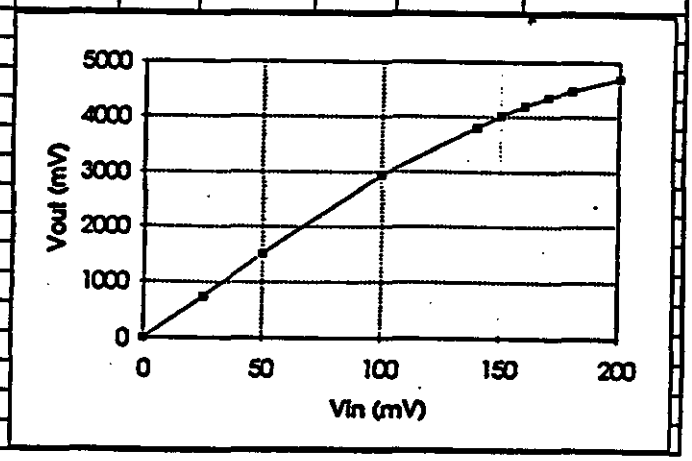

Gas amplification uniformity (%)

Chamber 2B

1.1	10.1	-9.8	4.7	-8.0	-9.8	-8.0	-13.4
6.4	10.1	-4.4	8.3	1.1	-8.0	-4.4	-15.2
10.1	8.3	-6.2	4.7	1.1	-6.2	-8.0	-13.4
17.3	17.3	-4.4	17.3	13.7	-4.4	-4.4	-15.2
6.4	10.1	-4.4	11.9	4.7	-4.4	-4.4	-11.6

Figure 12a

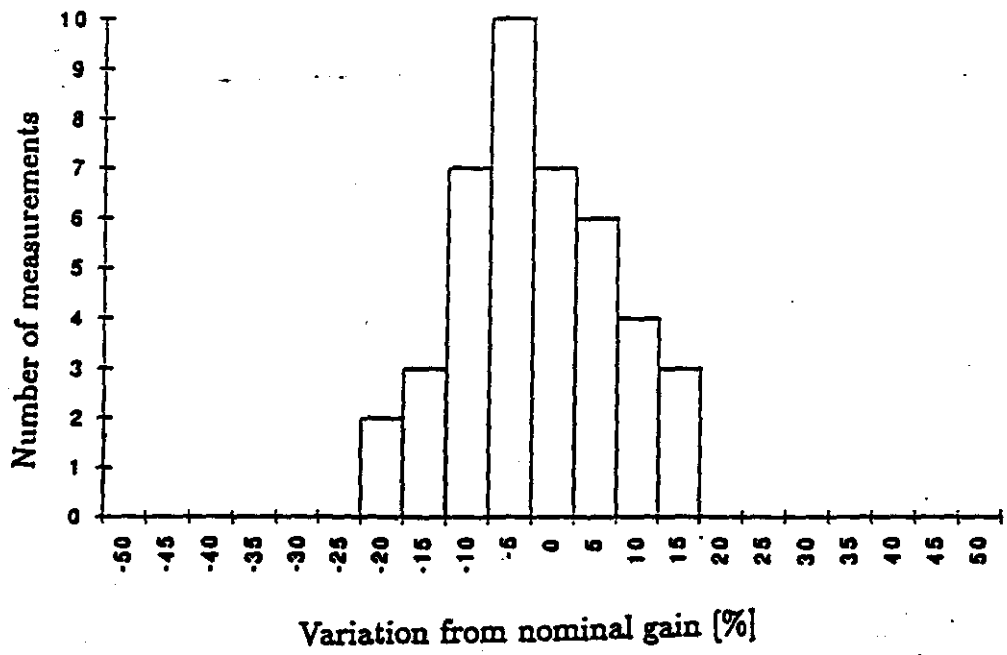

Figure 12b

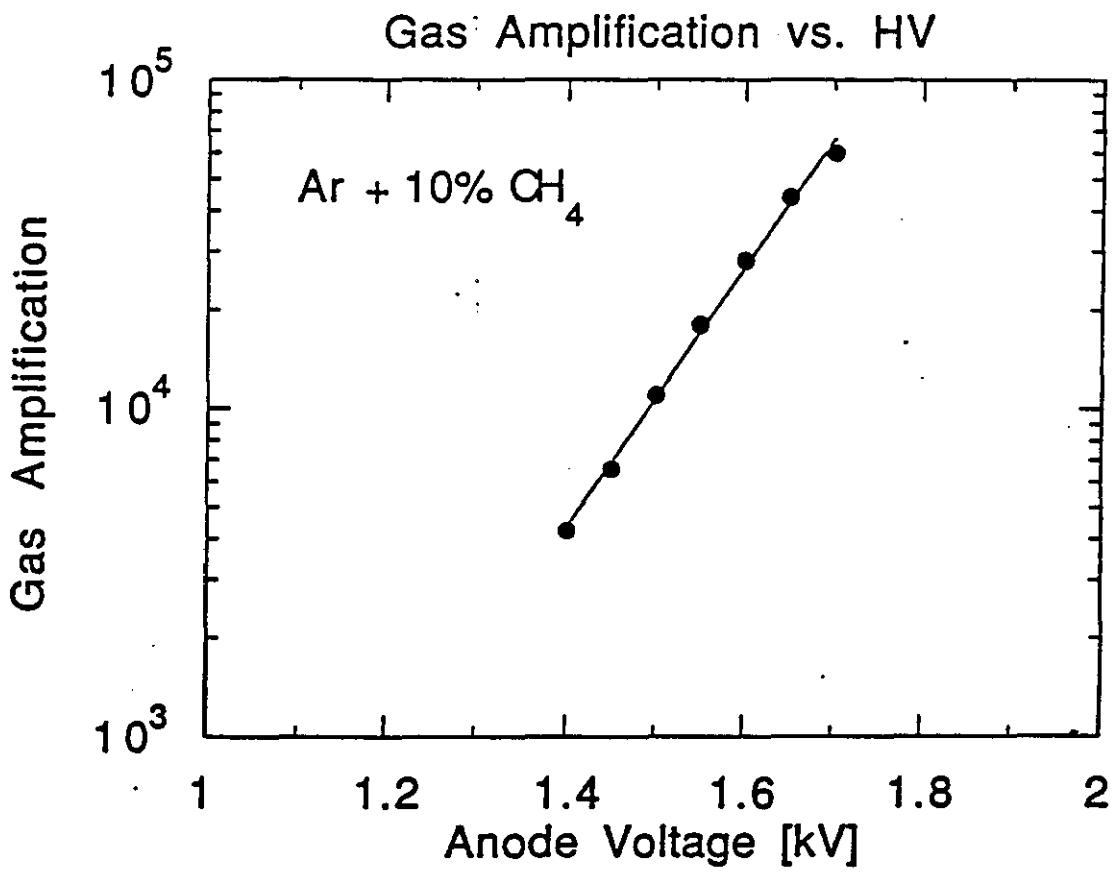
Gas Amplification vs. HV
Ar + 10% CH4
Gas Amplification
10^5
10^4
10^3
1
1.2
1.4
1.6
1.8
2
Anode Voltage [kV]

Figure 13

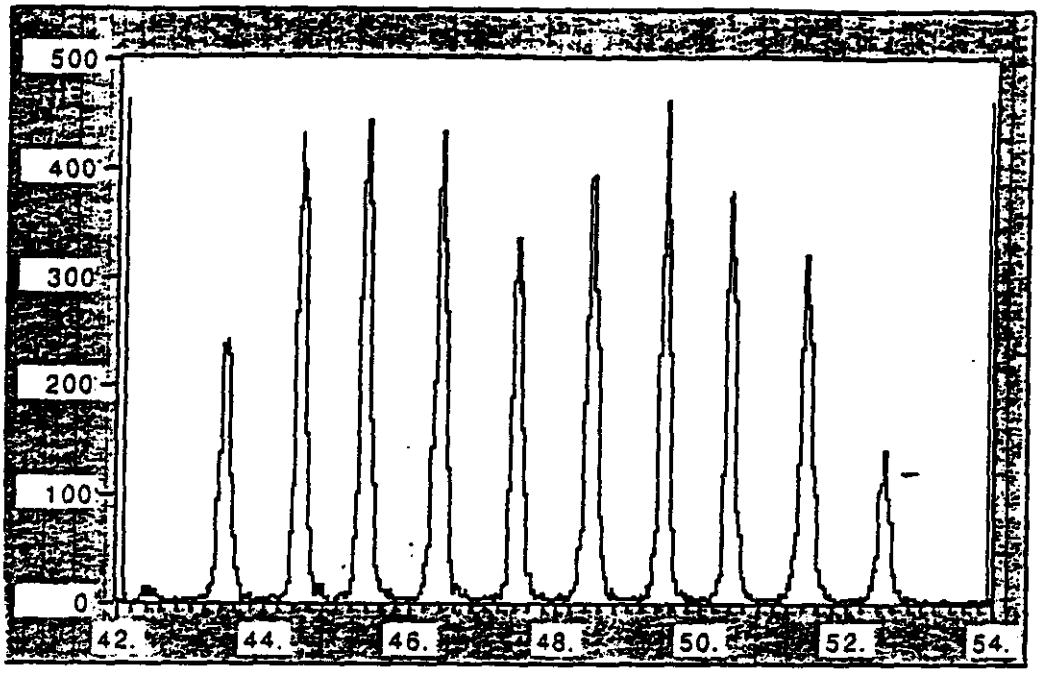

Figure 14a

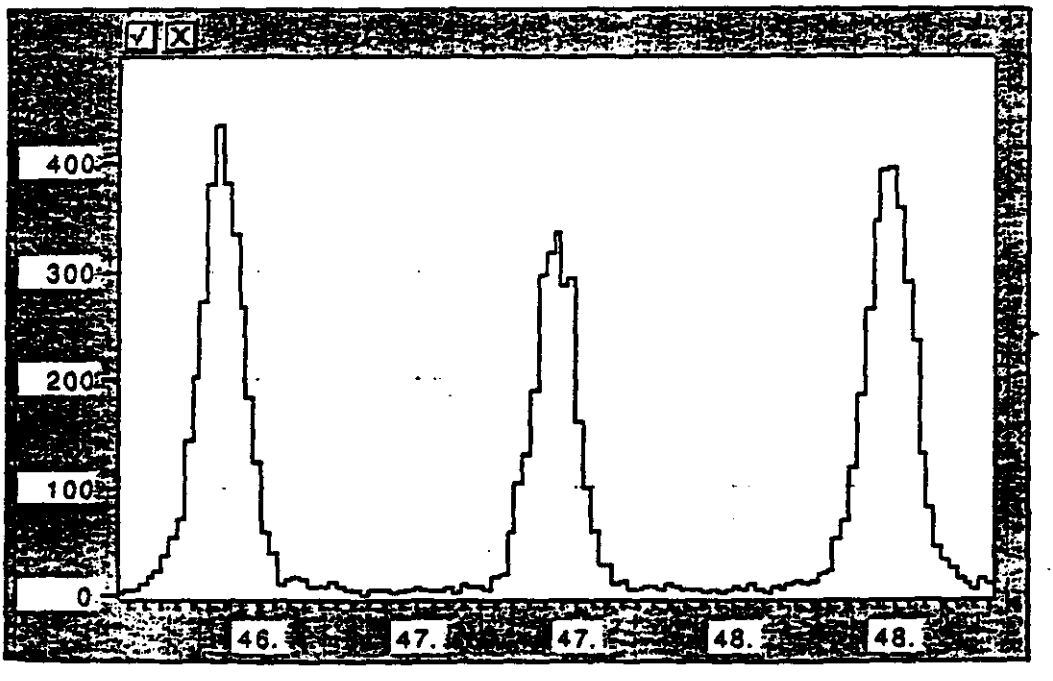

Figure 14b

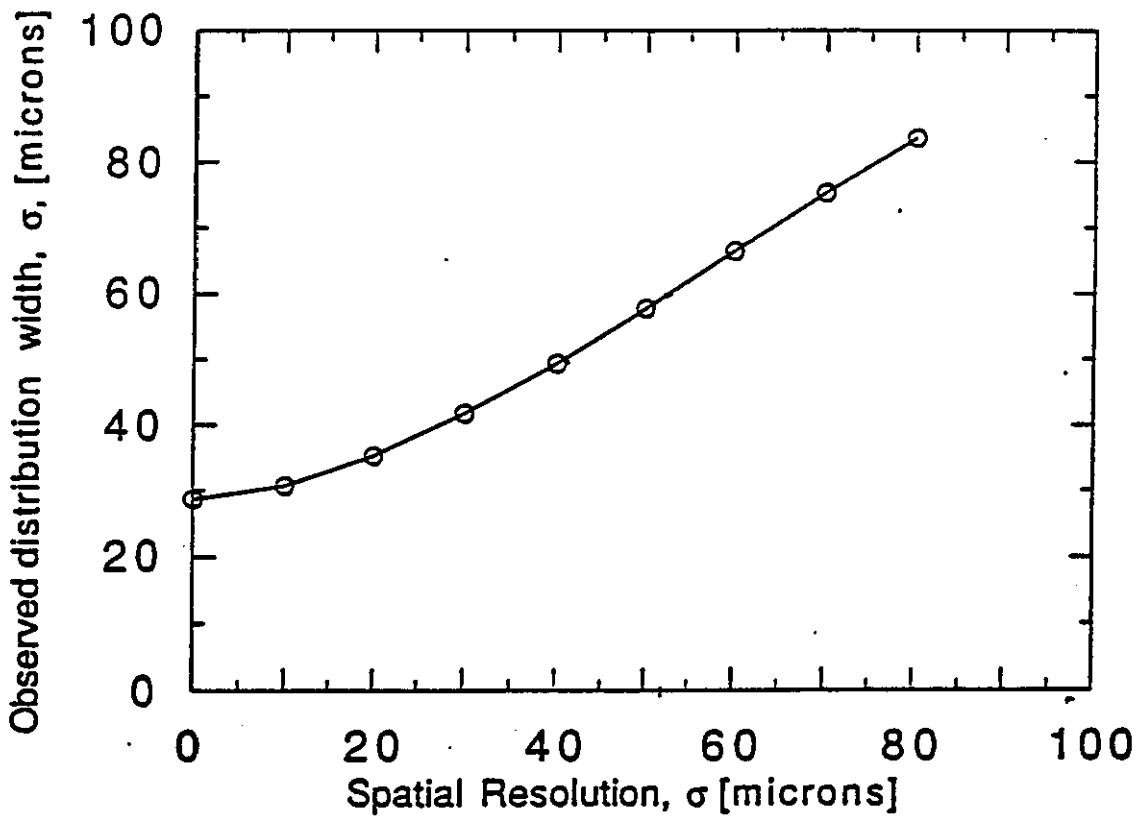
Observed distribution width, σ, [microns]
100
80
60
40
20
0
0
20
40
60
80
100
Spatial Resolution, σ [microns]

Figure 15

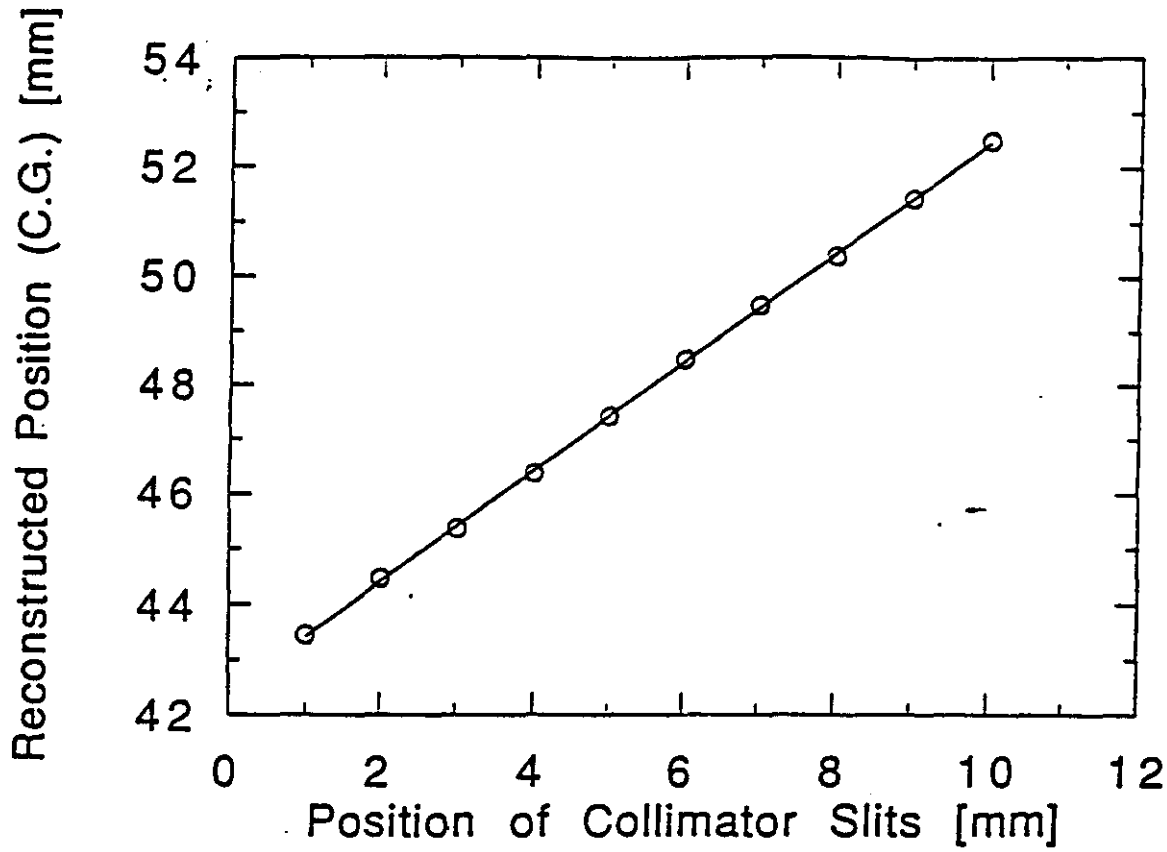

Figure 16a

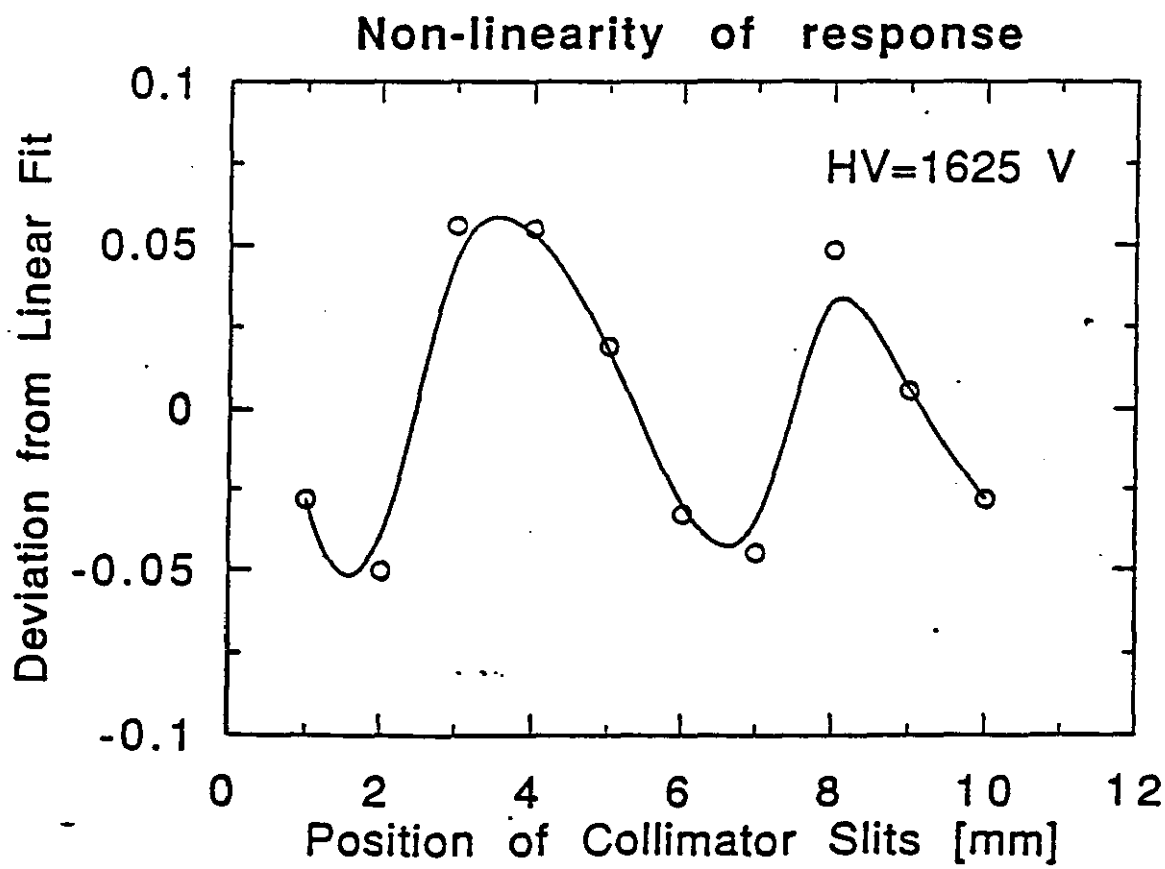

Figure 16b

Drift velocity

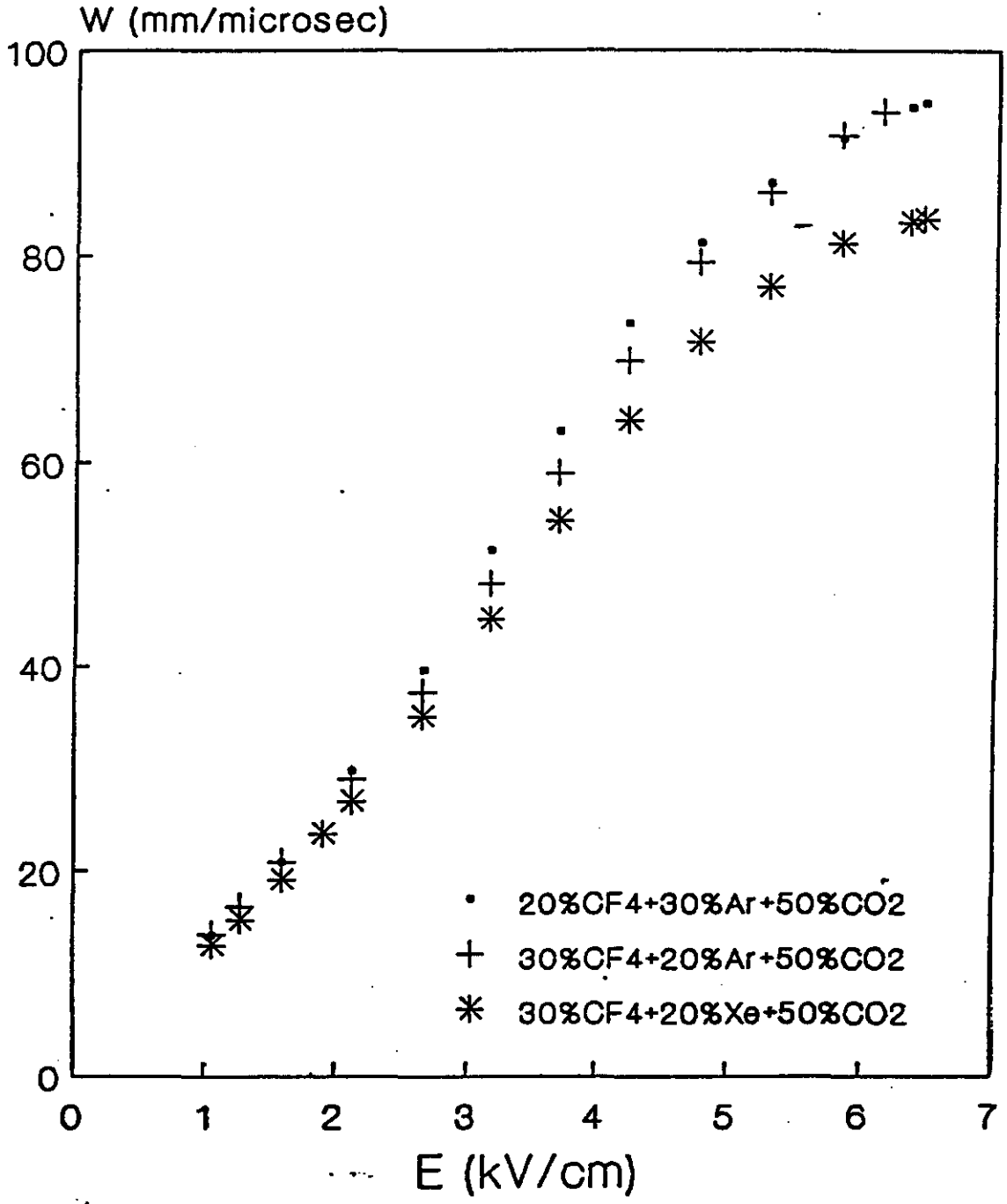

Fig. 17

Lorentz angle
B = 0.8 T

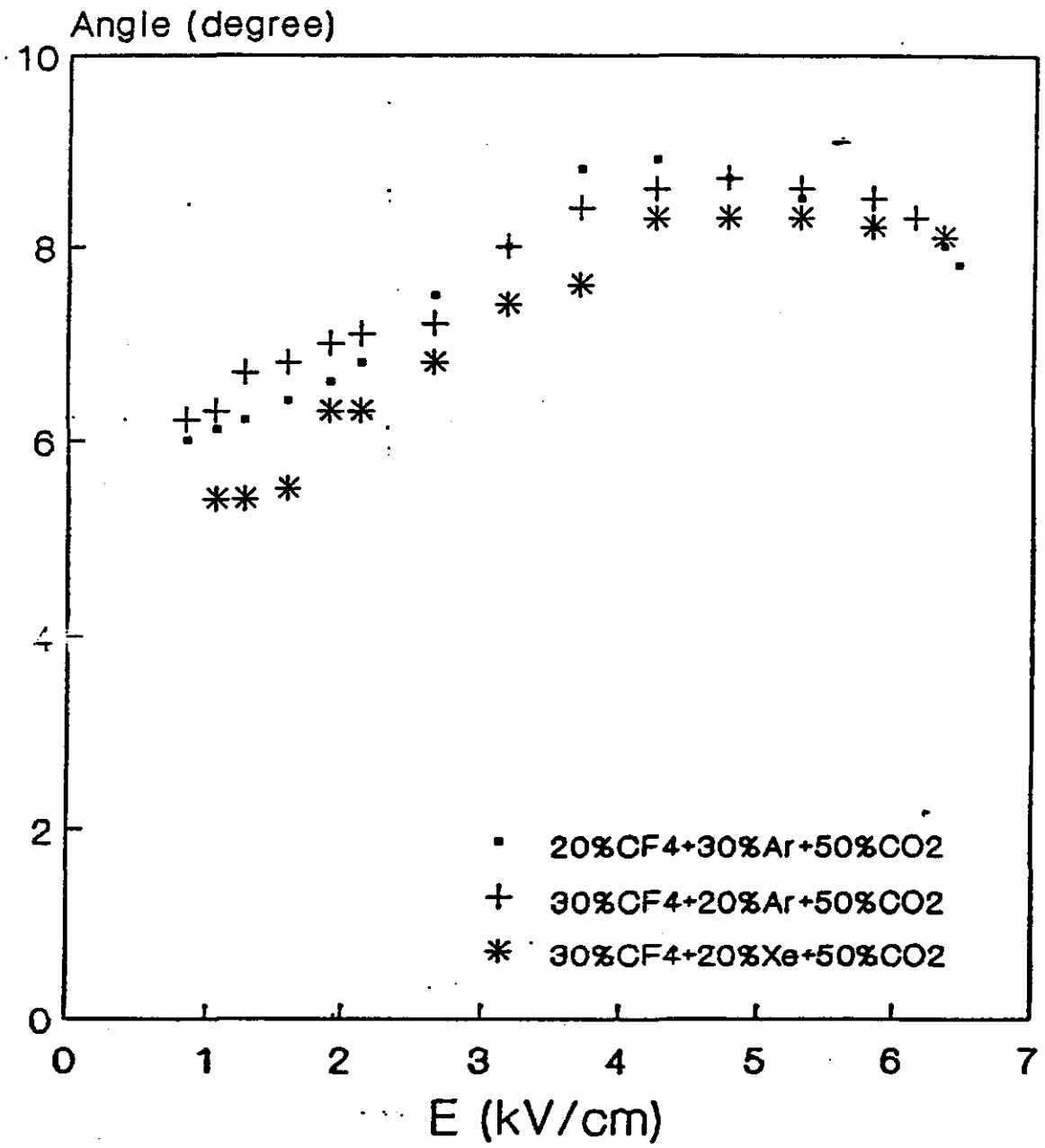

Fig. 18

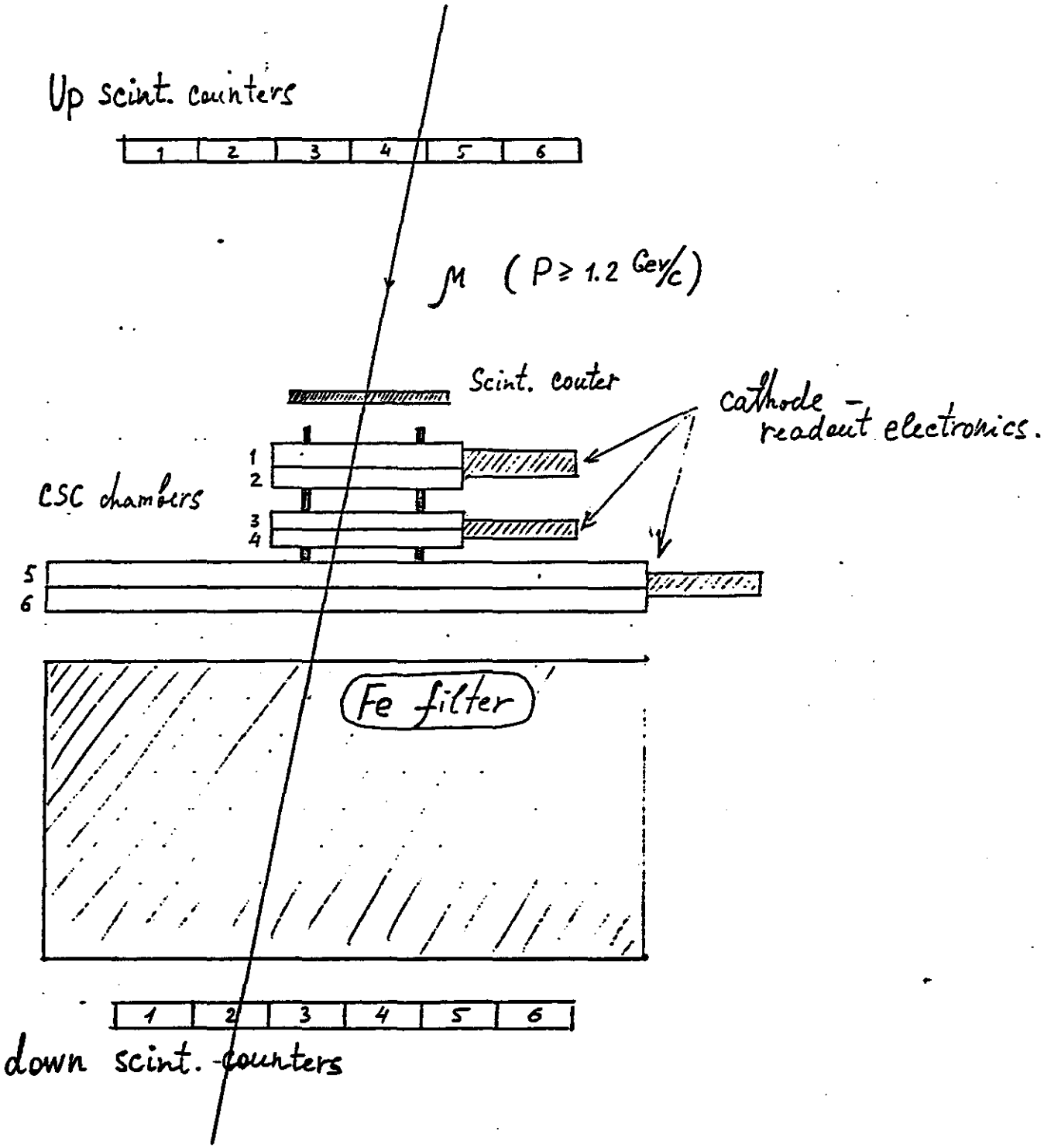
Up scint. counters
1
2
3
4
5
6
μ (P ≥ 1.2 Gev/c)
Scint. couter
cathode - readout electronics.
CSC chambers
1
2
3
4
5
6
Fe filter
1
2
3
4
5
6
down scint. counters

Fig 19

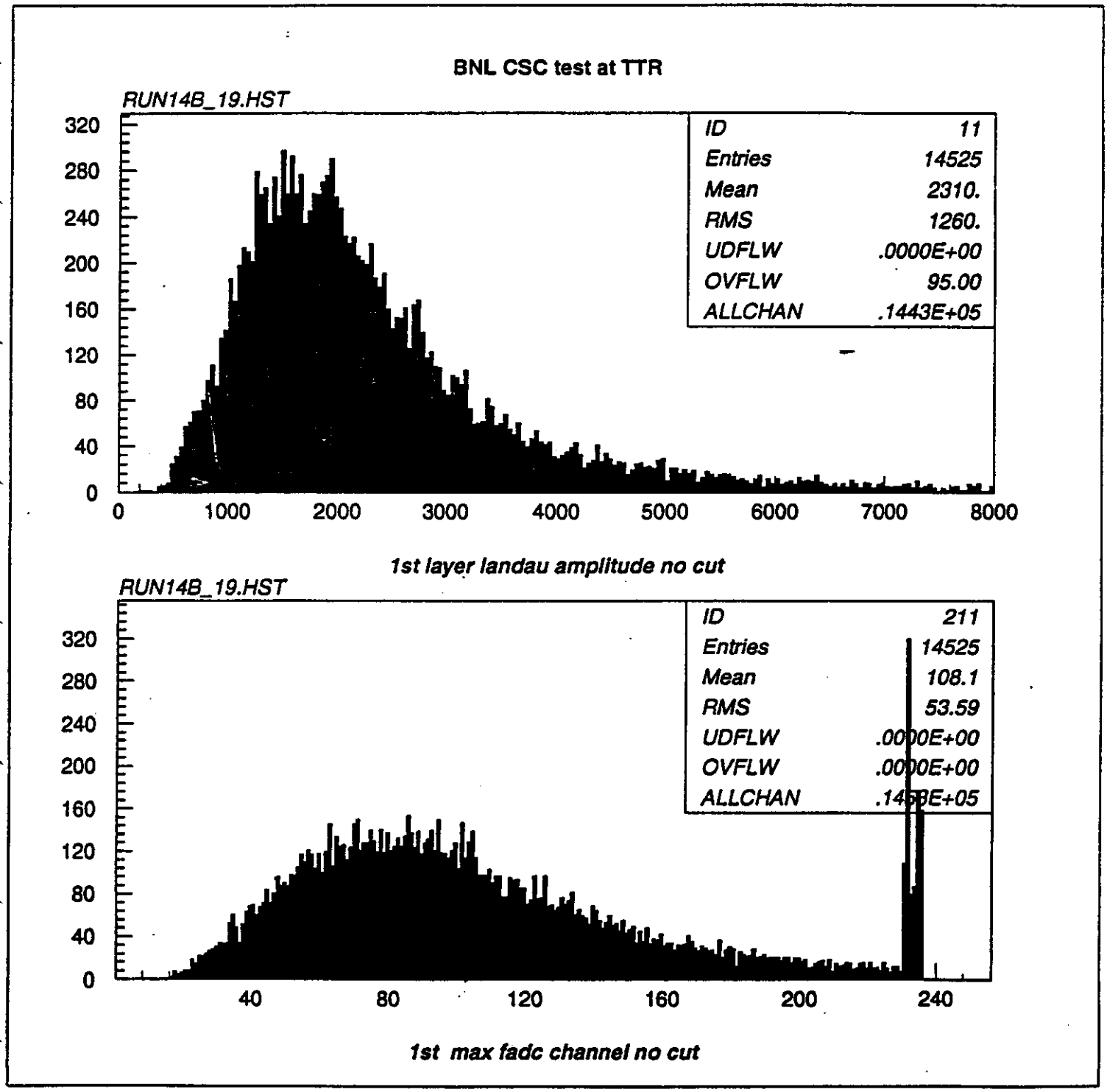
BNL CSC test at TTR
RUN14B_19.HST
ID 11
Entries 14525
Mean 2310.
RMS 1260.
UDFLW .0000E+00
OVFLW 95.00
ALLCHAN .1443E+05
1st layer landau amplitude no cut
RUN14B_19.HST
ID 211
Entries 14525
Mean 108.1
RMS 53.59
UDFLW .0000E+00
OVFLW .0000E+00
ALLCHAN .1458E+05
1st max fadc channel no cut

Fig 20

ont Panel

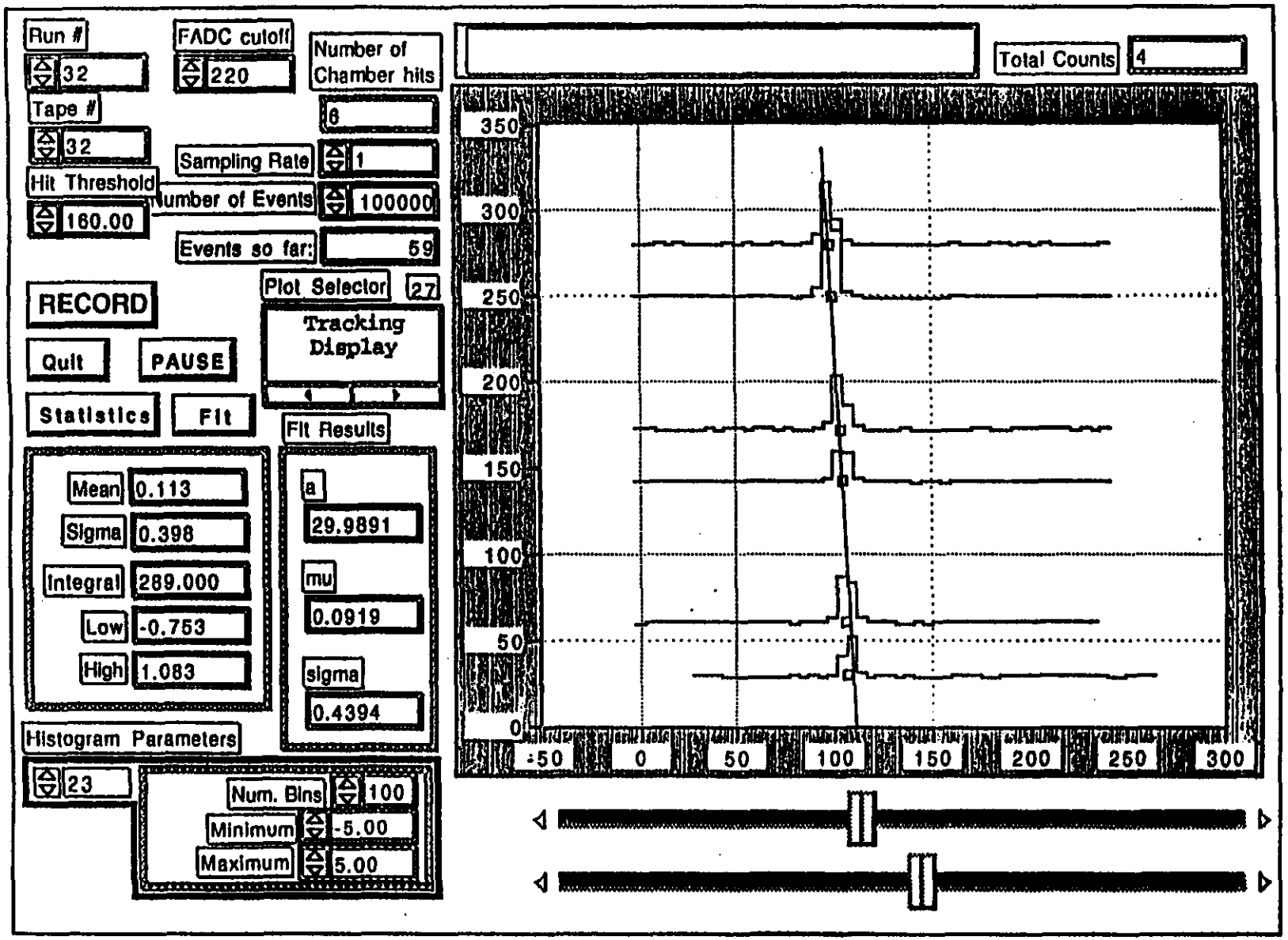

Fig 21

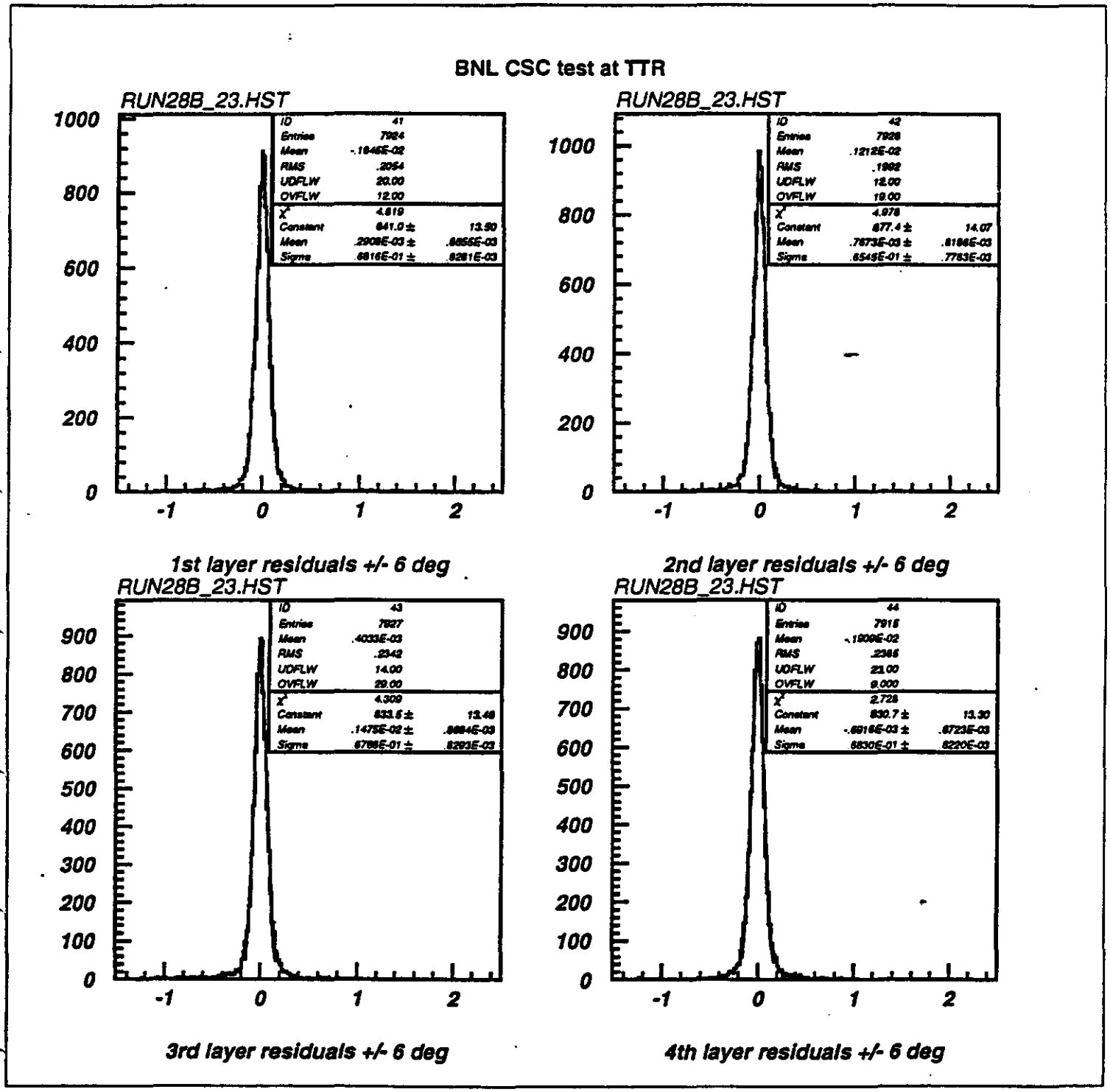
BNL CSC test at TTR
RUN28B_23.HST
ID 41
Entries 7924
Mean -.1846E-02
RMS .2054
UDFLW 20.00
OVFLW 12.00
χ² 4.819
Constant 841.0 ± 13.90
Mean .2908E-03 ± .8656E-03
Sigma .6816E-01 ± .6281E-03
1st layer residuals +/- 6 deg
RUN28B_23.HST
ID 42
Entries 7926
Mean .1212E-02
RMS .1992
UDFLW 12.00
OVFLW 19.00
χ² 4.976
Constant 877.4 ± 14.07
Mean .7673E-03 ± .8186E-03
Sigma .6545E-01 ± .7783E-03
2nd layer residuals +/- 6 deg
RUN28B_23.HST
ID 43
Entries 7927
Mean .4033E-03
RMS .2342
UDFLW 14.00
OVFLW 29.00
χ² 4.309
Constant 833.5 ± 13.48
Mean .1475E-02 ± .8884E-03
Sigma .6788E-01 ± .8293E-03
3rd layer residuals +/- 6 deg
RUN28B_23.HST
ID 44
Entries 7915
Mean -.1909E-02
RMS .2386
UDFLW 23.00
OVFLW 9.000
χ² 2.728
Constant 830.7 ± 13.30
Mean -.6916E-03 ± .8723E-03
Sigma .6830E-01 ± .8220E-03
4th layer residuals +/- 6 deg

Fig 22

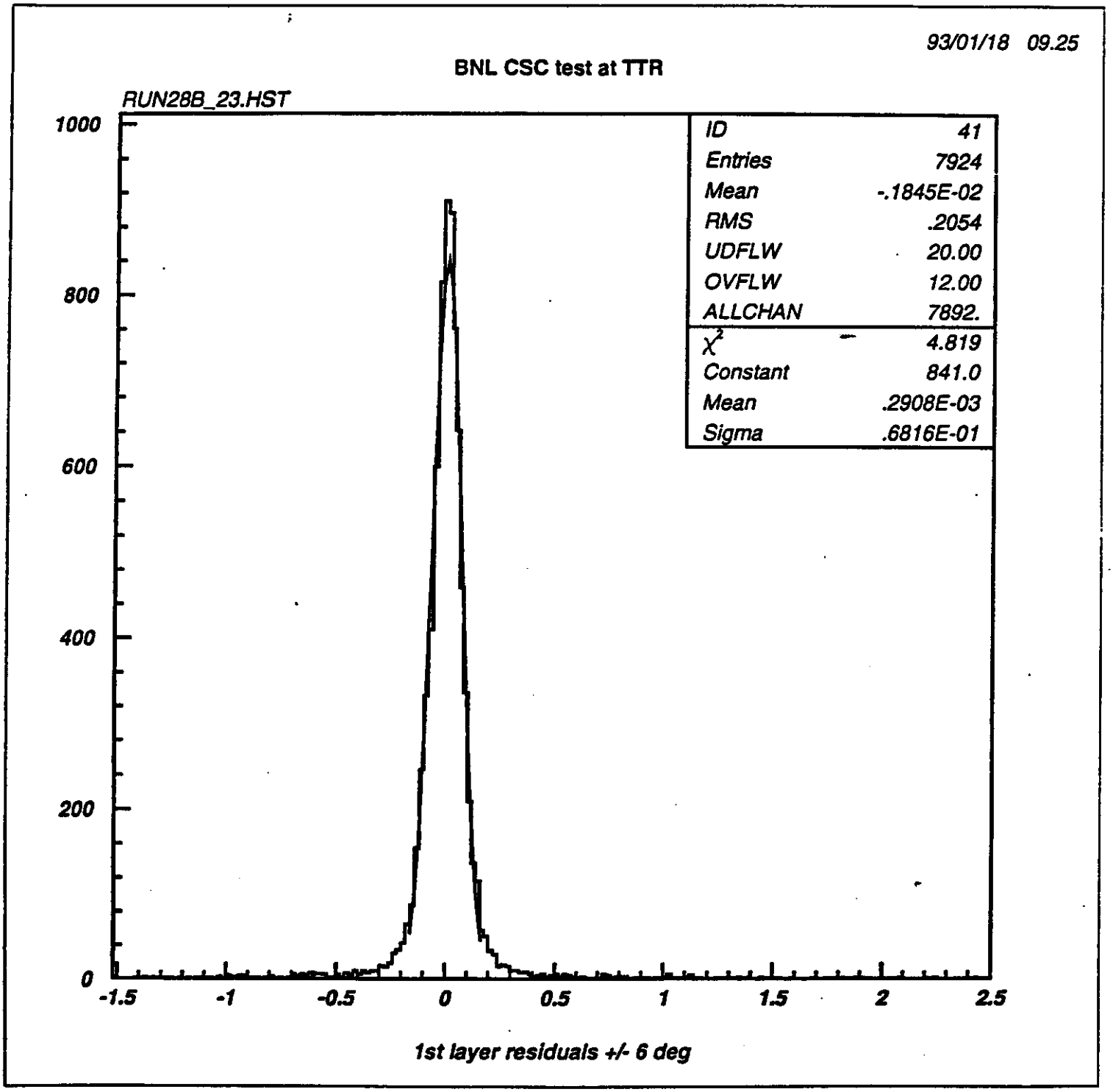
93/01/18 09.25
BNL CSC test at TTR
RUN28B_23.HST
ID 41
Entries 7924
Mean -.1845E-02
RMS .2054
UDFLW 20.00
OVFLW 12.00
ALLCHAN 7892.
χ² 4.819
Constant 841.0
Mean .2908E-03
Sigma .6816E-01
1000
800
600
400
200
0
-1.5
-1
-0.5
0
0.5
1
1.5
2
2.5
1st layer residuals +/- 6 deg

Fig 23

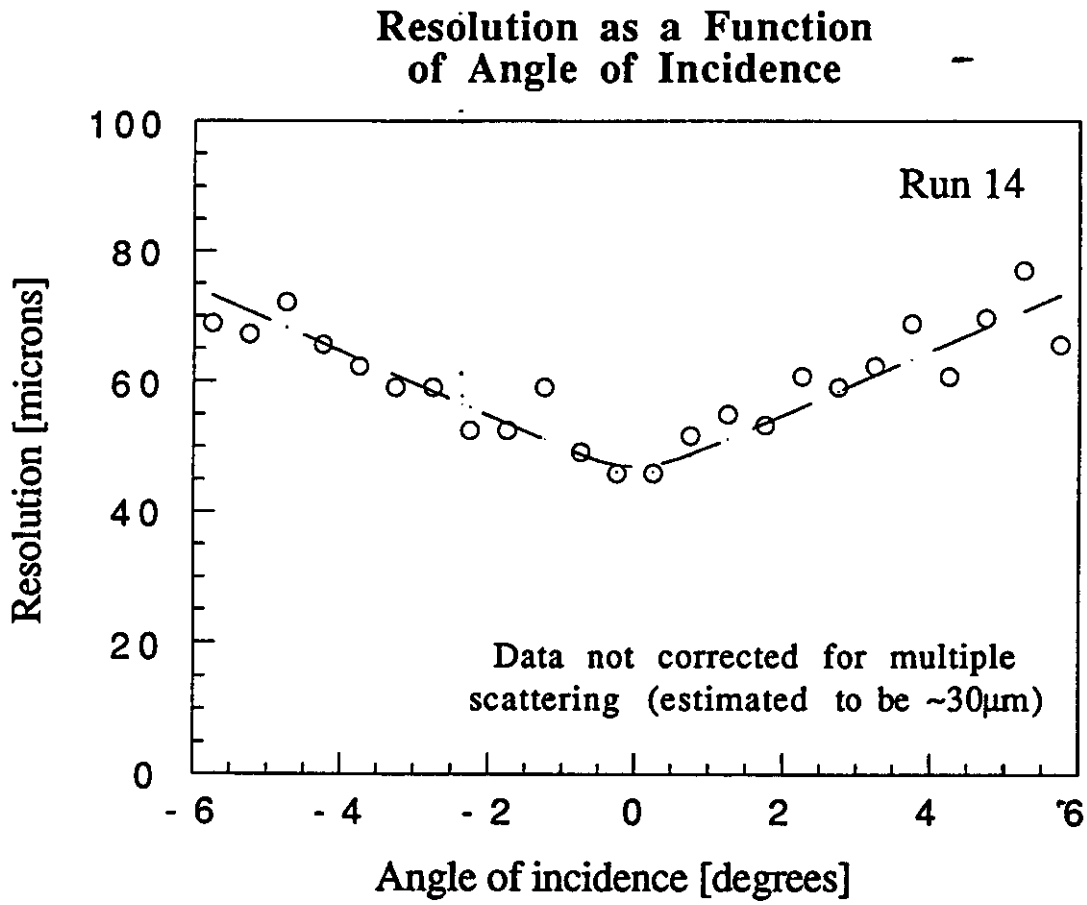
Resolution as a Function
of Angle of Incidence
Run 14
Data not corrected for multiple
scattering (estimated to be ~30μm)
Resolution [microns]
100
80
60
40
20
0
- 6
- 4
- 2
0
2
4
6
Angle of incidence [degrees]

Fig 24

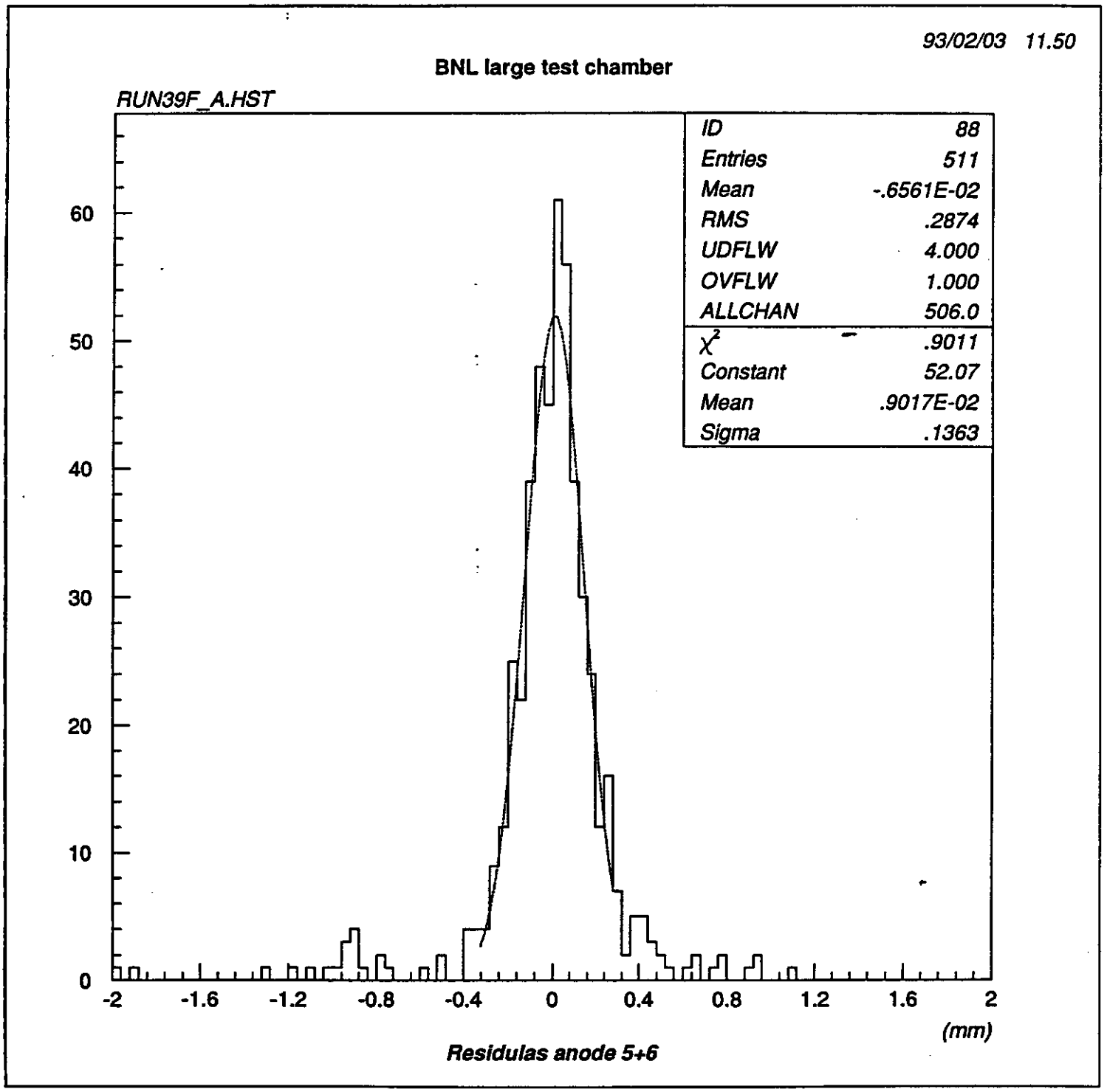
93/02/03 11.50
BNL large test chamber
RUN39F_A.HST
ID 88
Entries 511
Mean -.6561E-02
RMS .2874
UDFLW 4.000
OVFLW 1.000
ALLCHAN 506.0
χ² .9011
Constant 52.07
Mean .9017E-02
Sigma .1363
0
10
20
30
40
50
60
-2
-1.6
-1.2
-0.8
-0.4
0
0.4
0.8
1.2
1.6
2
(mm)
Residulas anode 5+6

Fig 27

Dubna CSC resolution

Resolution

93/01/16 15.24

run 1127

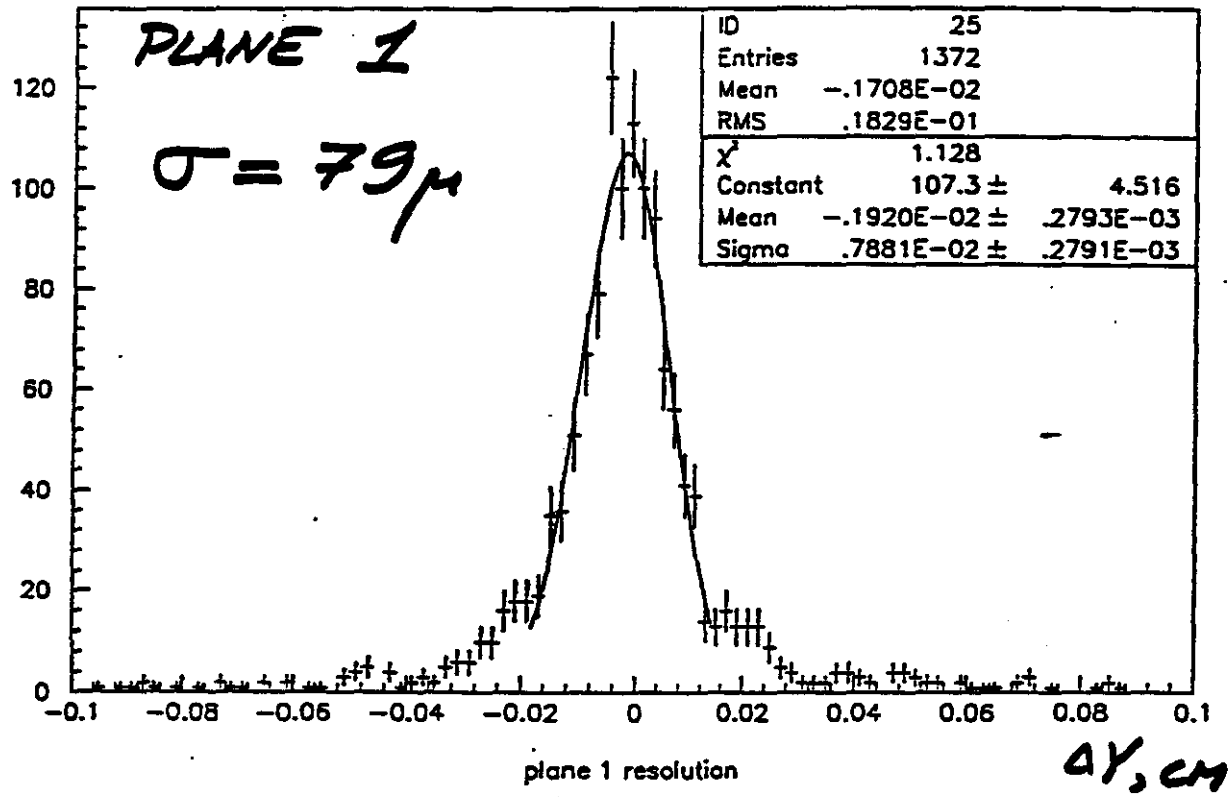

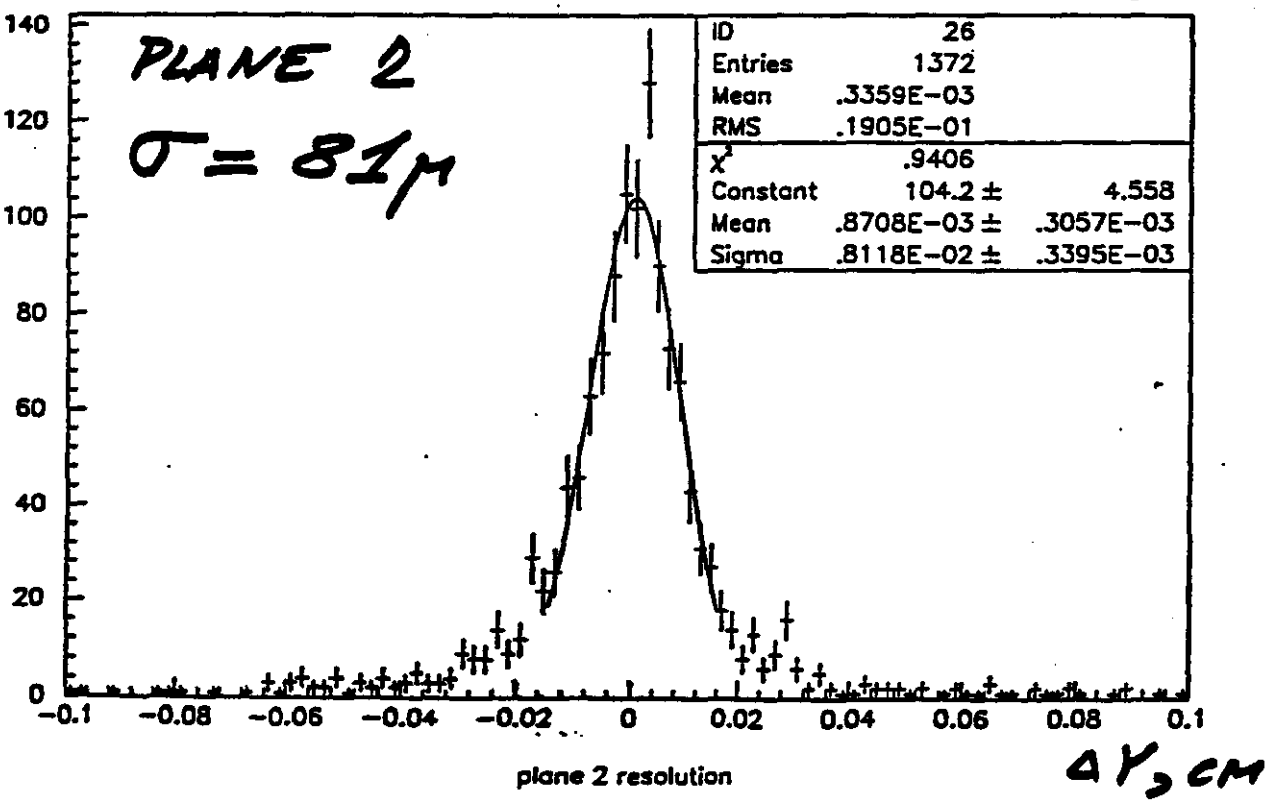

4 inner channels in the same preamp chip

Fig 25

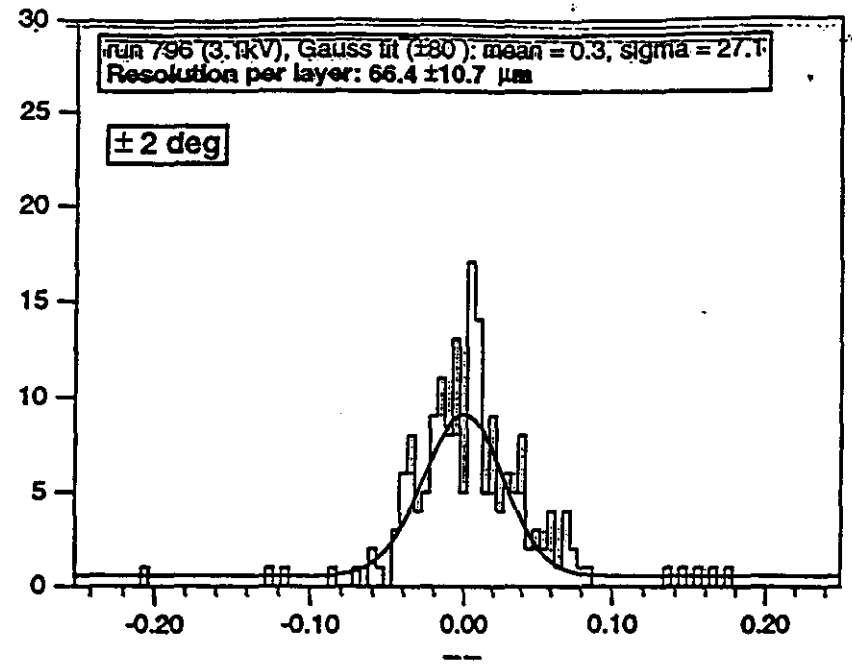
run 796 (3.1kV), Gauss fit (±80): mean = 0.3, sigma = 27.1
Resolution per layer: 66.4 ±10.7 µm
± 2 deg
30
25
20
15
10
5
0
-0.20
-0.10
0.00
0.10
0.20

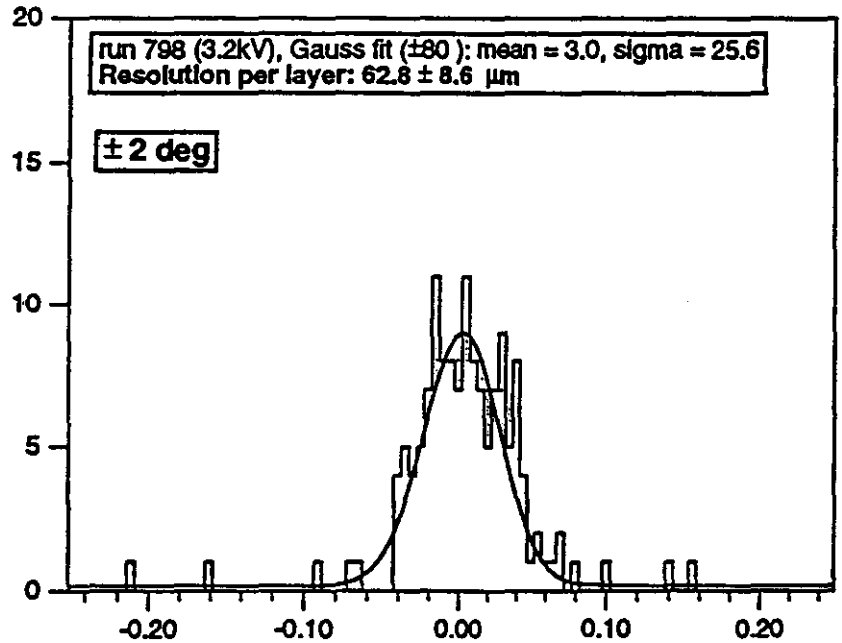
run 798 (3.2kV), Gauss fit (±80): mean = 3.0, sigma = 25.6
Resolution per layer: 62.8 ± 8.6 µm
± 2 deg
20
15
10
5
0
-0.20
-0.10
0.00
0.10
0.20

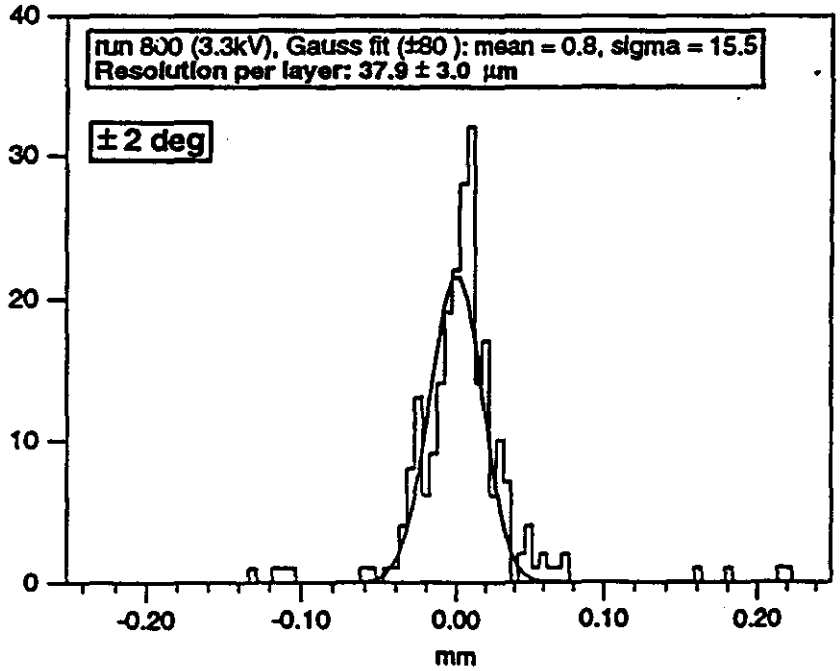
run 800 (3.3kV), Gauss fit (±80): mean = 0.8, sigma = 15.5
Resolution per layer: 37.9 ± 3.0 µm
± 2 deg
40
30
20
10
0
-0.20
-0.10
0.00
0.10
0.20
mm

Efficiency

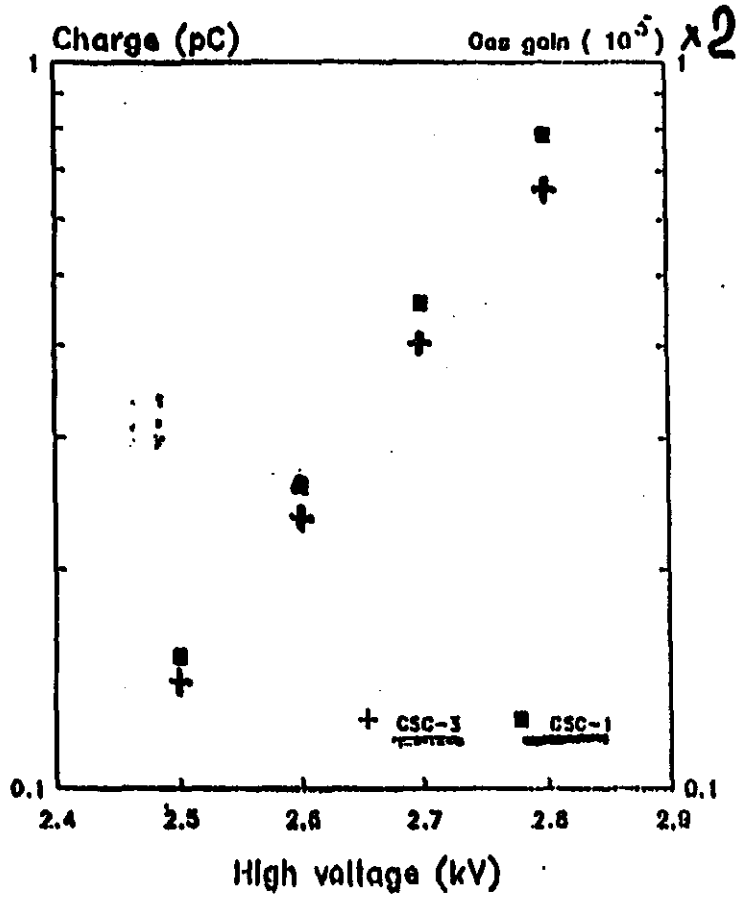

20% difference in gain

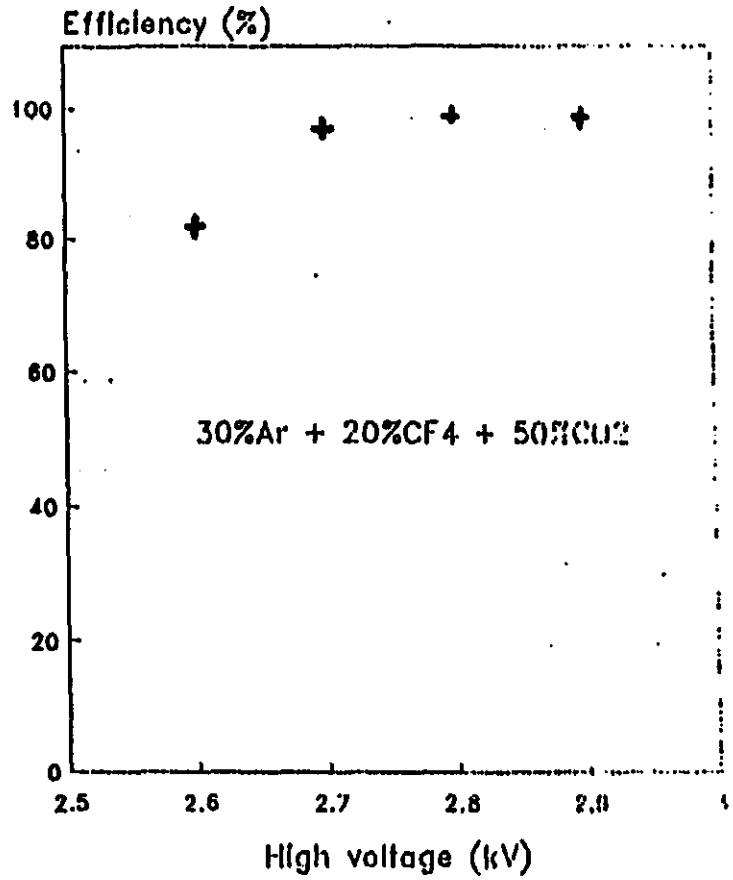

99.8% efficiency

Fig. 2X
45

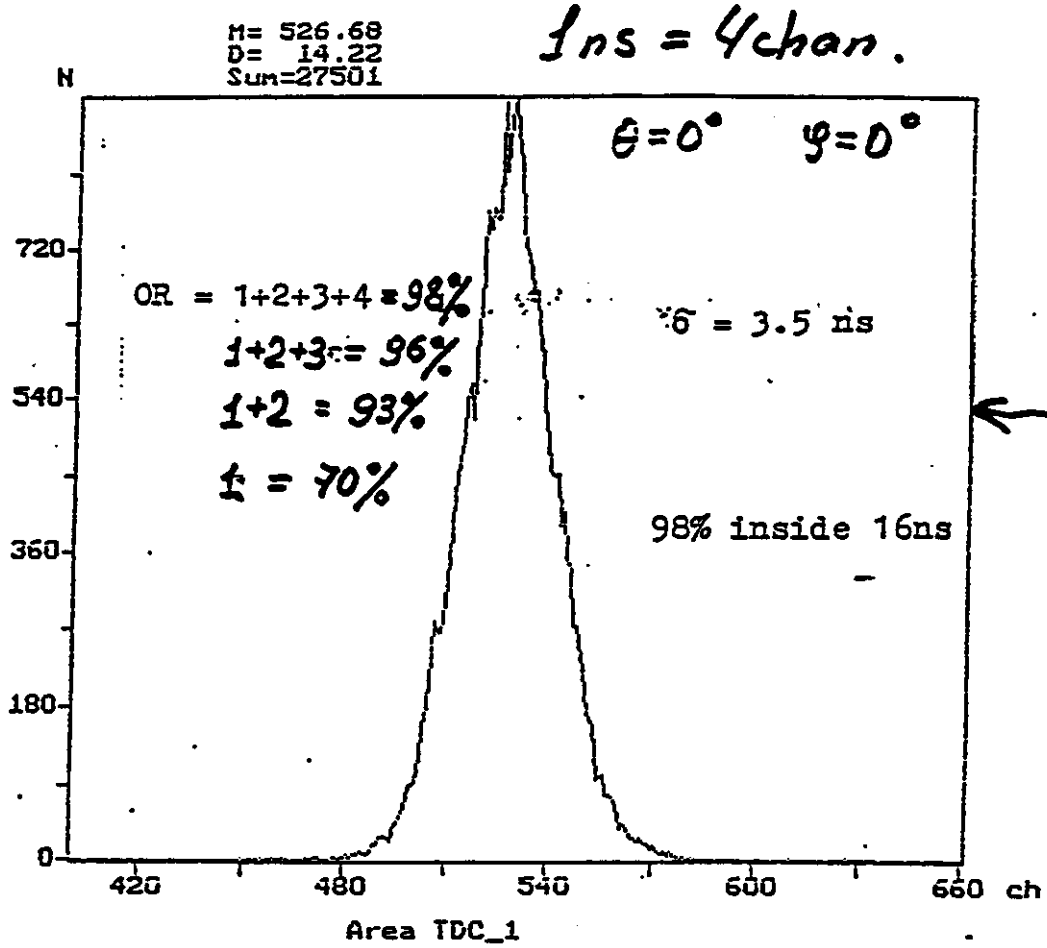

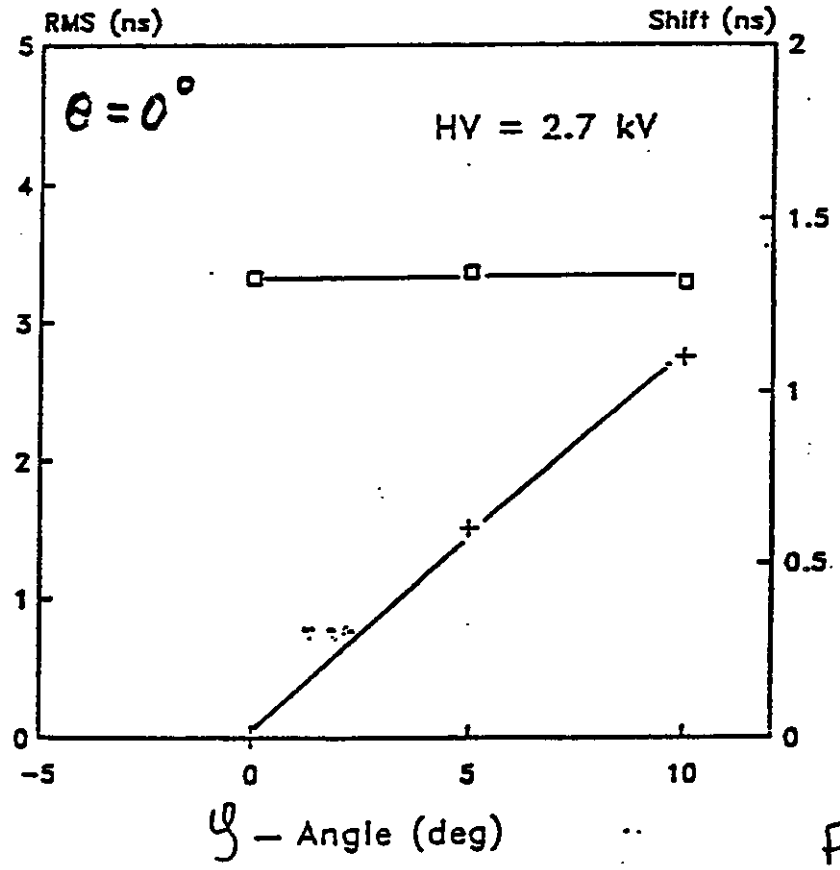

HV = 2.7 kV
σ = 3.5 ns

Fig 29

gem

γeμ

Presentation by:

Yu. Fisyak
A. Golutvin

Yu. Fisyak
A. Golutvin

PATTERN RECOGNITION IN MUON SYSTEM

2 MAJOR STEPS:

1. FIND MUON TRACK IN THE PRESENCE OF NEUTRONS

   (presence of associated background helps)

2. FIND "GOOD" HITS TO MEASURE MUON MOMENTUM

Muon associated background (δ, γ) represents the main difficulty!

$d_{1,2} = 8$ мм
$d_3 = 40$ мм

Muon efficiency (n only)
3 SL (8/3.0, 4/2.4, 4/3.4m)
neff=4.E-3, dtau=0.5E-6sec

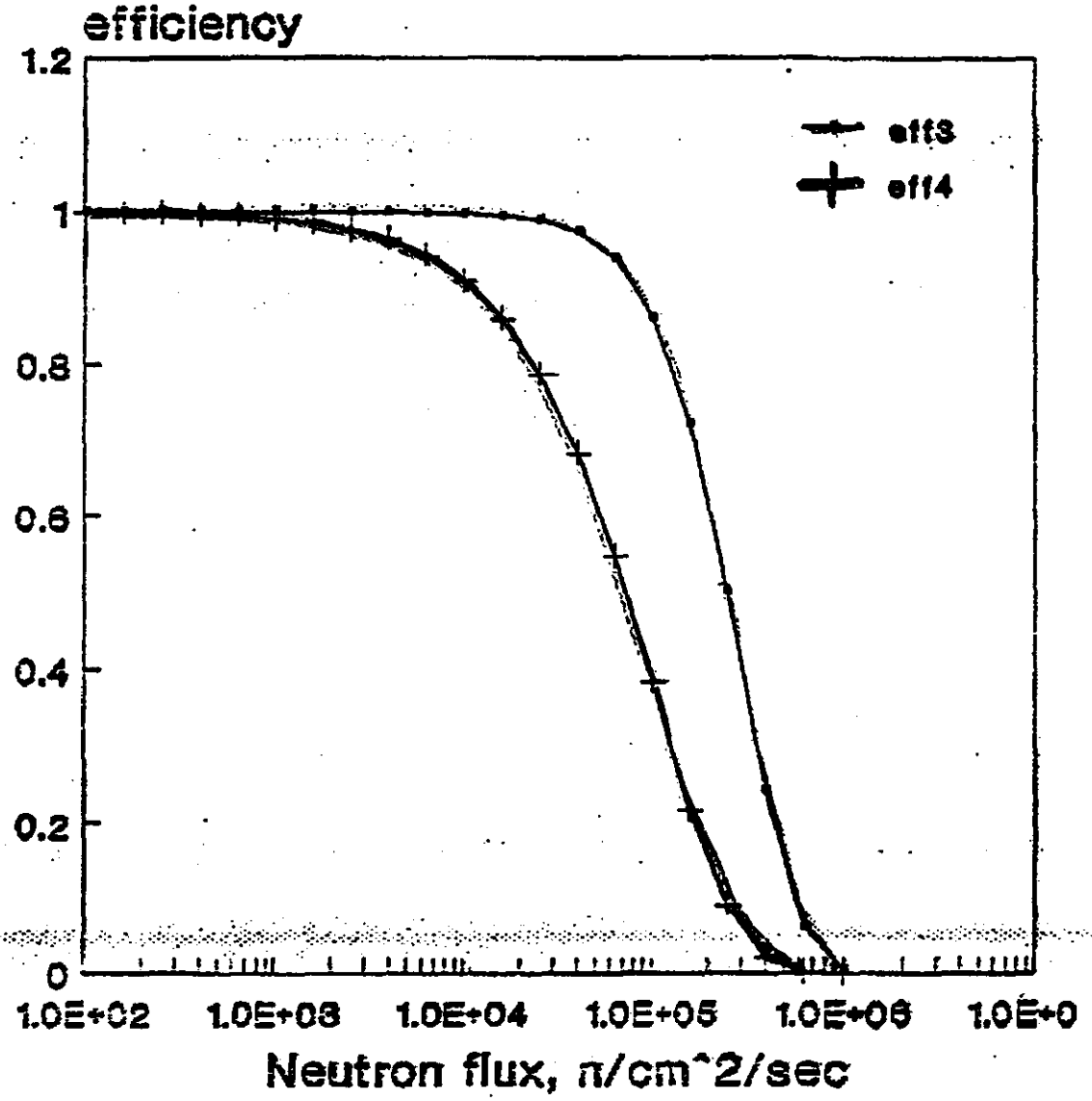

d1=d2=8mm, d3=12mm

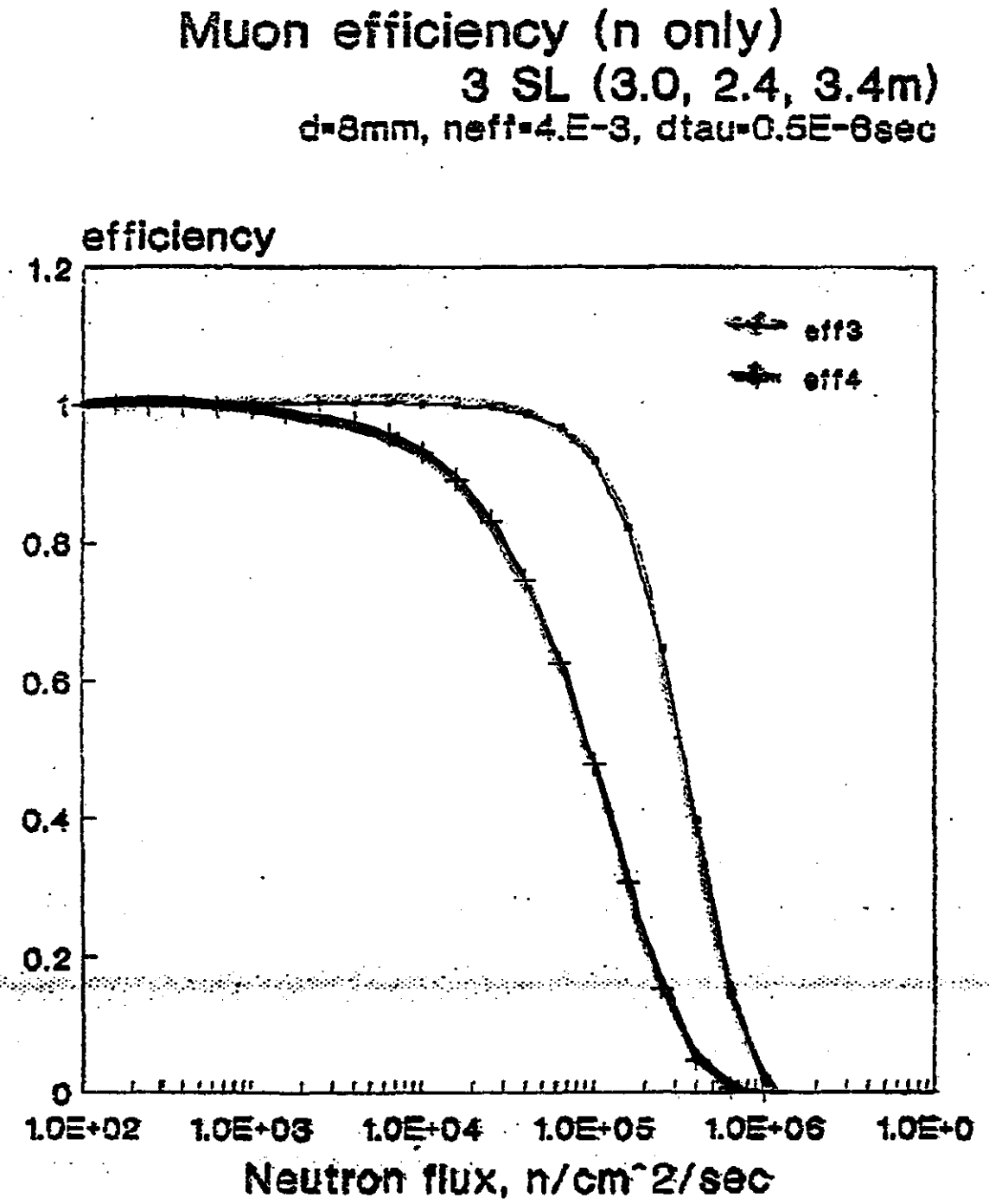
Muon efficiency (n only)
3 SL (3.0, 2.4, 3.4m)
d=8mm, neff=4.E-3, dtau=0.5E-6sec
efficiency
1.2
1
0.8
0.6
0.4
0.2
0
eff3
eff4
1.0E+02
1.0E+03
1.0E+04
1.0E+05
1.0E+06
1.0E+0
Neutron flux, n/cm^2/sec

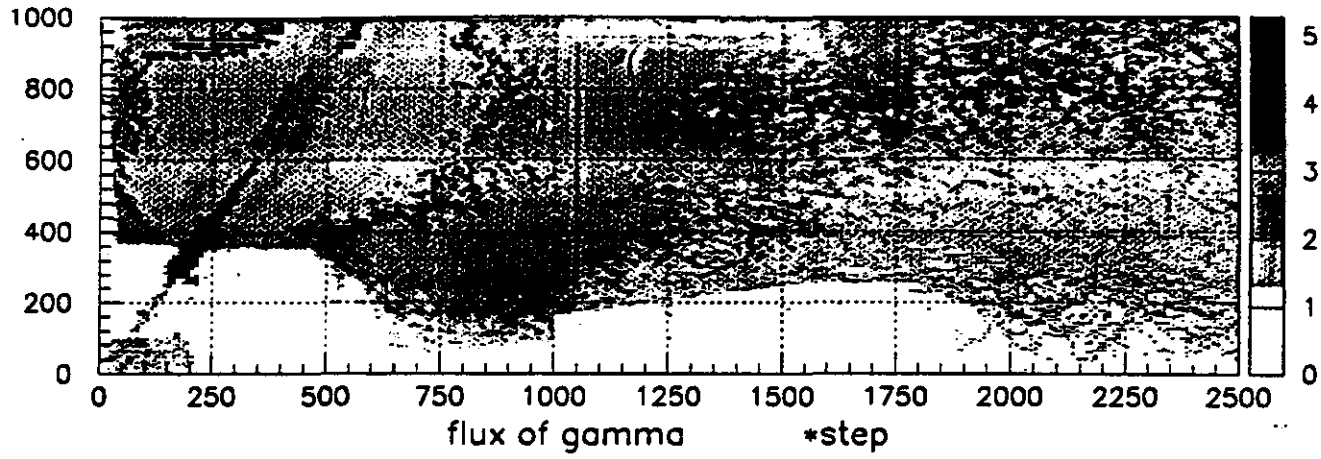
1000
800
600
400
200
0
0 250 500 750 1000 1250 1500 1750 2000 2250 2500
flux of gamma *step
5
4
3
2
1
0

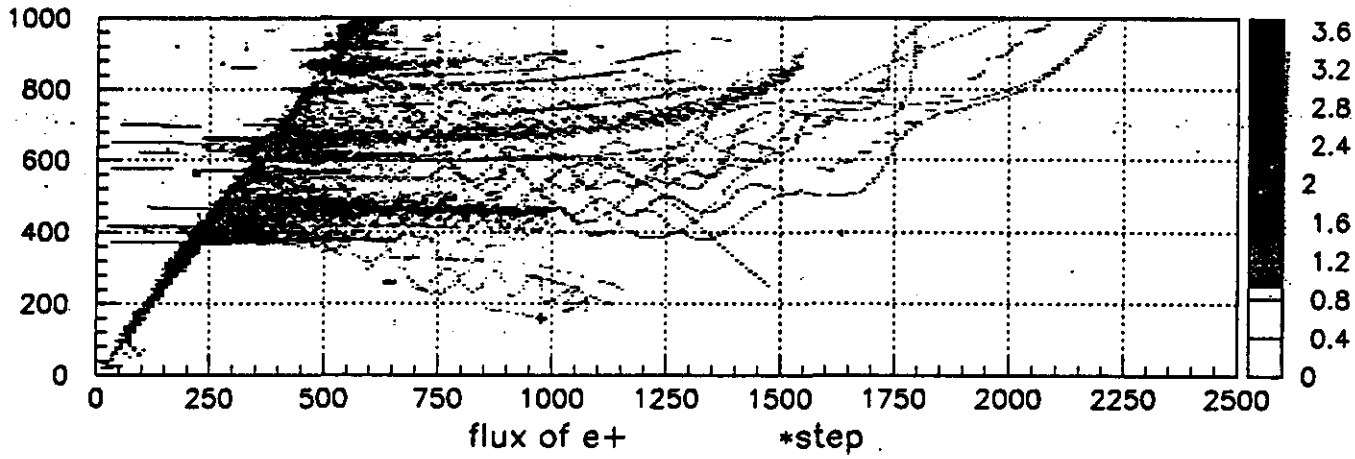
1000
800
600
400
200
0
0 250 500 750 1000 1250 1500 1750 2000 2250 2500
flux of e+ *step
3.6
3.2
2.8
2.4
2
1.6
1.2
0.8
0.4
0

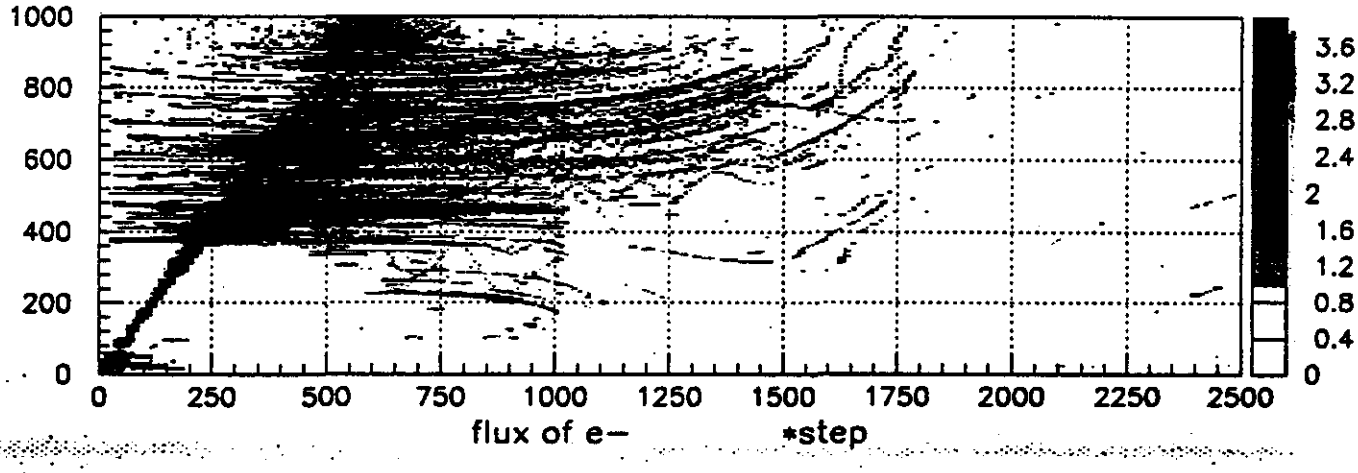
1000
800
600
400
200
0
0 250 500 750 1000 1250 1500 1750 2000 2250 2500
flux of e− *step
3.6
3.2
2.8
2.4
2
1.6
1.2
0.8
0.4
0

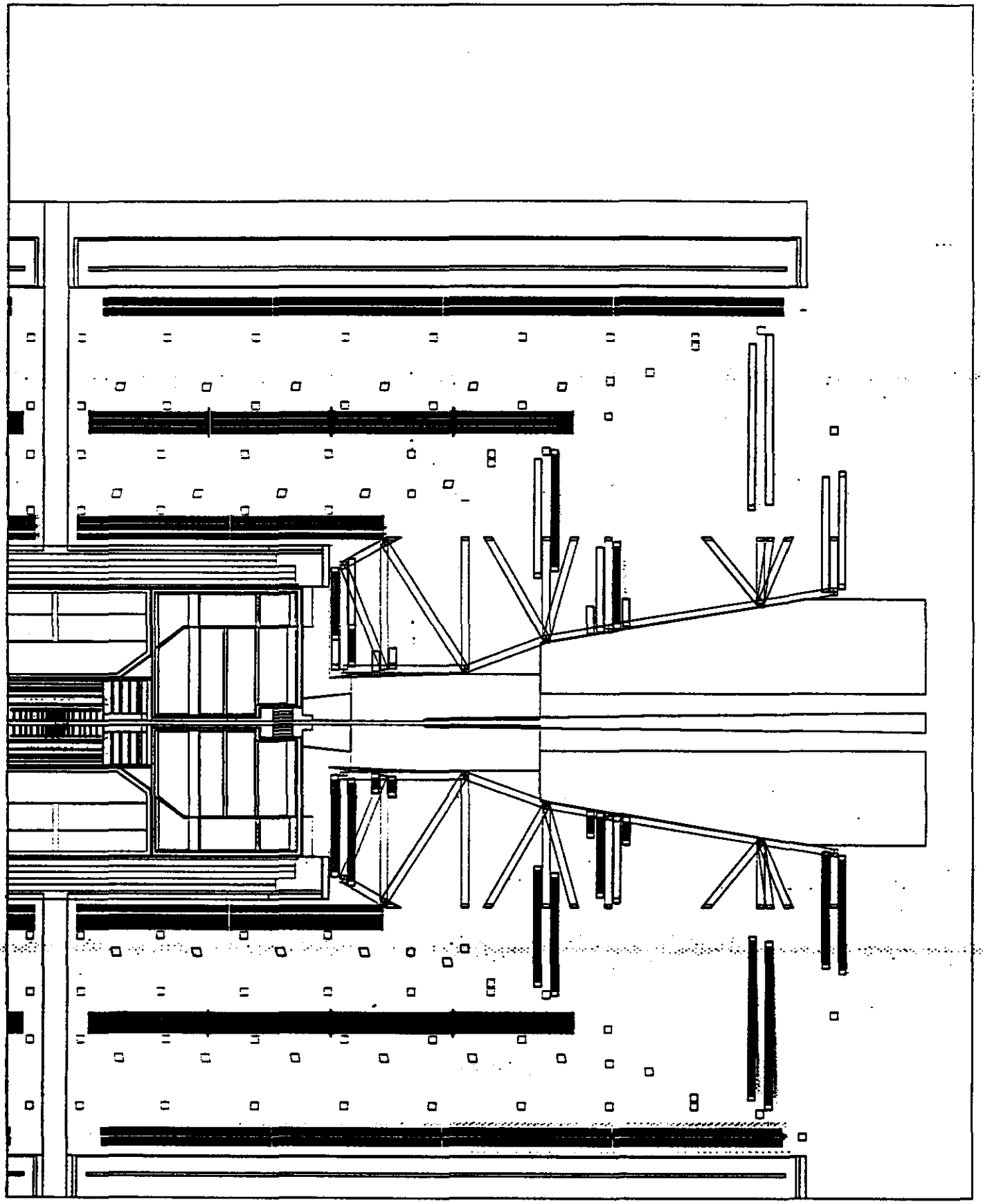

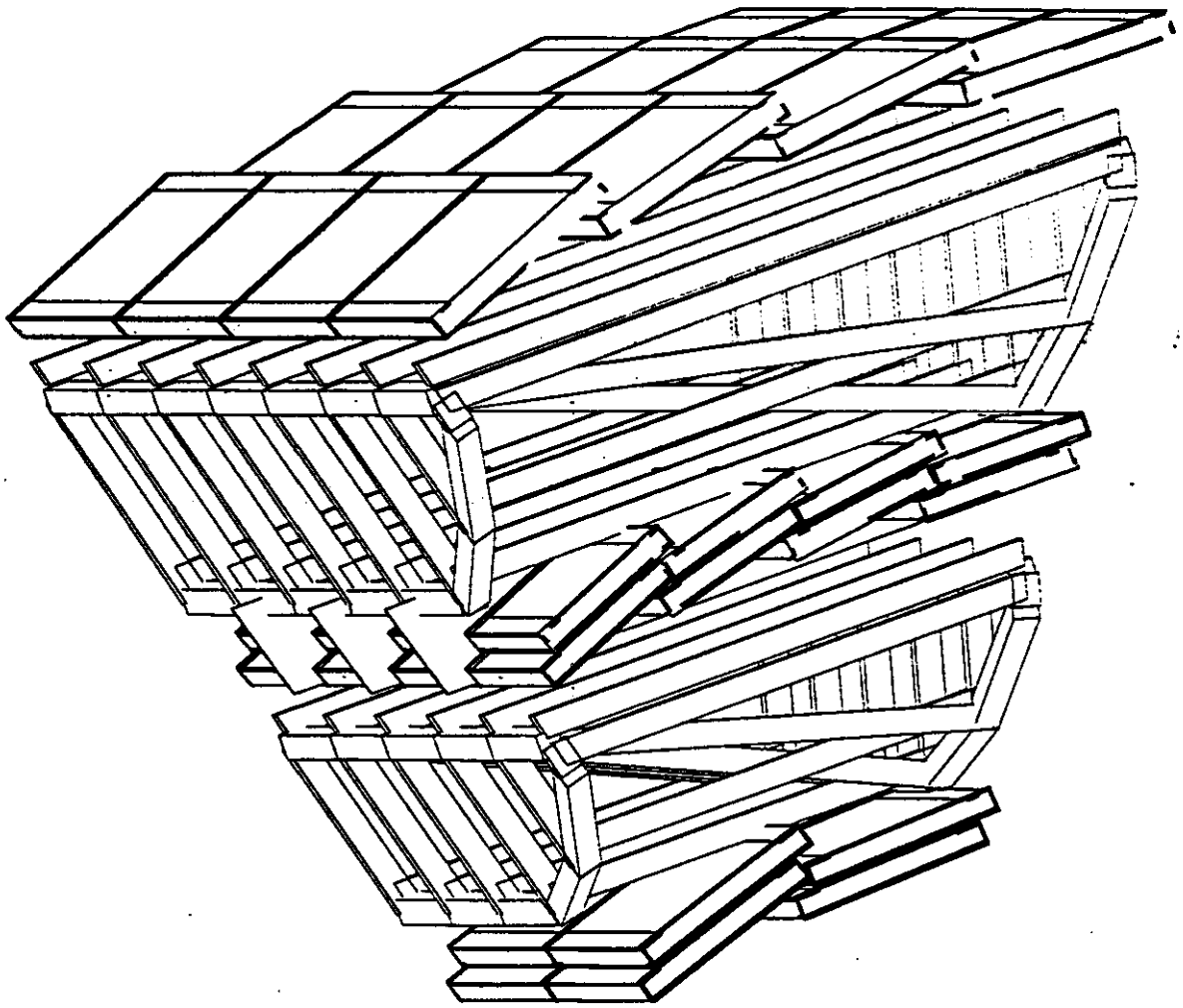

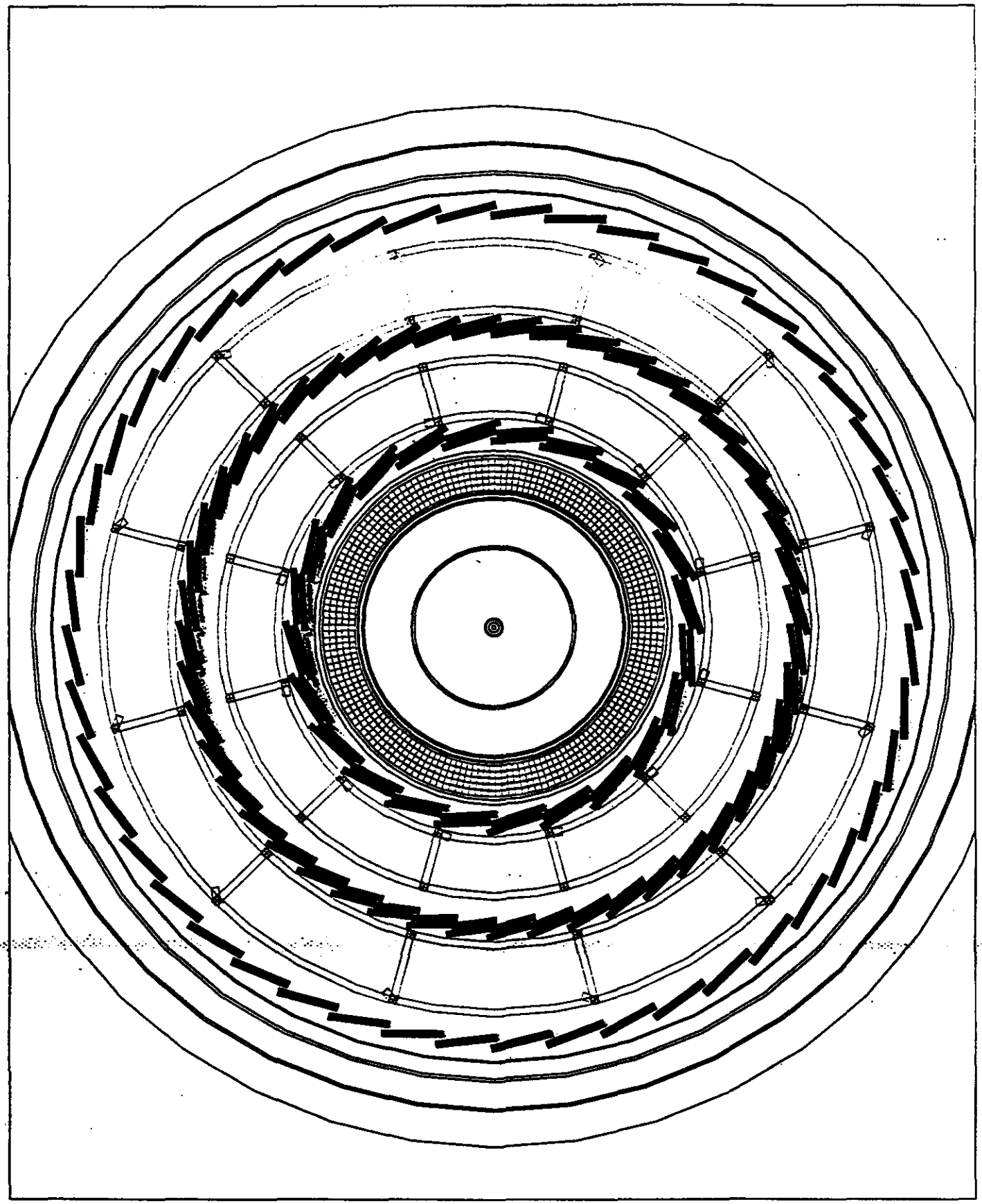

MUON ASSOCIATED BACKGROUND

(in the vicinity of muon)

Generate 1 TeV μ using SIGEM
(Baseline II – Yu. Fisyak)

$\theta_\mu = 60°$
$\varphi_\mu = 87°$ (track goes through the middle of μ-chambers)

Cut-off:

10 keV for: Scint. catcher (including iron support)
Muon system (everywhere!)

Statistics: 1500 μ

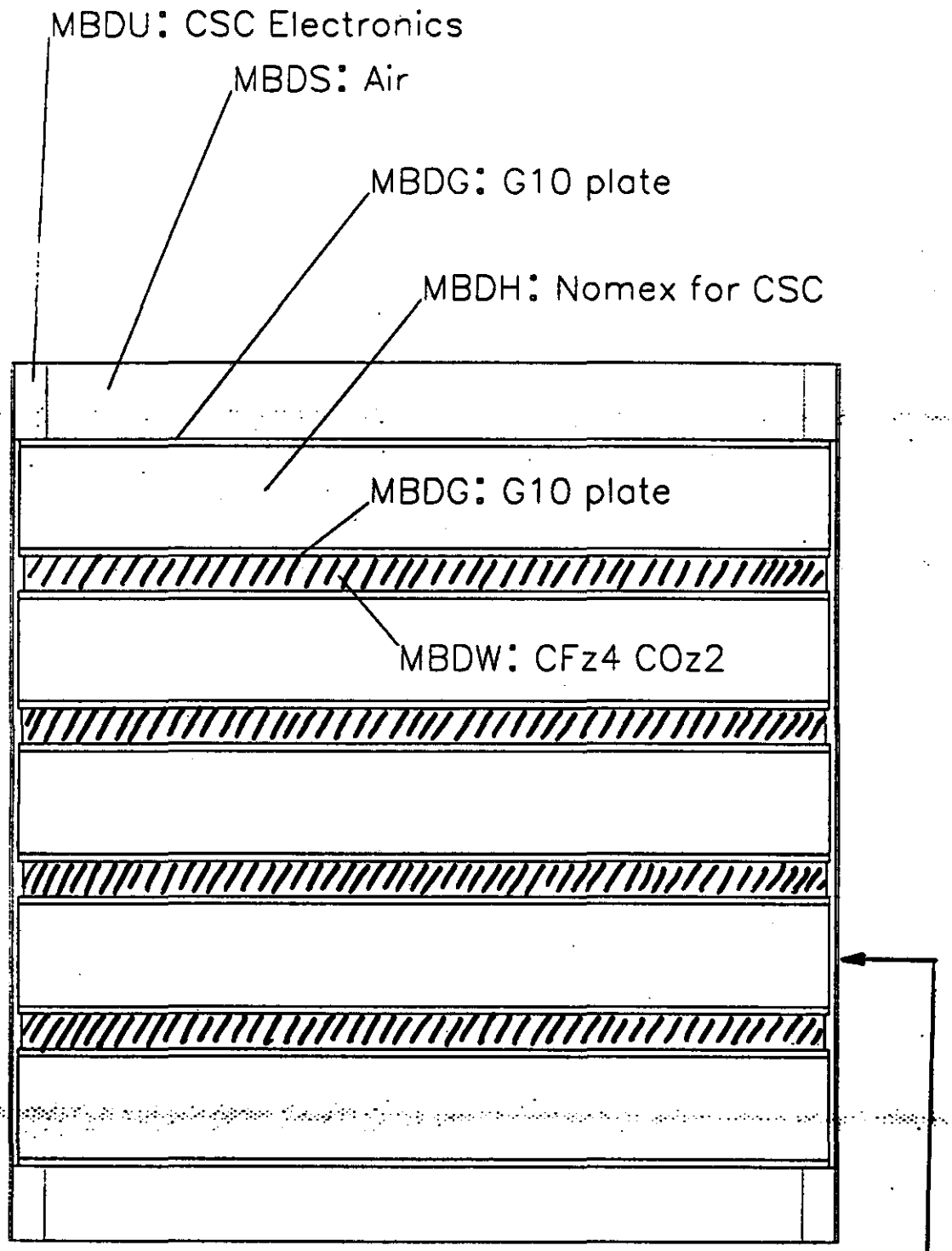

Cu = 17μ

Nomex = 2 cm

G10 = 1.29 mm

(conservative estimate of the amount of matherial)

Cu	—	0.12%
G10	—	0.66%
Nomex	—	0.14%
G10	—	0.66%
Cu	—	0.12%

≃ 1.7%

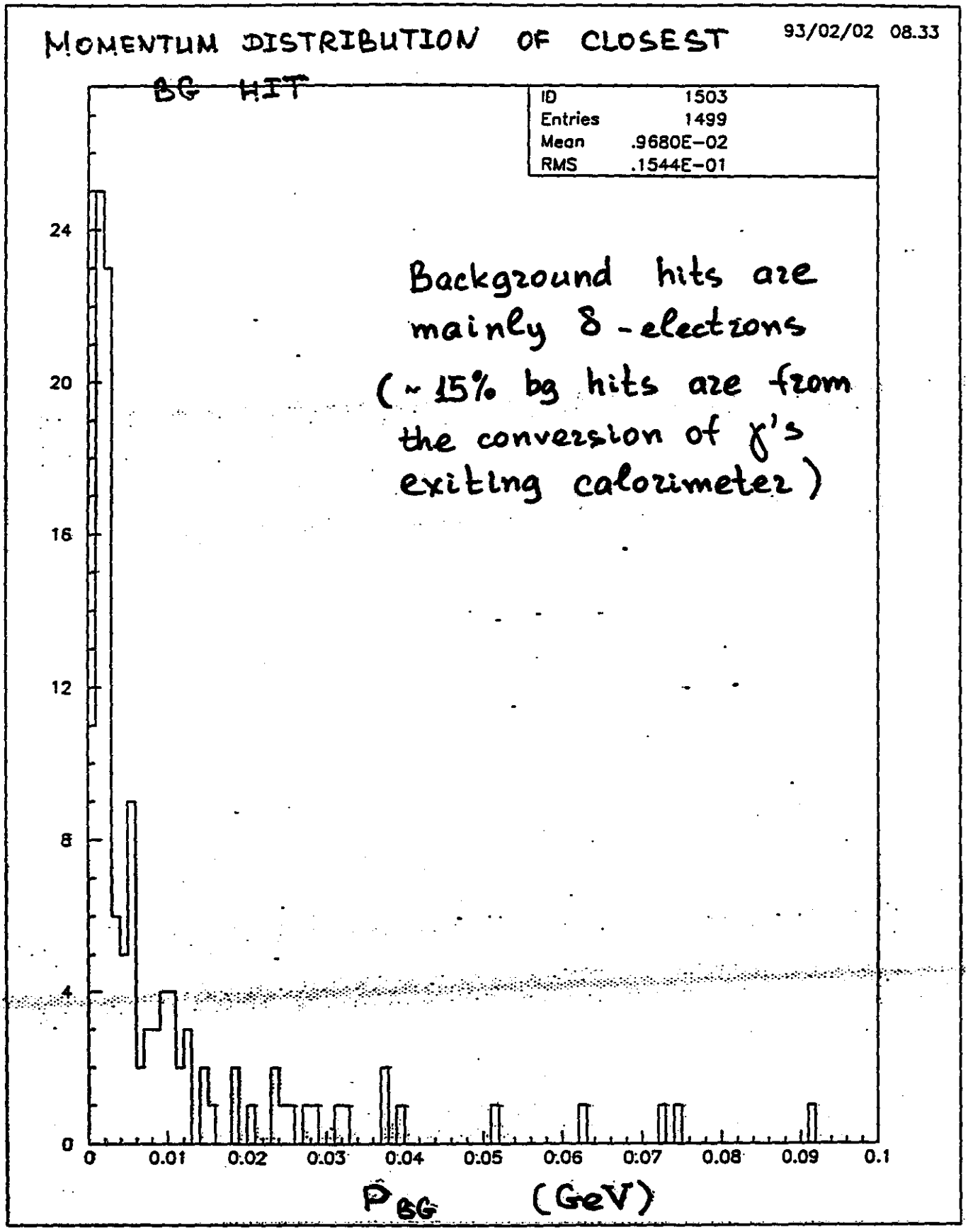
MOMENTUM DISTRIBUTION OF CLOSEST BG HIT
93/02/02 08.33
ID 1503
Entries 1499
Mean .9680E-02
RMS .1544E-01
Background hits are mainly δ-electrons
(~15% bg hits are from the conversion of γ's exiting calorimeter)
24
20
16
12
8
4
0
0
0.01
0.02
0.03
0.04
0.05
0.06
0.07
0.08
0.09
0.1
P_BG (GeV)

SL3

ORIGIN OF THE CLOSEST BG HIT

93/02/02 08.33

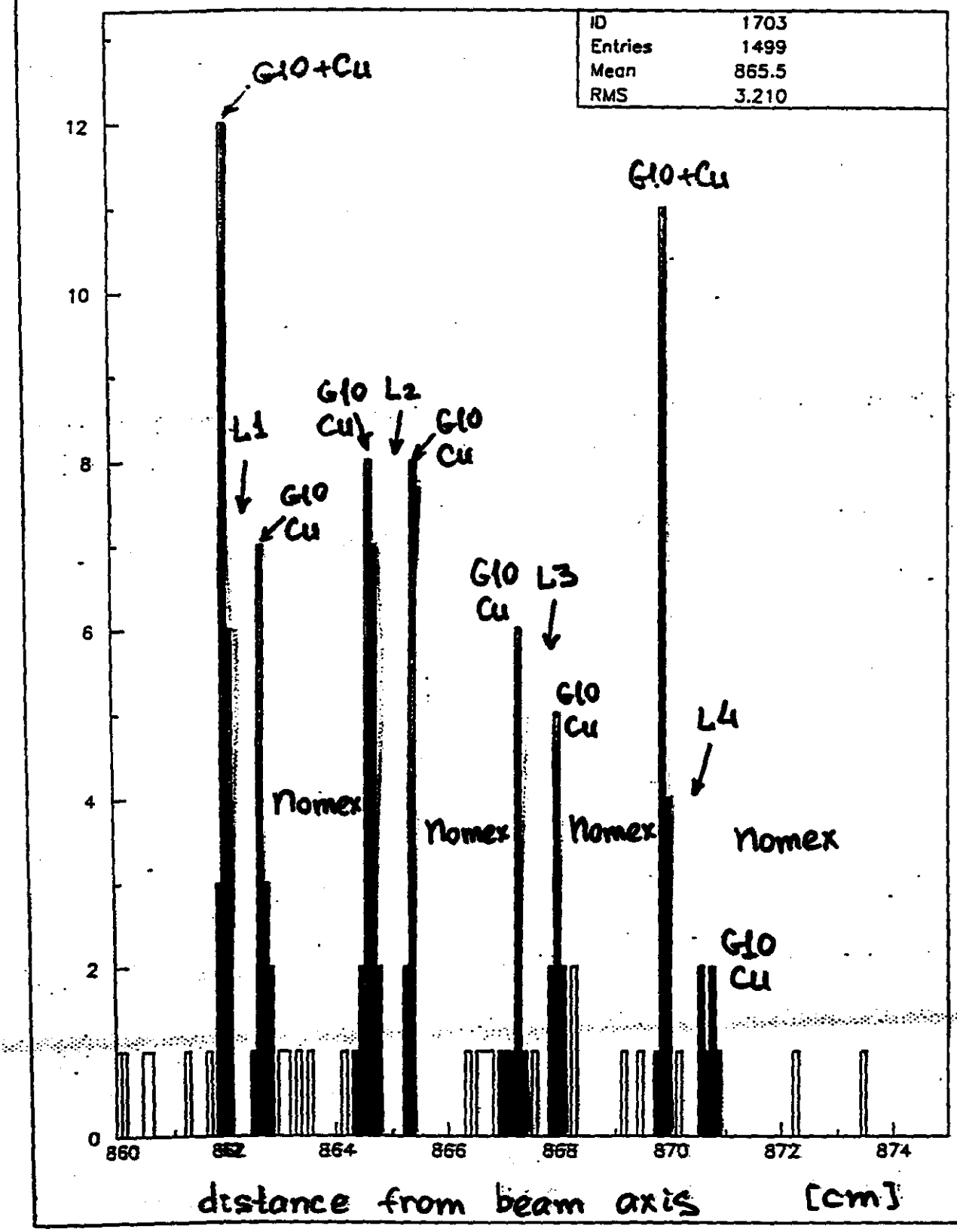

SL 3 -

DISTANCE BETWEEN MUON AND CLOSEST BACKGROUND HIT

93/02/02 08.32

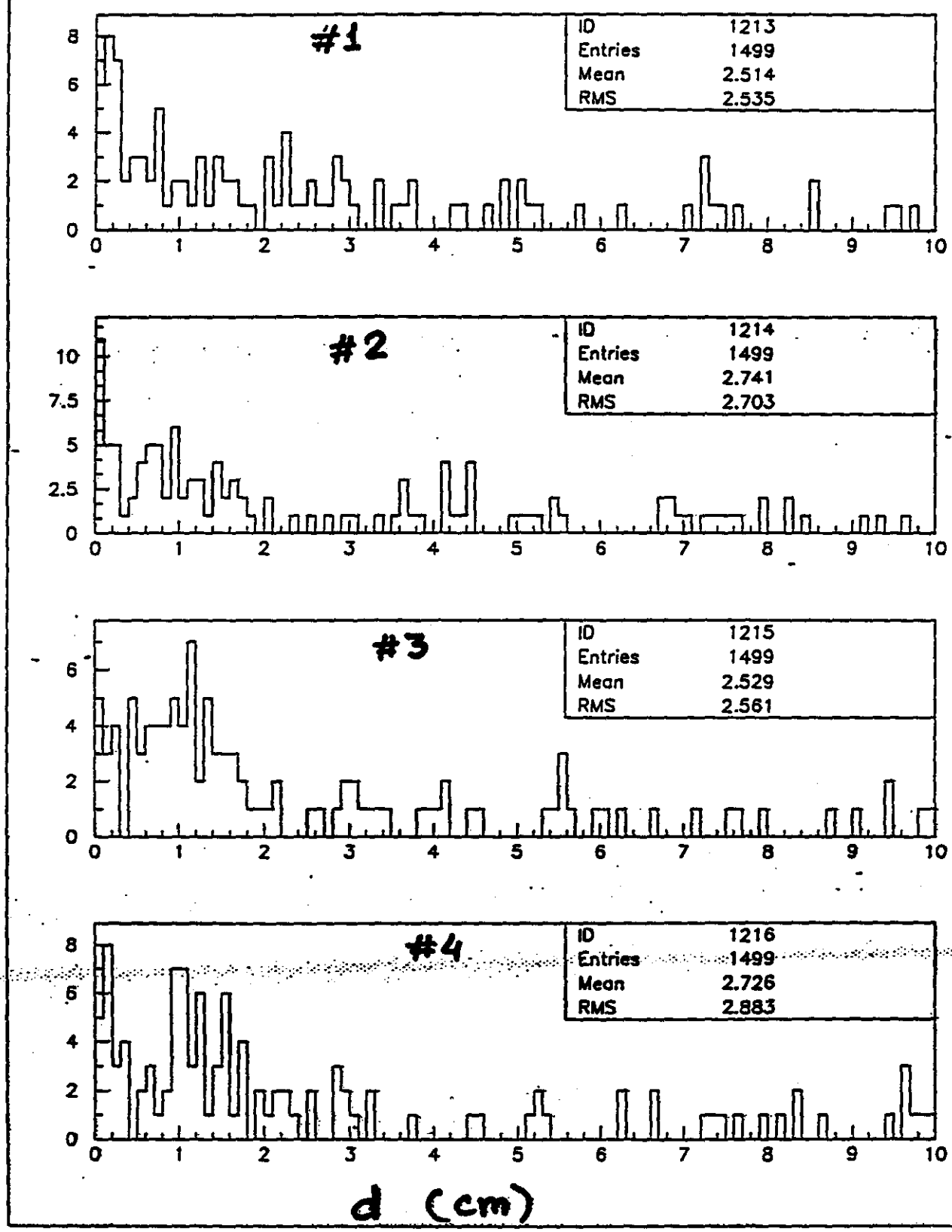

SL3

THE PROBABILITY TO HAVE n "GOOD" HITS OUT OF 4

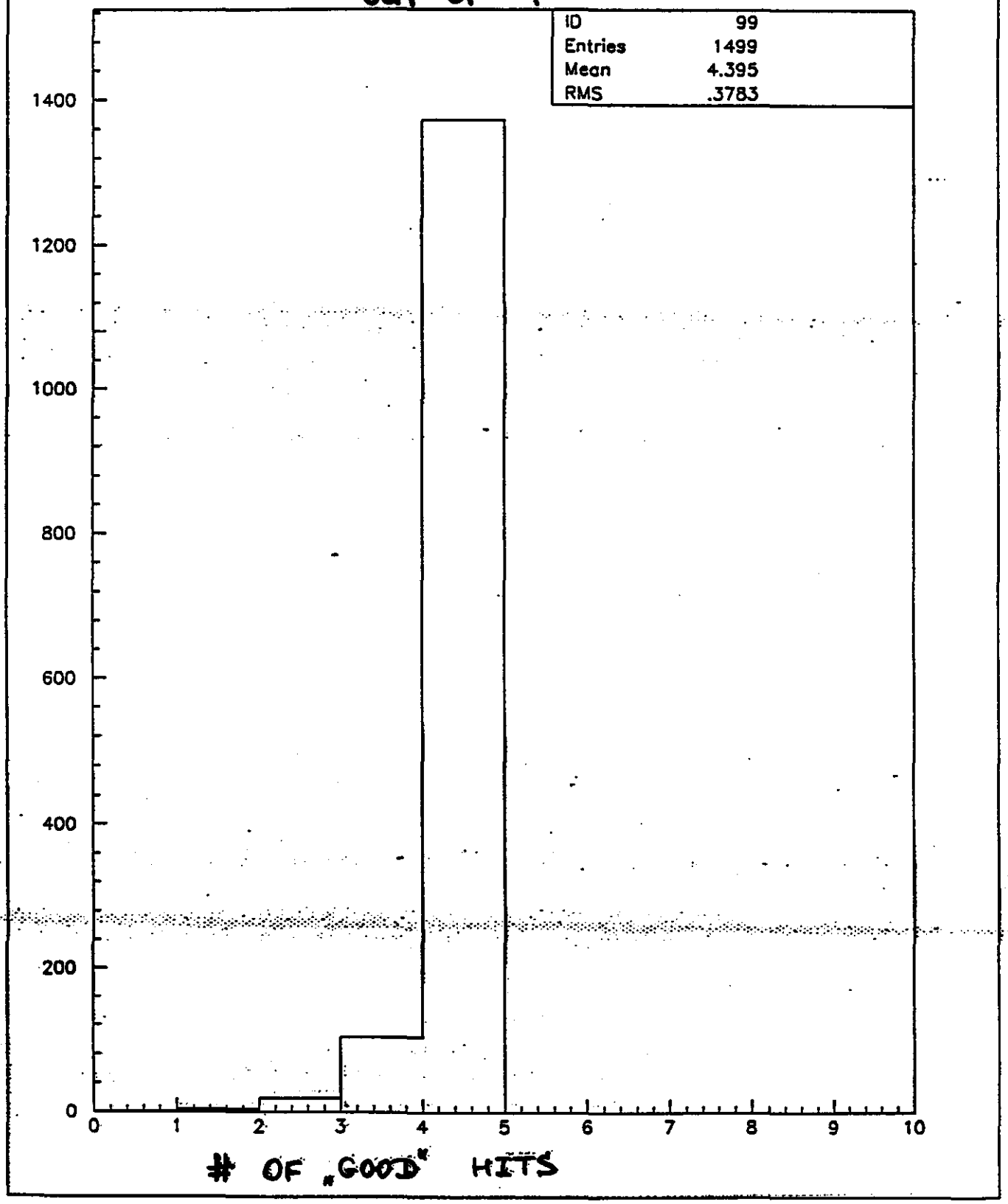

FRACTION OF "BAD" HITS PER PLANE OF 3 SUPERLAYER

d – distance between muon and closest background hit

# of plane	d < 1cm	d < 2cm
1	2.6%	3.7%
2	3.1%	4.5%
3	2.5%	4.5%
4	2.5%	4.5%

↓

THE PROBABILITY TO HAVE 3 OUT OF 4 "GOOD" HITS IS 98.7% (for d<1cm)

96.5% (for d<2cm)

gem γeμ

Presentation by:

I. Golutvin

THE BARREL CSC's LAYOUT CONCEPT

I. GOLUTVIN

2/3/1993

★ 6/6/6

$$\Downarrow$$

6/6/4

(B)

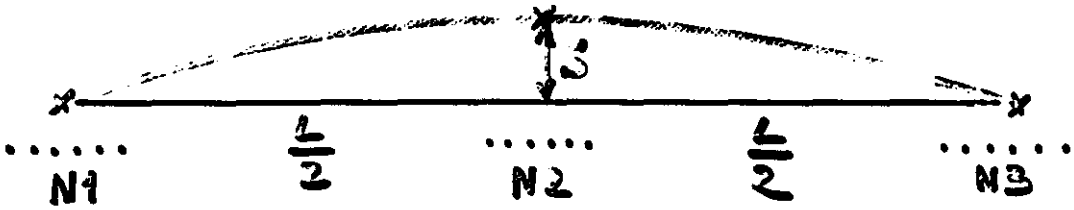

$$\frac{\Delta p}{p} = \frac{\Delta S}{S} = \frac{27\, p\left[\frac{TeV}{c}\right]}{BL^2\,(Tm)} \sqrt{\frac{\sigma_{s1}^2}{2} + \sigma_{s2}^2 + \frac{\sigma_{s3}^2}{2}} + \frac{0.1}{BL\,(Tm)} \sqrt{X_2/X_0}$$

$\sigma_{s1}, \sigma_{s2}, \sigma_{s3}$ — RESOLUTION OF SUPERLAYERS 1, 2, 3

$$\sigma_{si}^2 = \frac{\sigma_i^2}{N_i\, \epsilon_i}$$

σ_i - SINGLE LAYER RESOLUTION IN SUPERLAYER i

N_i - NUMBER OF LAYERS IN SUPERLAYER i

X_2/X_0 - RAD. LENGTH OF SUPERLAYER 2

ϵ_i - SINGLE LAYER EFFICIENCY

(1) RESOLUTION OF SUPERLAYER 2 SHOULD BE OPTIMIZED

$$\rightarrow \text{MIN}\left\{\frac{\sigma_2^2}{N_2\, \epsilon_2}\right\}$$

(2) MULTIPLE SCATTERING IN SUPERLAYER 2 SHOULD BE MINIMIZED

$$\text{MIN}\left\{X_2/X_0\right\}$$

NUMBER OF SECTORS ?

DOMINATING CONSTRAINS:

→ MINIMUM NUMBER OF CHAMBERS IN THE MIDDLE PLANE

↓

MINIMUM NUMBER OF FRAMES

↓

MINIMIZE MULTIPLE SCATTERING

→ MAXIMUM POSSIBLE LENGTH OF ANODE WIRES

→ ANGLE RANGE IN THE MIDDLE CHAMBER

MAX ANODE WIRE LENGTH

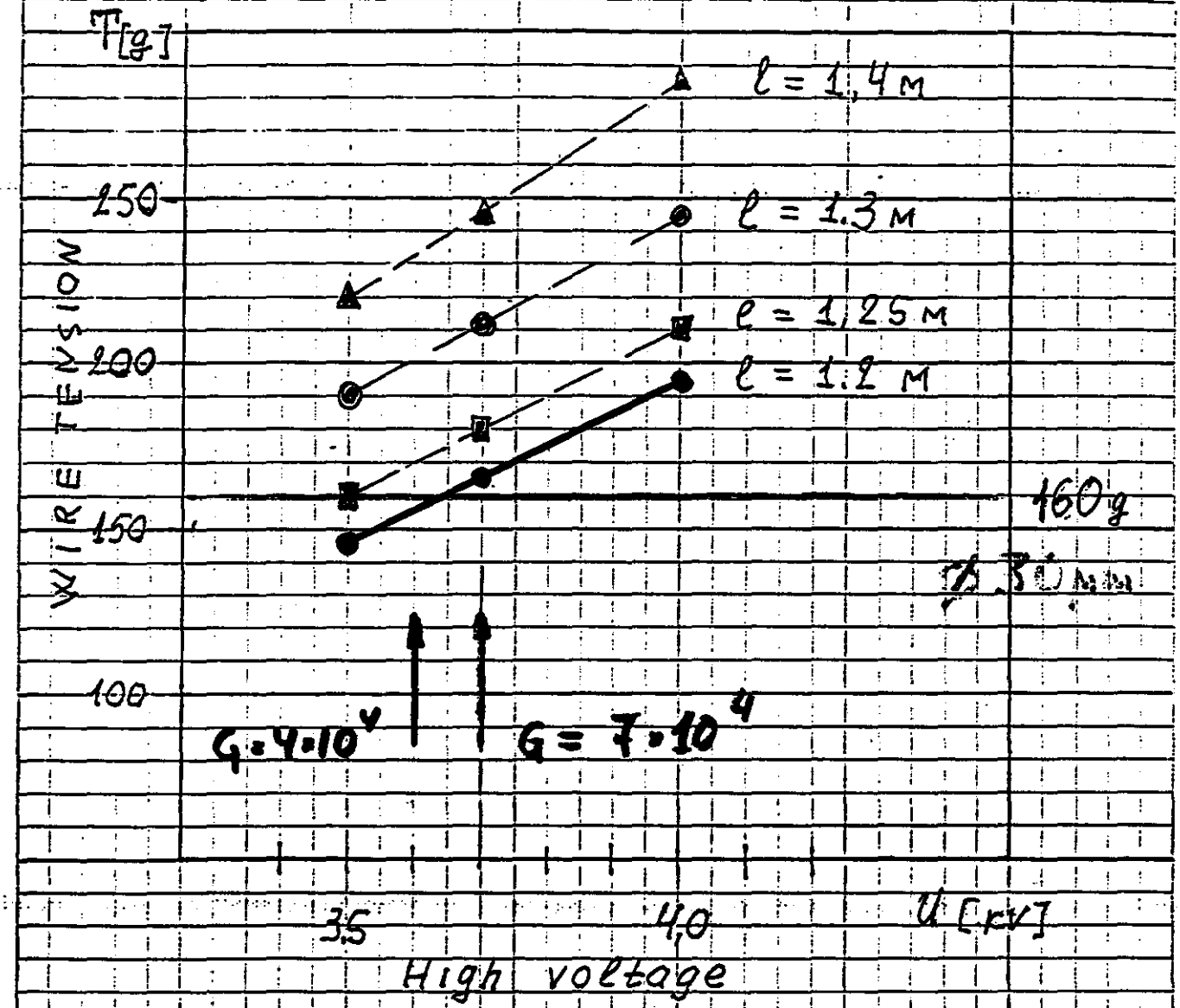

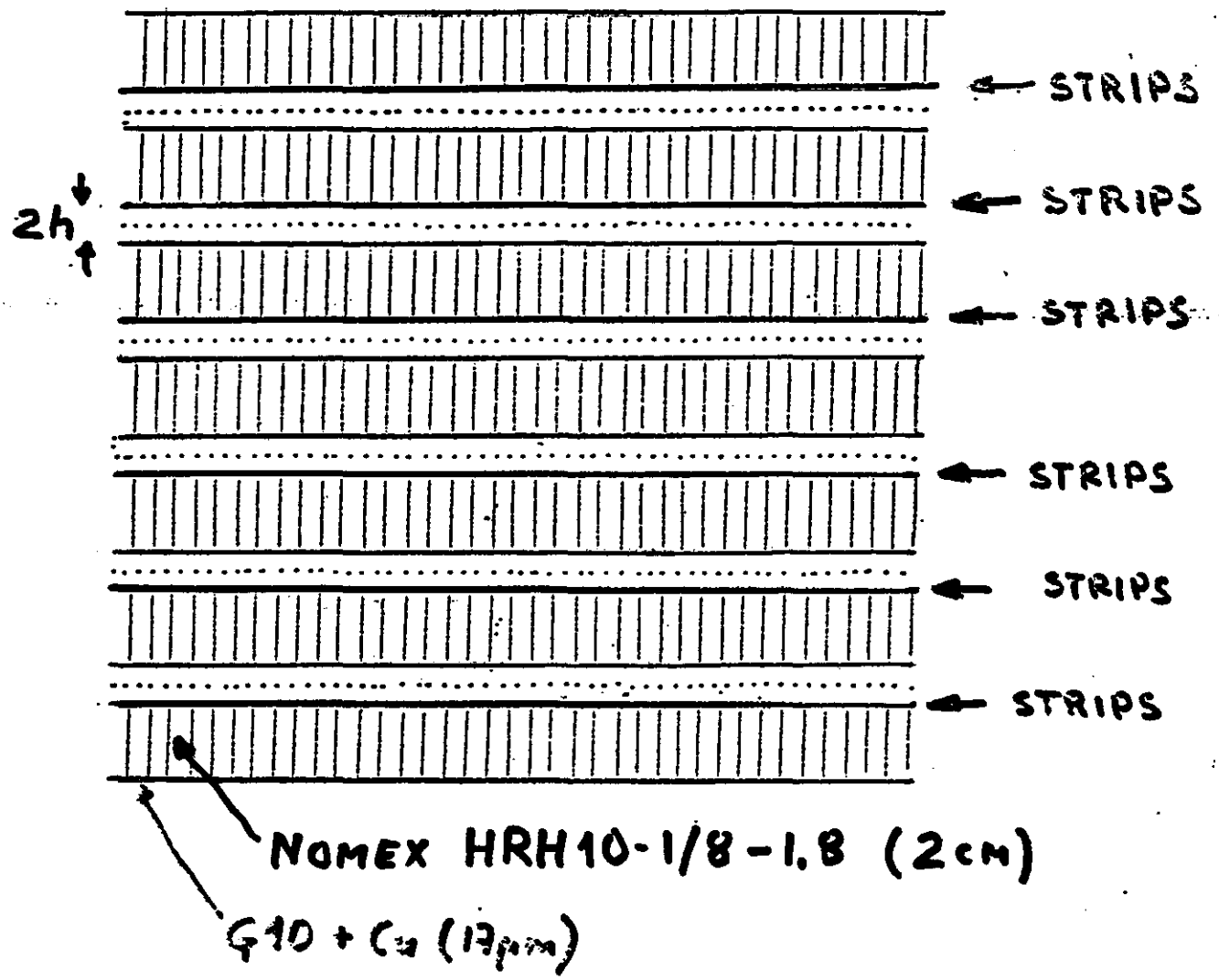
STRIPS
STRIPS
STRIPS
STRIPS
STRIPS
STRIPS
2h
NOMEX HRH10-1/8-1.8 (2cm)
G10 + Cu (17μm)

THE MIDDLE SUPERLAYER

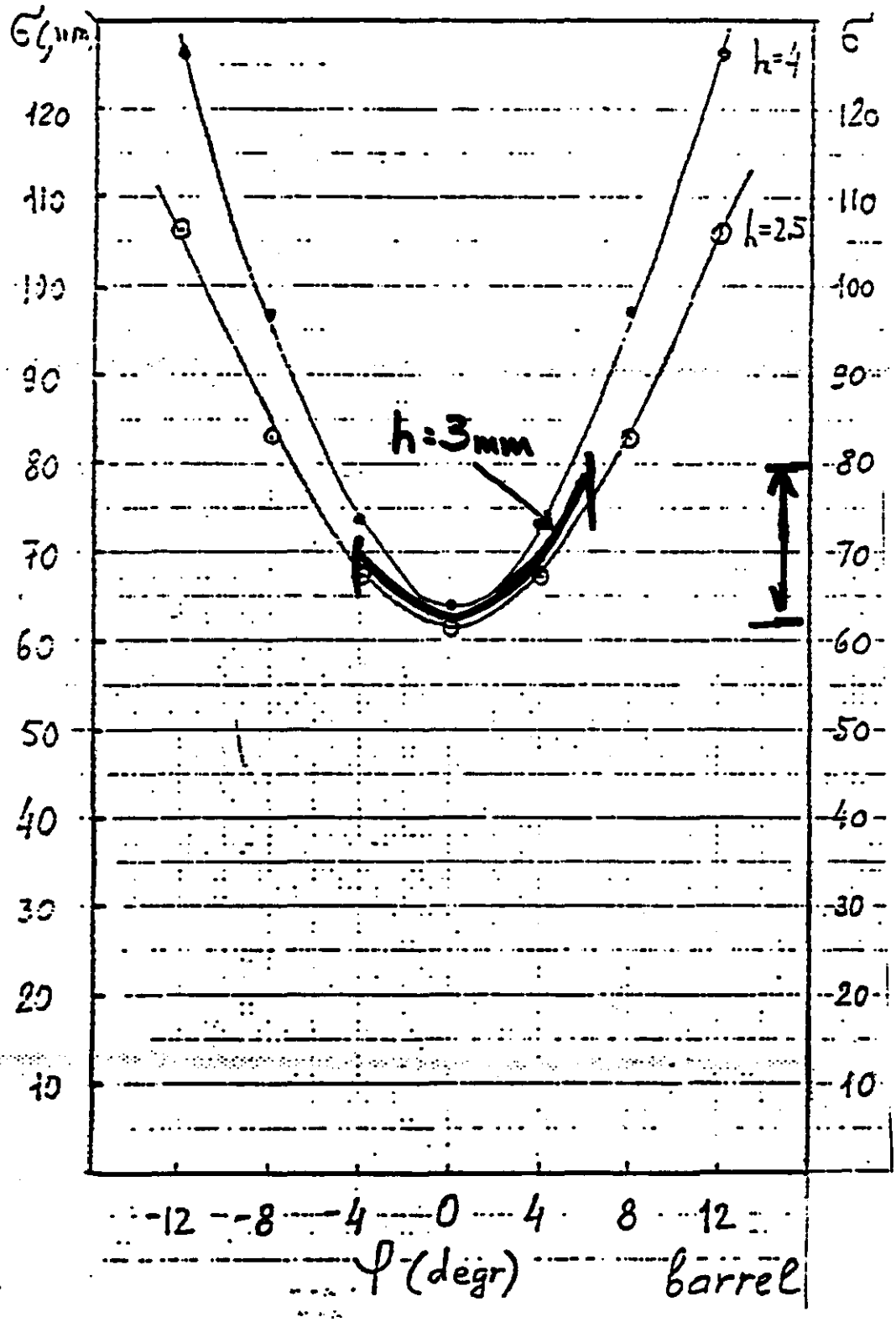

< TCHERNIATIN >

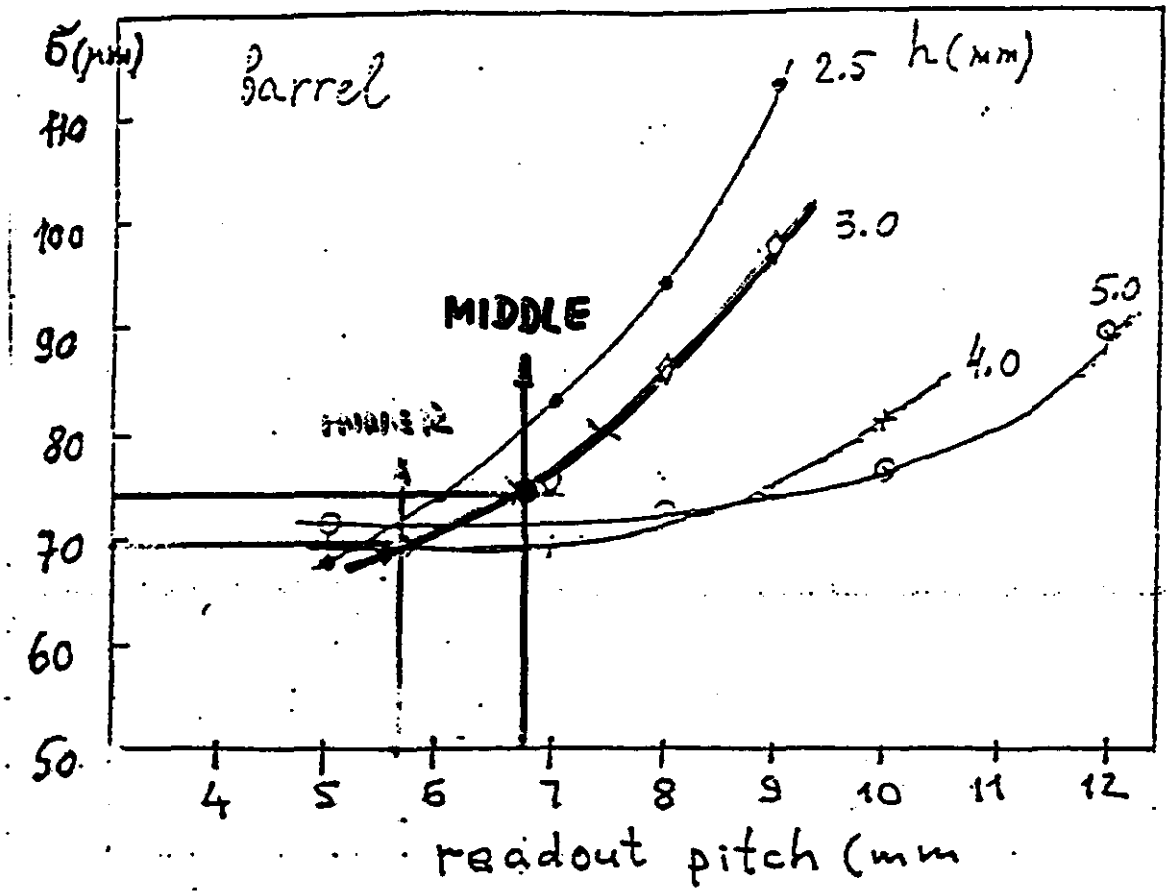

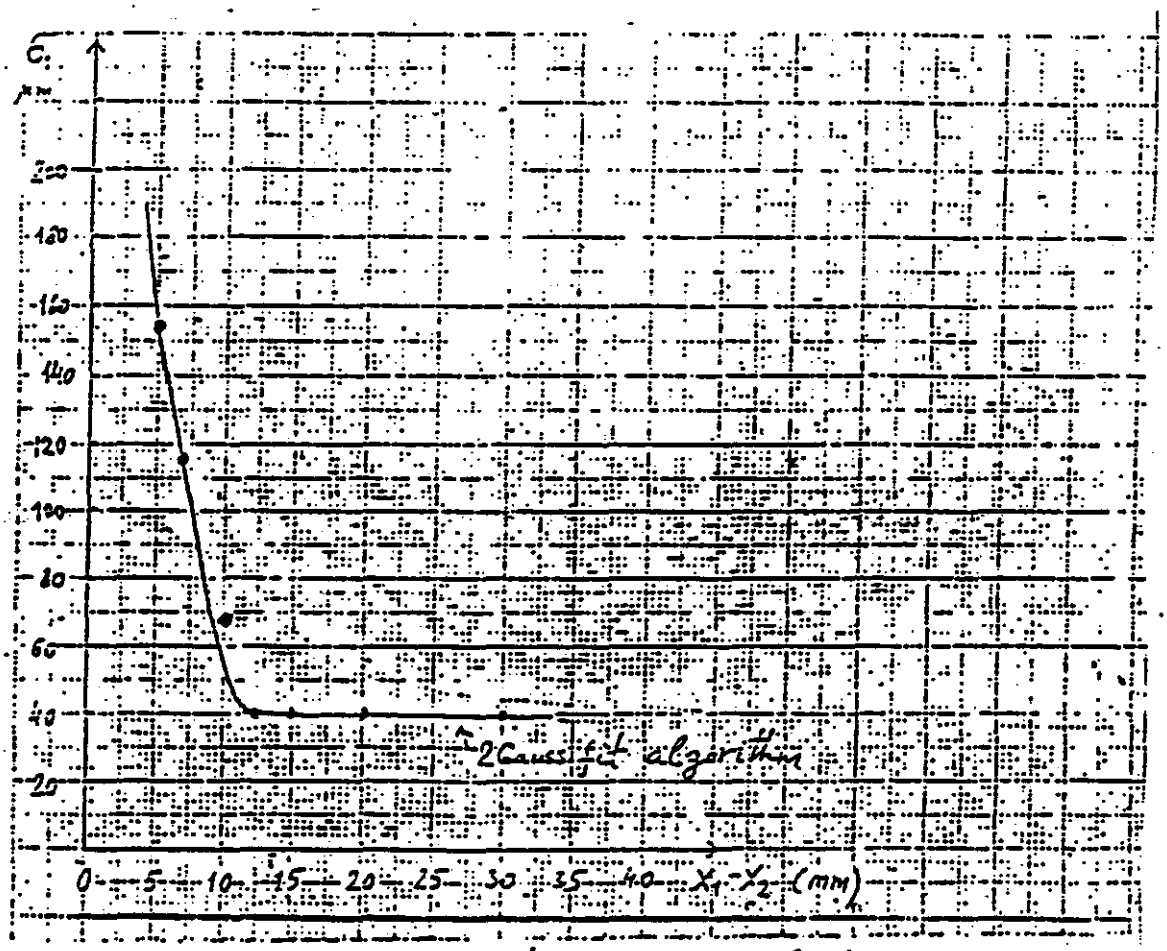

two partical resolution.
$X_1 - X_2$ – distance between particals.

SUPERLAYER 2
(MIDDLE)

W (WIRE LENGTH) = 120 cm

— MAXIMUM POSSIBLE LENGTH

— U.S. G-10 PRODUCTION (MAX 49")

h (GAP) = 3 mm

S (PITCH) = 6.8 mm ← RESOLUTION

COMPENSATION ANGLE → 9.2°

$\Theta_L = 8°$

ANGULAR RANGE $4.4° \leq \varphi \leq 6.8°$

NUMBER OF CHAMBERS IN 1 SECTOR 4

NUMBER OF STRIP CHANNELS IN CHAMBER 256

NUMBER OF CHAMBERS IN THE BARREL 1056

NUMBER OF STRIP CHANNELS IN THE BARREL 270,336

SUPERLAYER 1
(INNER)

$W = 914$ MM

$h = 3$ MM

$S = 5{,}7$ MM

} OPTIMIZE 2-TRACK RESOLUTION
⇓
MAX LAYER EFFICIENCY

COMPENSATION ANGLE → 13°

$\theta_L = 8°$

ANGULAR RANGE $0{,}5° \leq \varphi \leq 11°$

NUMBER OF CHAMBERS IN 1 SECTOR 2

NUMBER OF STRIP CHANNELS IN CHAMBER 960

NUMBER OF CHAMBERS IN THE BARREL 128

NUMBER OF STRIP CHANNELS IN THE BARREL 122,880

Inner Superlayer

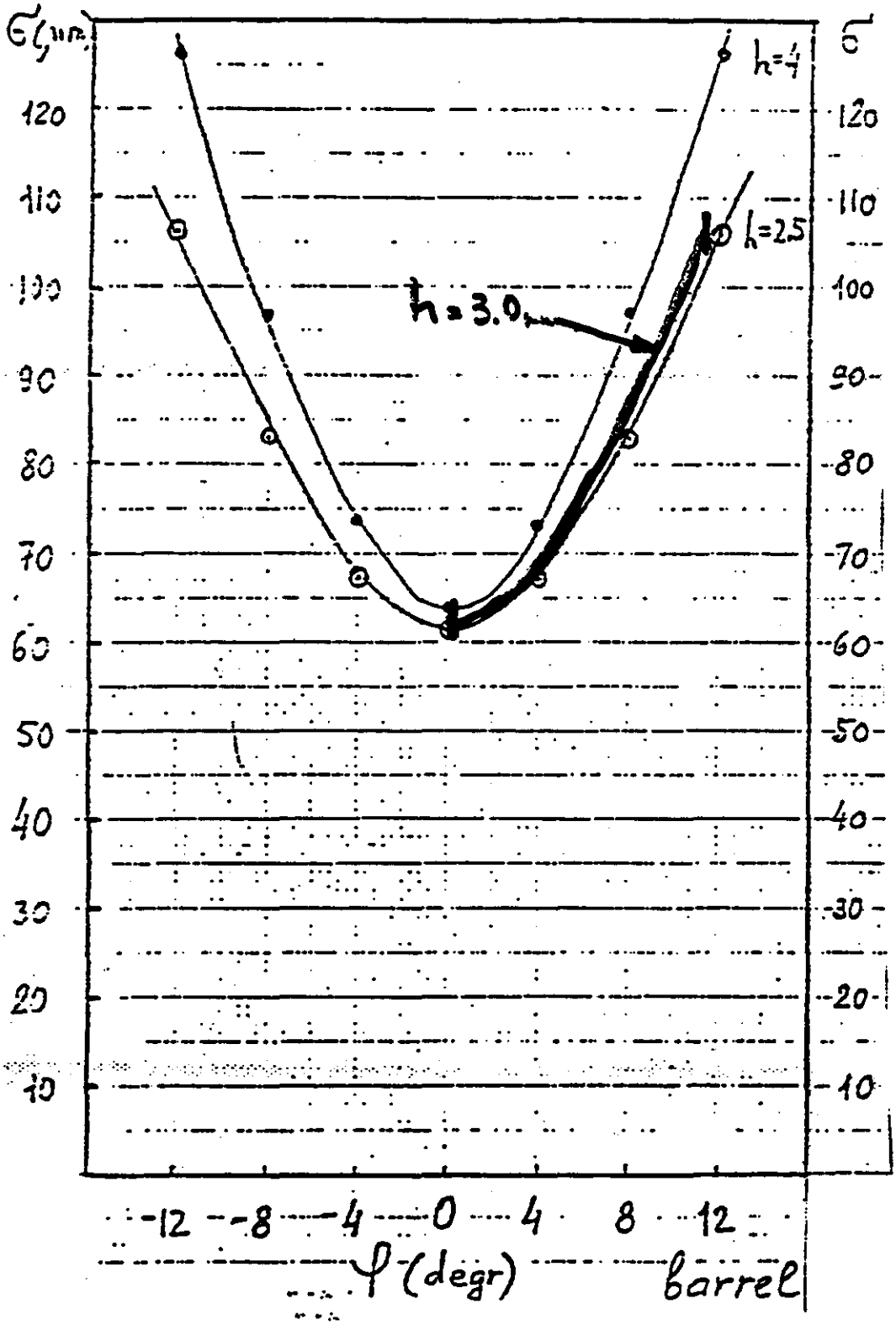

<TCHERNIATIN>

SUPERLAYER 3
(OUTER)

W (WIRE LENGTH) = 893 mm

h (GAP) = 6 mm

S (PITCH) = 11,2 mm

COMPENSATION ANGLE → 7.4°

$\Theta_L = 8°$

ANGULAR RANGE $5° < \varphi < 6.2°$

NUMBER OF CHAMBERS IN 1 SECTOR 8

NUMBER OF STRIP CHANNELS IN CHAMBER 480

NUMBER OF CHAMBERS IN THE BARREL 512

NUMBER OF STRIP CHANNELS IN THE BARREL 245,760

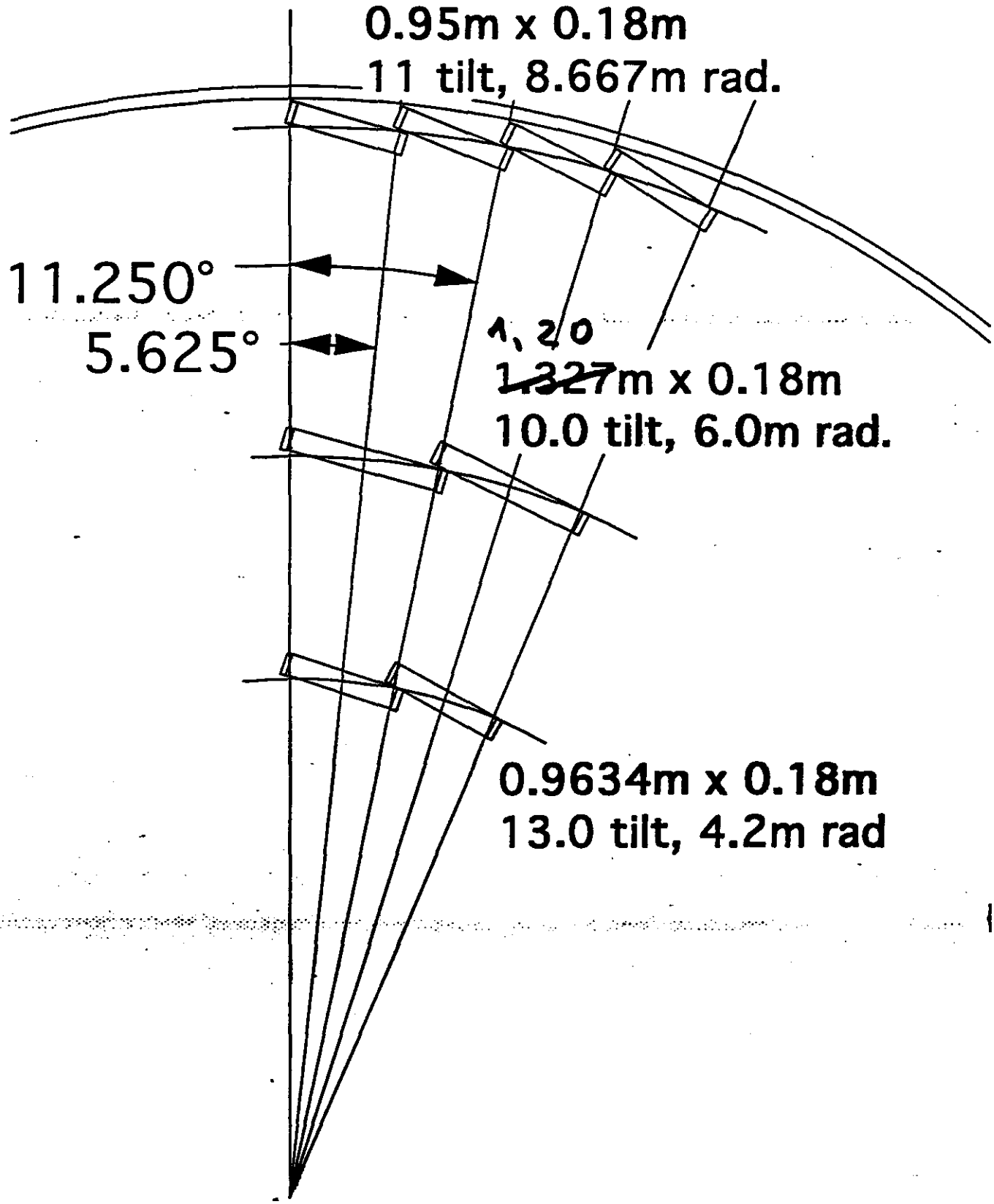
0.95m x 0.18m
11 tilt, 8.667m rad.
11.250°
5.625°
1.20
~~1.327~~m x 0.18m
10.0 tilt, 6.0m rad.
0.9634m x 0.18m
13.0 tilt, 4.2m rad

93/02/02 21.19

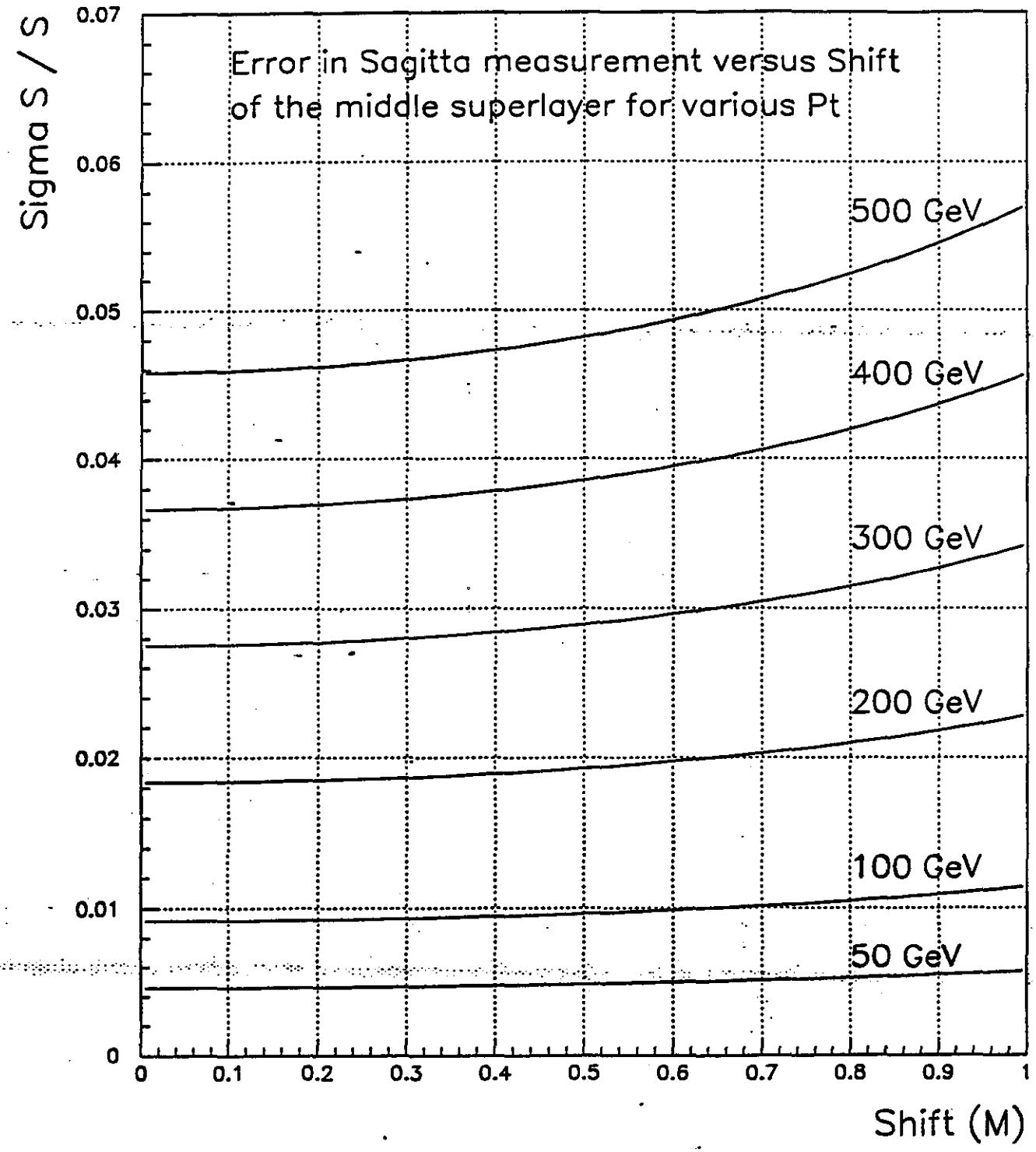

< BONUSHKIN >

	SL1	SL2	SL3
#CHAMBERS	128	256	512
# CHANNEL	123 K	270K	246 K

TOTAL

CHAMBERS → 896

STRIP CHANNELS → 638,976

gem

γeμ

Presentation by:

A. Ostapchuk

U. Ostapchuk
02.03.93

Coverage of the GEM barrel muon system

Two types of coverage:

- muon momentum measurement (all 3 SL)
- muon identification (any 1 of SL)

Two kinds of coverage characteristics

- pseudorapidity (η) } full coverage
- solid angle ($\cos\theta$) } over φ

Three sources of coverage losses

- membrane
- muon chamber dead zones (60 mm) and clearance (50 mm)
- projective alignment paths (lense ϕ 50 mm)

GEM barrel muon system coverage

All three superlayers (p_t - measurement)

	η (0 ÷ 1.33)	$\cos\theta$ (0 ÷ 0.87)
Membane	0.11 (8%)	0.11 (13%)
Dead Zones	0.124 (9.4%)	0.070 (8%)
Alignment	0.030 (2.3%)	0.015 (1.8%)
Total	0.264 (19.7%)	0.195 (22.8%)

Any one of superlayers (muon identification)

	η (0 ÷ 1.33)	$\cos\theta$ (0 ÷ 0.87)
Membrane	0.05 (3.8%)	0.05 (5.7%)
Dead Zones	0.057 (4.3%)	0.031 (3.6%)
Alignment	0	0
Total	0.107 (8.1%)	0.081 (9.3%)

gem

γeμ

Presentation by:

A. Korytov

February 3, 1993
A. Korytov
MIT

Axial + Projective Alignment for the Barrel CSC's.

"No Axial Alignment" disadvantages:

- **many projective paths:**
  either loss of coverage or fancy chambers;

- **high accuracy, wide range detectors**
  are apparently costly;

Axial Alignment might solve these problems.

Axial + Projective Alignment:

+ small number of projective paths;

+ does NOT contradict to projective ideology:
Brief analysis made by A.Ostapchuk showed:
±3 mm requirements on chamber placement;
~10 μm accuracy requirements for axial alignment;

+ allows to have ~10 μm accuracy
over 10 mm range
in both transverse and 'vertical' directions;

+ systematic errors in alignment detectors/channels
are relaxed up to ~0.5%
(compare to ~0.1% in LED/Lens System);

+ has NO transfer points:
ministrips and regular strips are on the same photo mask.

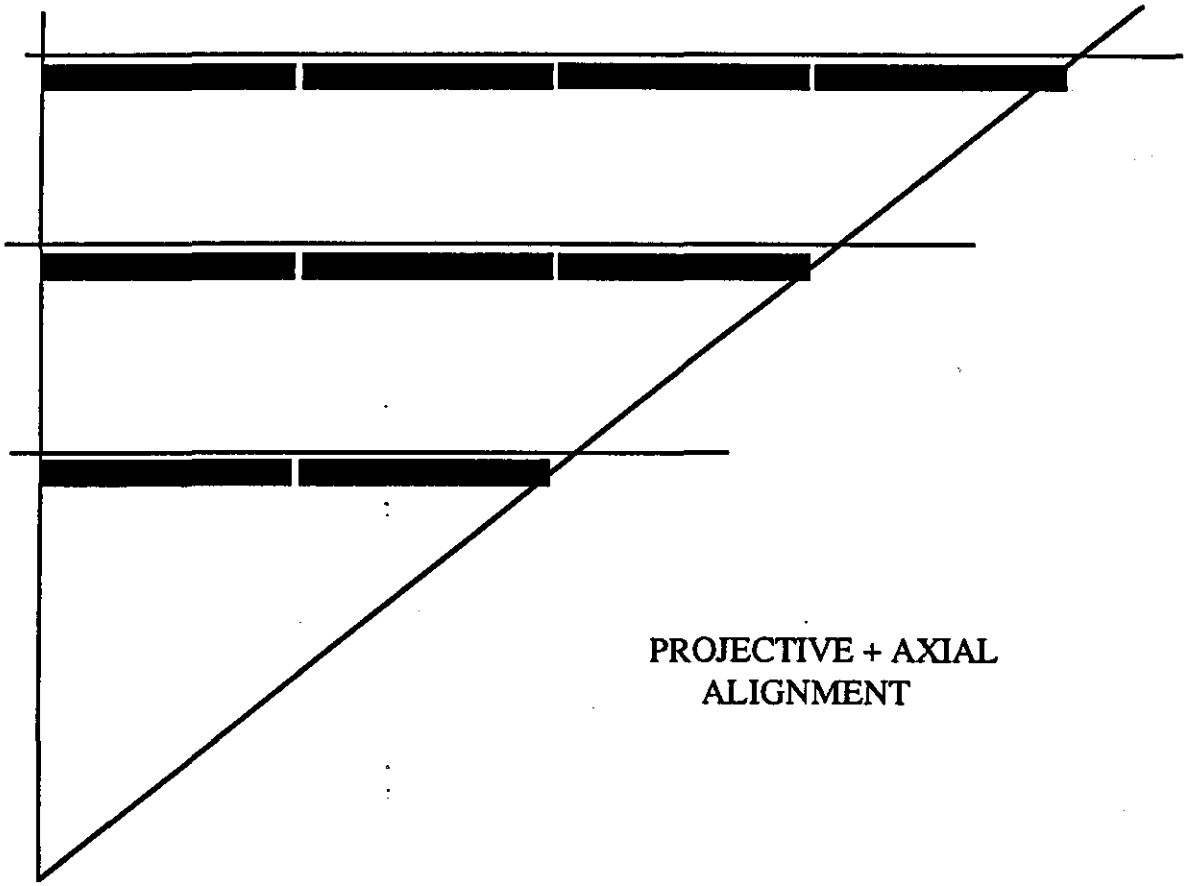
PROJECTIVE + AXIAL
ALIGNMENT

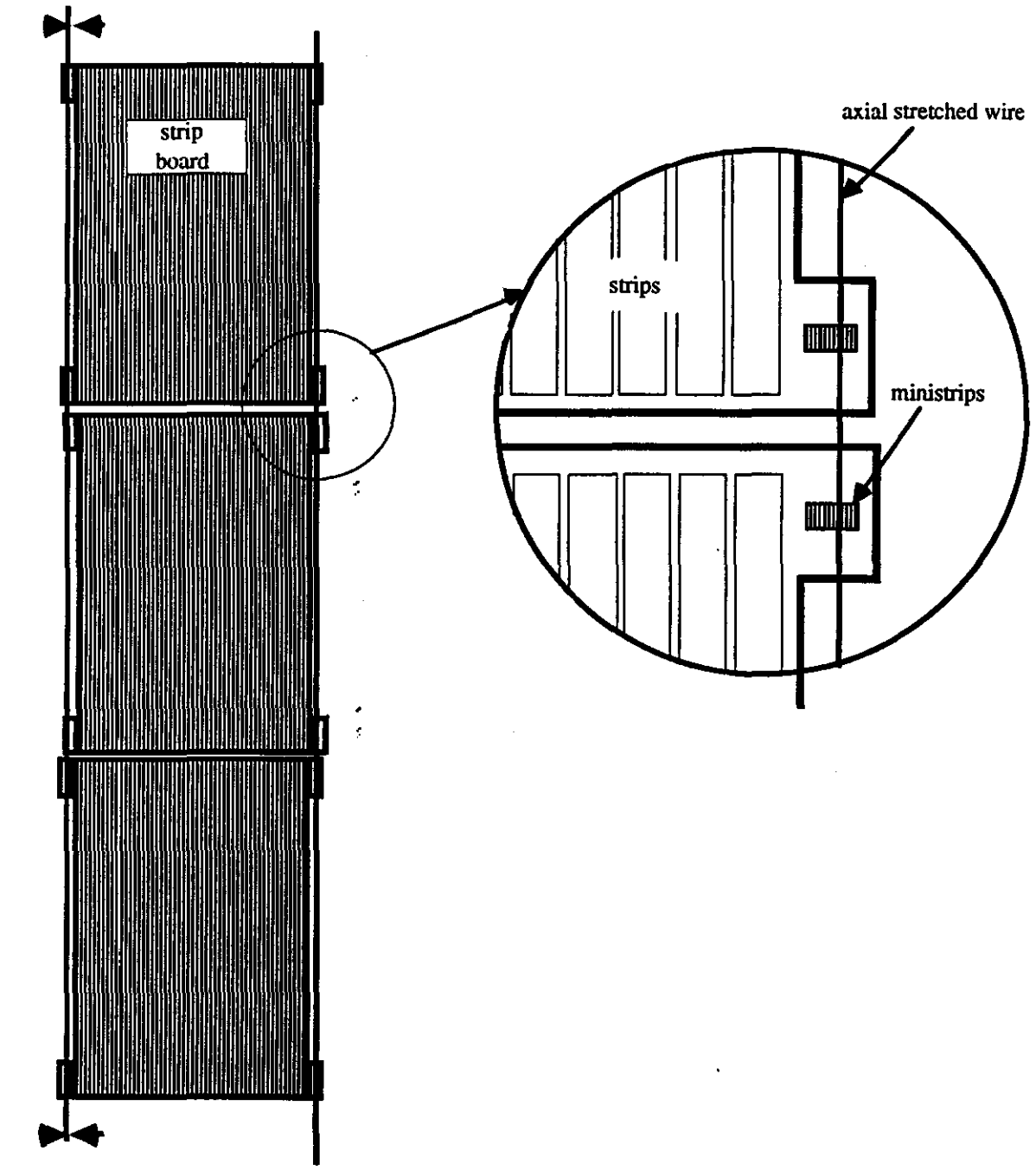

wire fixture
is NOT attached to
strip boards

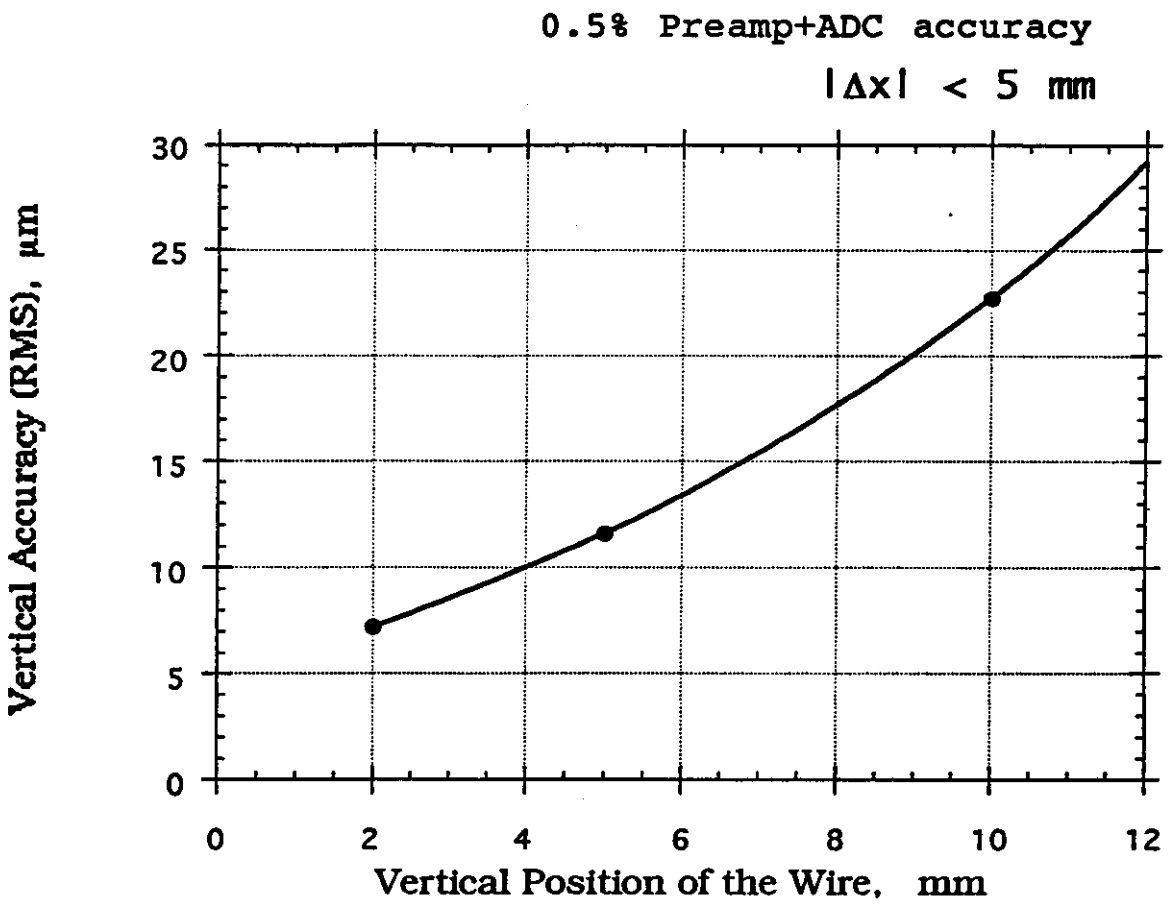
0.5% Preamp+ADC accuracy
|Δx| < 5 mm
Vertical Accuracy (RMS), μm
30
25
20
15
10
5
0
0
2
4
6
8
10
12
Vertical Position of the Wire, mm

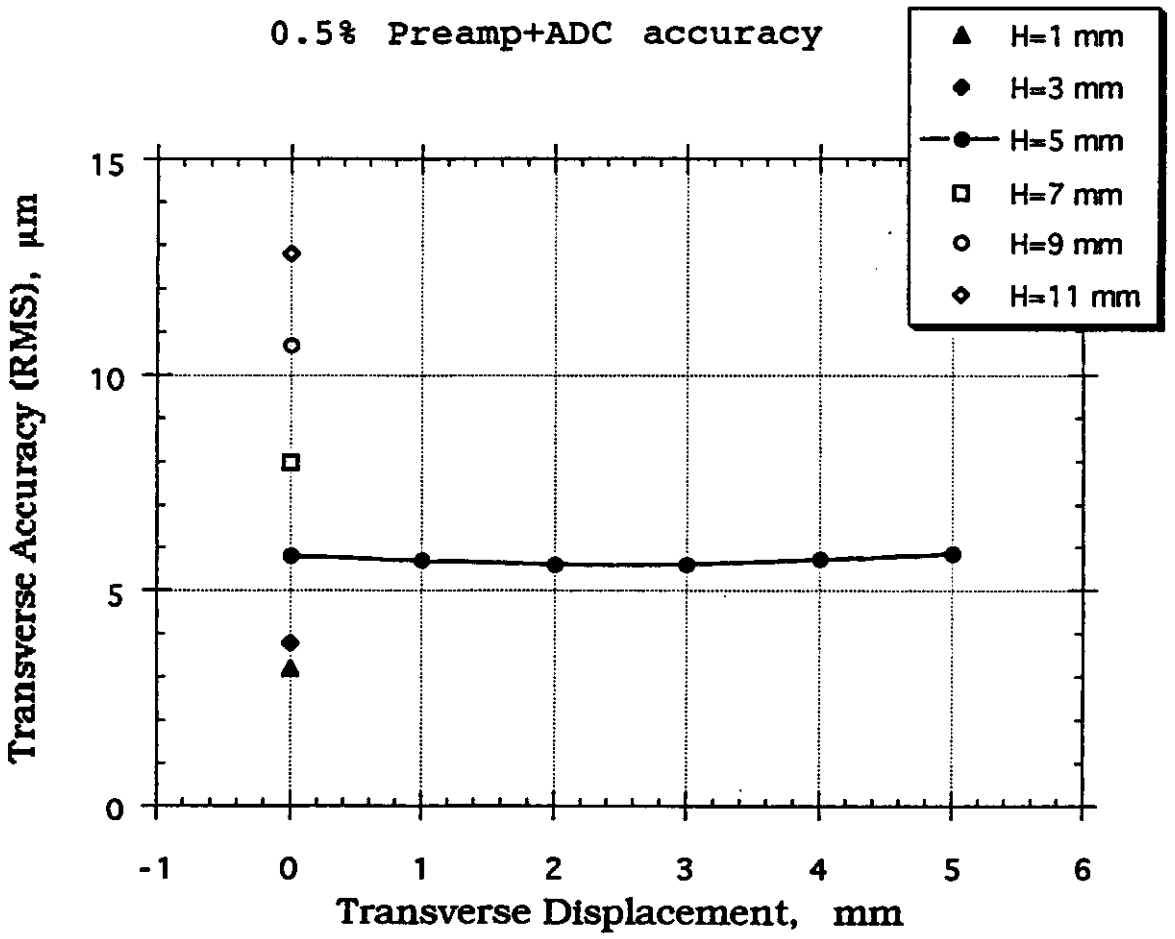
0.5% Preamp+ADC accuracy
H=1 mm
H=3 mm
H=5 mm
H=7 mm
H=9 mm
H=11 mm
Transverse Accuracy (RMS), µm
15
10
5
0
-1
0
1
2
3
4
5
6
Transverse Displacement, mm

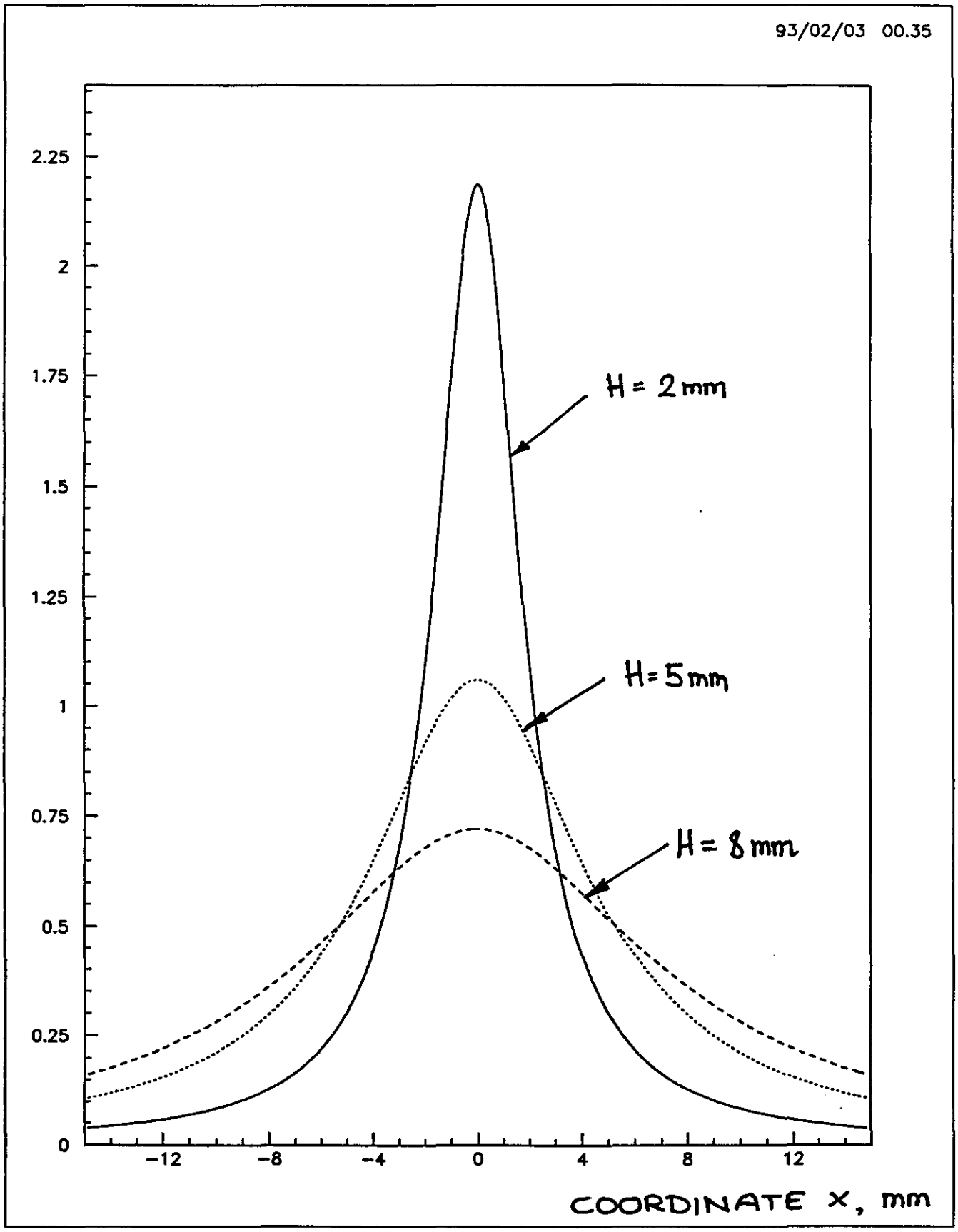
93/02/03 00.35
2.25
2
1.75
1.5
1.25
1
0.75
0.5
0.25
0
−12
−8
−4
0
4
8
12
H = 2mm
H=5mm
H = 8mm
COORDINATE X, mm

x=4

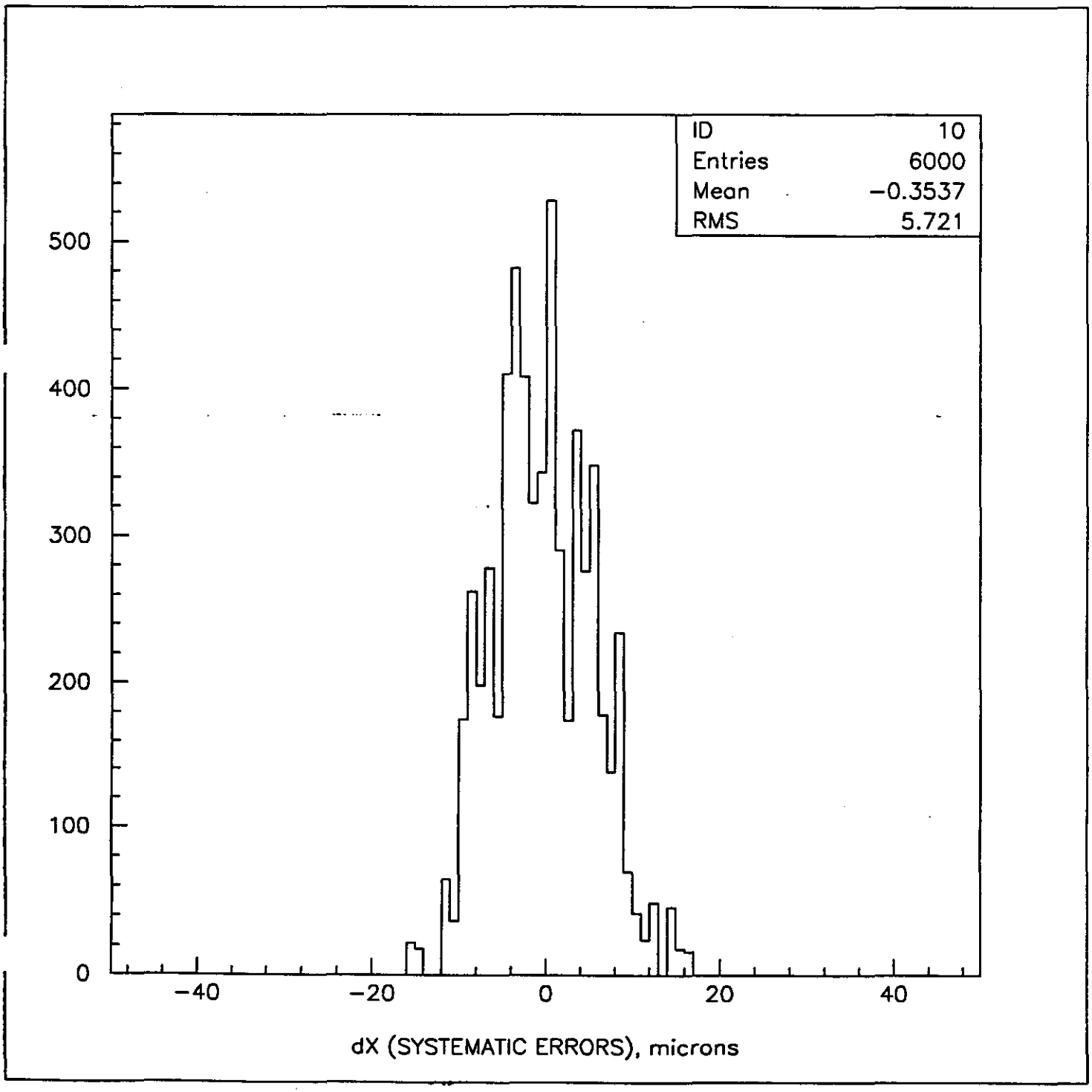
ID 10
Entries 6000
Mean −0.3537
RMS 5.721
500
400
300
200
100
0
−40
−20
0
20
40
dX (SYSTEMATIC ERRORS), microns

gem

γeμ

Presentation by:

J. Paradiso

Extended Range Alignment @

Schedule

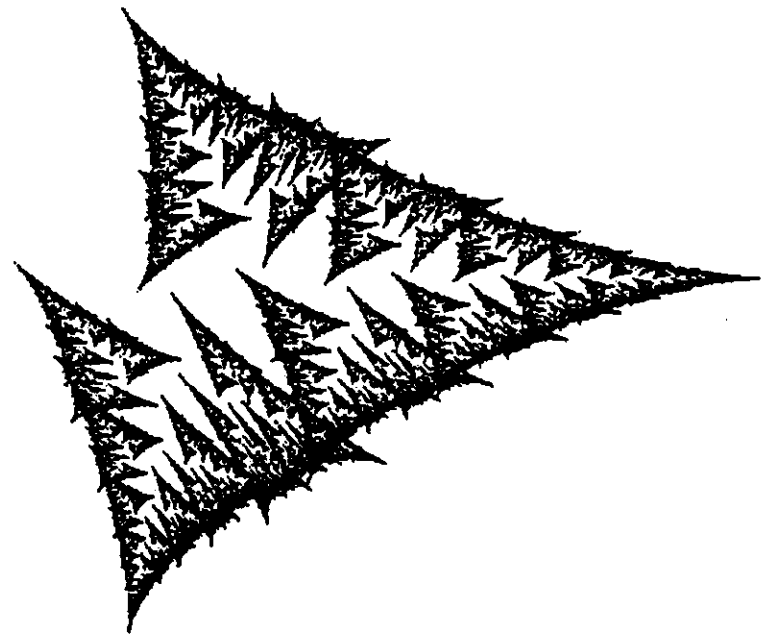

- *CCD alignment*
  - Background
  - Procedure
  - First results
- *Multiple LED's*
  - Plans, Status
- Activities in the Optics Lab
  - LED/lens, fencepost, proximity sensors
- Visit from Sokkia reps; "Monomos" demo

- J. Paradiso 27-Jan-92

GEM

Application of CCD

Modification of LED/Lens approach discussed w. Harry VanDerGraff

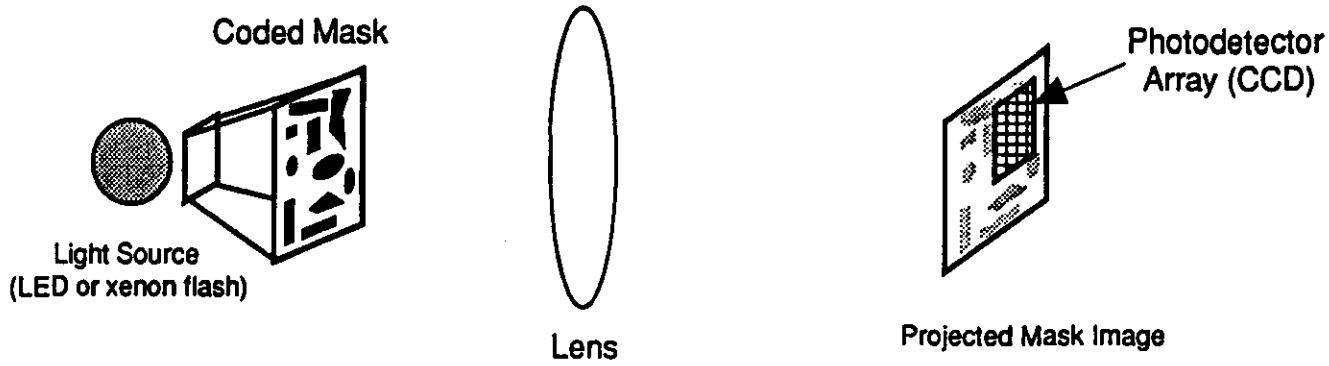

- Wide dynamic range entails large quad cell or lateral effect photodiode
  -> Expensive...
- Image onto 2D CCD array instead of quadrant detector
- Project "complicated" image instead of simple square
- Projected image is larger than the sensitive detector area
  - Do pattern recognition; use information from entire CCD surface
  - Can accurately establish detector position within large field
  - Use small, commercial-grade CCD from cheap TV cameras
- Encode several features in the projected image
  - Less sensitive to ambient light, optical gradients & inhomogeneities
- LED with field lens works to efficiently map smooth LED source into coded image (no need for flash)!

GEM

Deployed System

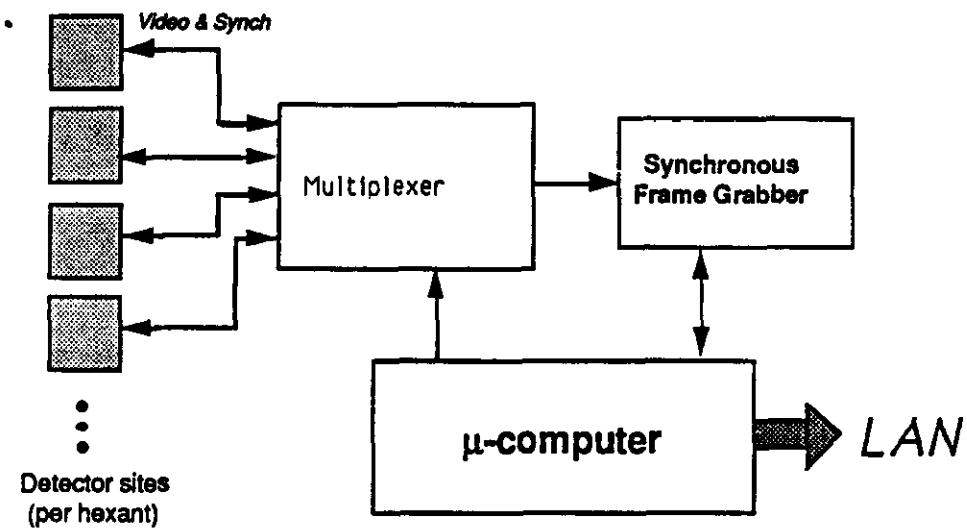

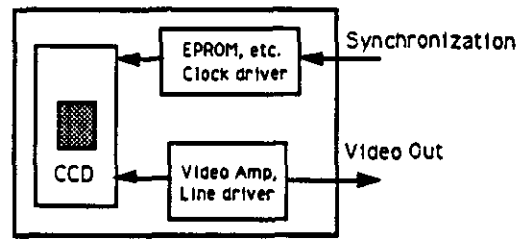

Detector Site

- Minimize hardware at detector sites
  - Need only one μ-processor, frame-grabber per sector
- Processing is fairly simple; since small image motion expected, 2D autocorrelation provides offsets (plus correction for rotation, scale shift, if necessary) ☞☞☞ *Note: can do simple centroiding/parsing!*
  - Star trackers for guidance & control; fast updates attained (but not needed here...)
- Must determine best image encoding; dot pattern, ☞☞☞ *"bar code"*..
  - Since image not too much larger than array, not difficult...
- Other information available from system
  - Differential rotation between imager & mask, imager scale shift

GEM

RS170 Imaging Chips

- Commercial CCD area imagers for miniature cameras.
- Single chip needs power, clock (≈ 2 phases?)
- Outputs composite RS-170 signal for frame grabber.
  - => Simple and cheap!! (circa $40./chip; cost of quad cell!)
  - => Cabling is minimal (need power, 75Ω video out)

Note: RS-170 chips in development (SONY, etc.), but cheap CCD camera cards (<$100. in kilo-quantities) now available!

- Issues...

✔ - Light sensitivity, S/N

✔? - Neutron background/damage

Card probably no (has inductors) but simple mod! → Runs in magnetic field?

"No Problem" M.A., 12/92 → - Clocked (≈3 Mhz) device near pickup strips?

[No need for distributed clock; synch to composite RS170]

Trivial to try...

GEM

John Grace
508-460-0749

CHINON

CX-102

Pat Bibby / Purchasing

MINIATURE SINGLE BOARD MONOCHROME SOLID STATE CHIP CAMERAS

- MOS Image Sensor For Long Camera Life
- Ultra Compact Solid State One Board Camera
- Automatic Electronic Shutter Adjusts for Lighting Conditions
- 2 LUX Minimum Illumination
- Extremely Low Power Consumption
- Operating Range of DC 7V to 14V
- Alternate Lens Configuration
- Small Size Allows for Unique Applications and Installations

1/3" CCD
RS170 Output
$172.- single q.
$117.- 24-unit quantity

CL-83

CL-115

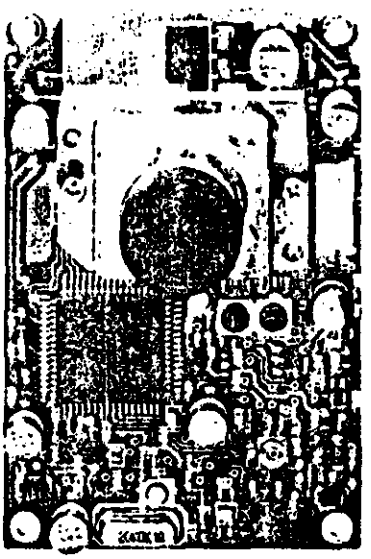

CX-102/3
CX-102/4

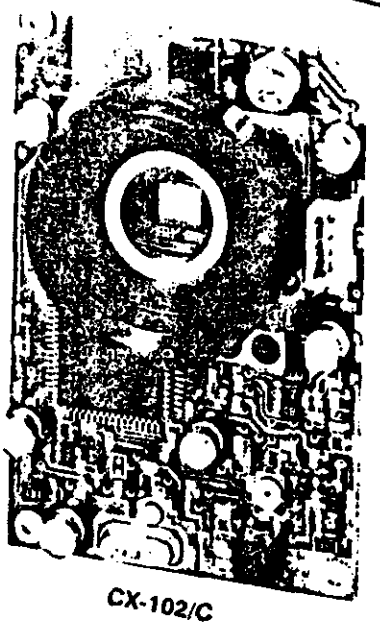

CX-102/C

ACTUAL SIZE

PRODUCT CODE	PRODUCT DESCRIPTION
CAMERA VERSIONS:	
600109	CX-102/4, 4mm F1.8 Camera (78° Field of View)
600110	CX-102/3, 3mm F1.8 Camera (110° Field of View)
600106	CX-102/C, C-Mount: Accepts C-Mount Lenses
OPTIONAL ACCESSORIES:	
600212	CX-MH, Housing, Metal: For 4mm and 3mm CX-102 Cameras
600211	CX-MHC, Housing, Metal: For the CX-102 C-Mount Camera
600501	CL-83, 8.3mm F1.8 Lens, (55° Field of View)
600503	CL-115, 11.5mm F1.8 Lens (43° Field of View)

4/92

2D Barcode Mask

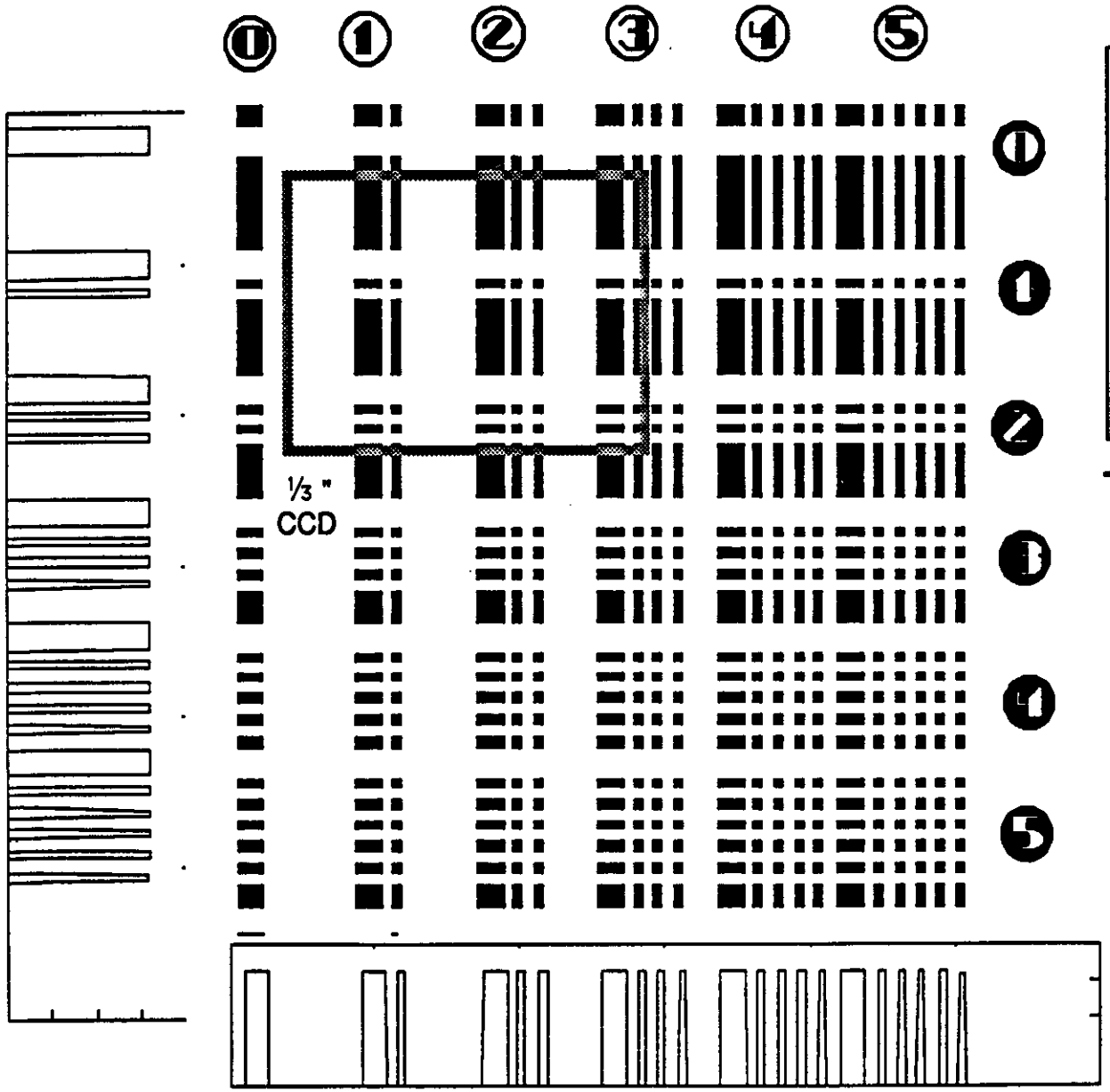

- Take x,y projections & separately match to code features
  - Converts 2D problem into 2 1D calculations!
  - Now nonotonic linear code; could binary-encode digits or use 2-digit numbers for *much* wider range!

12 x 12 mm

- Current code hand-generated in Canvas (PICT oblect positions used to determine alignment), printed on Linotype.
  - Accurate pattern with direct postscript!
- Now on murky negative
  - Inexpensive (≈$20.) to put precisely on glass!

GEM

5

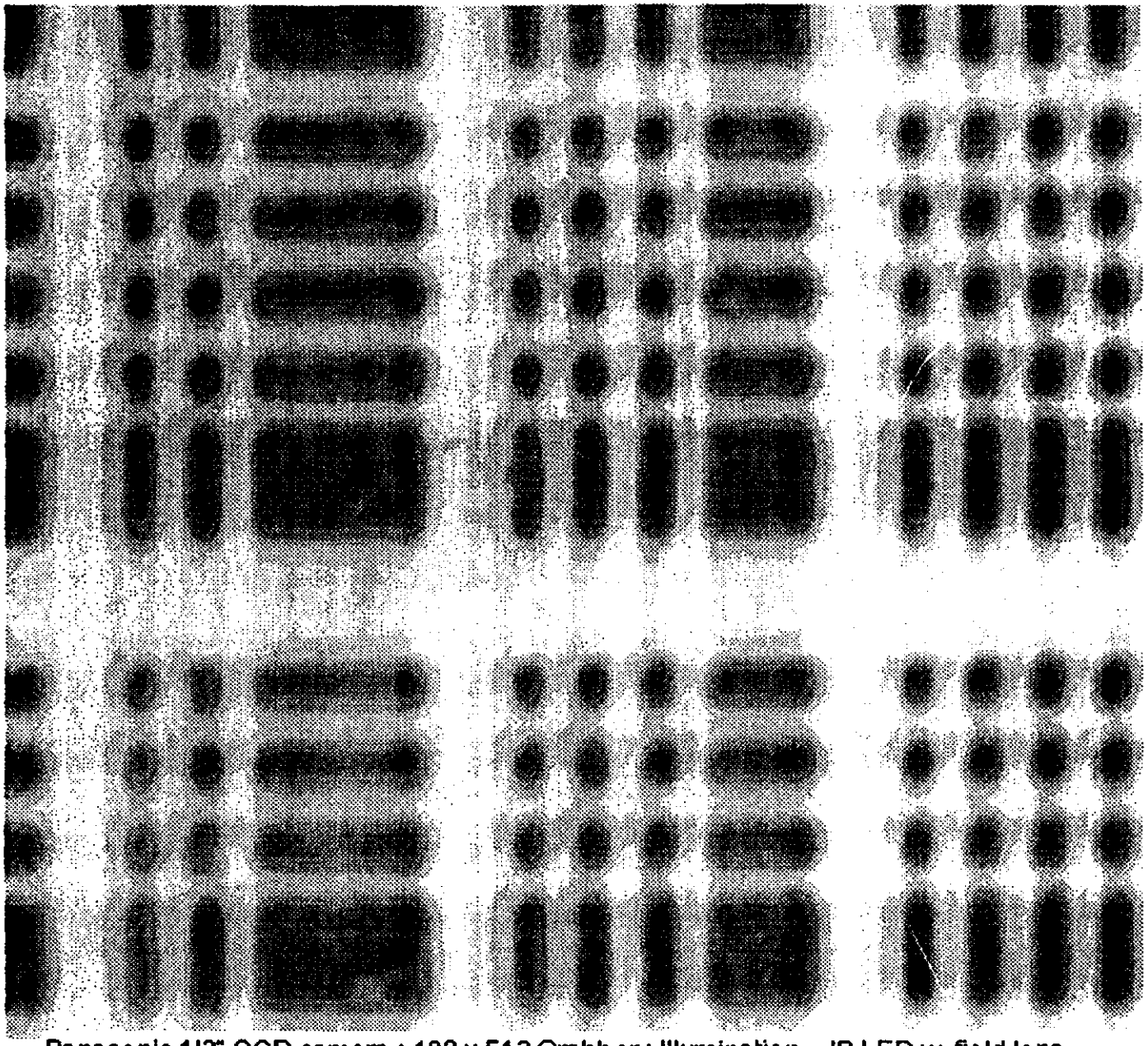

Panasonic 1/3" CCD camera : 480 x 512 Grabber : Illumination = IR LED w. field lens
Imaged over a 9 meter path through 1.5" lens aperture

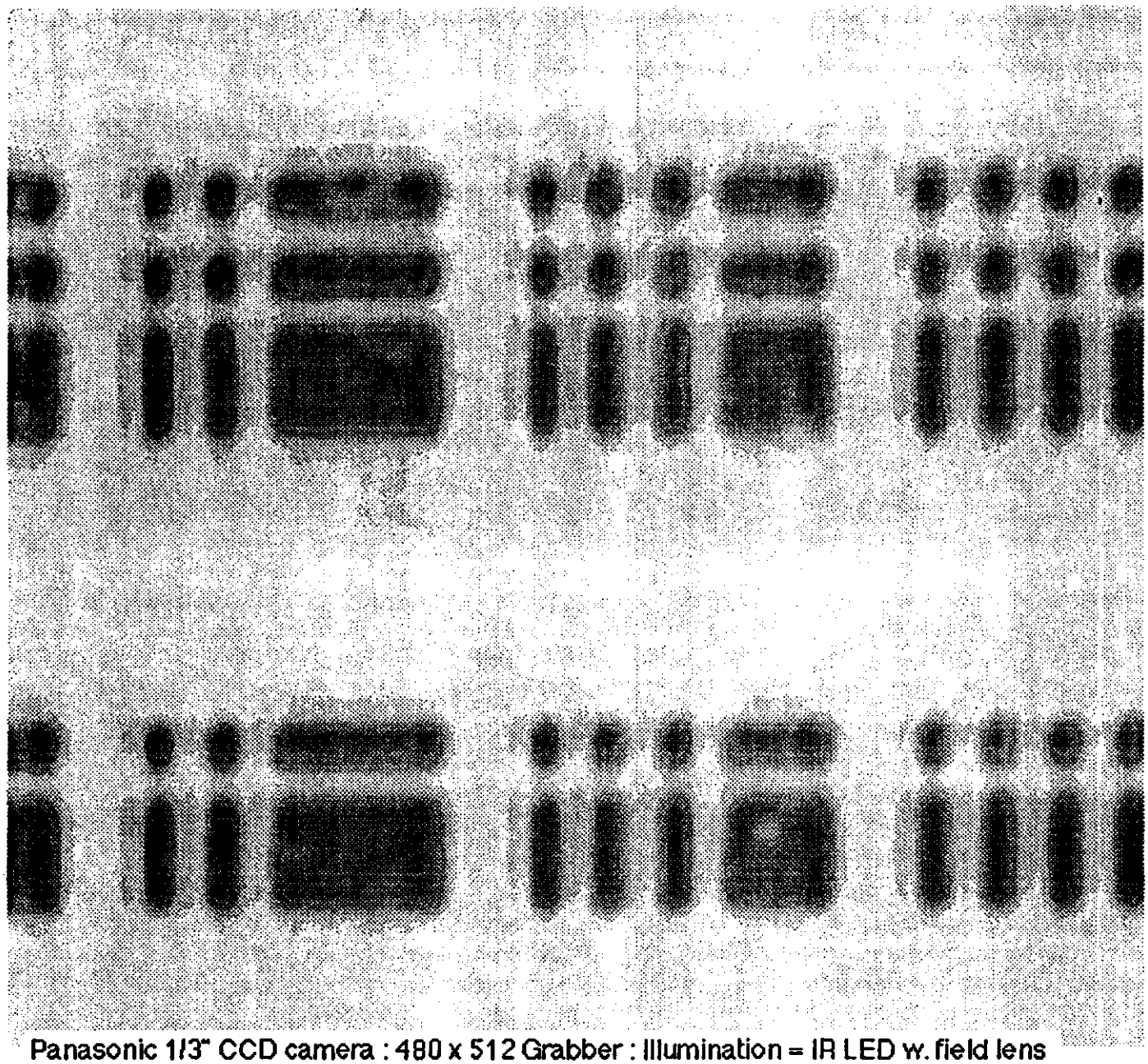

Panasonic 1/3" CCD camera : 480 x 512 Grabber : Illumination = IR LED w. field lens
Imaged over a 9 meter path through 1.5" lens aperture

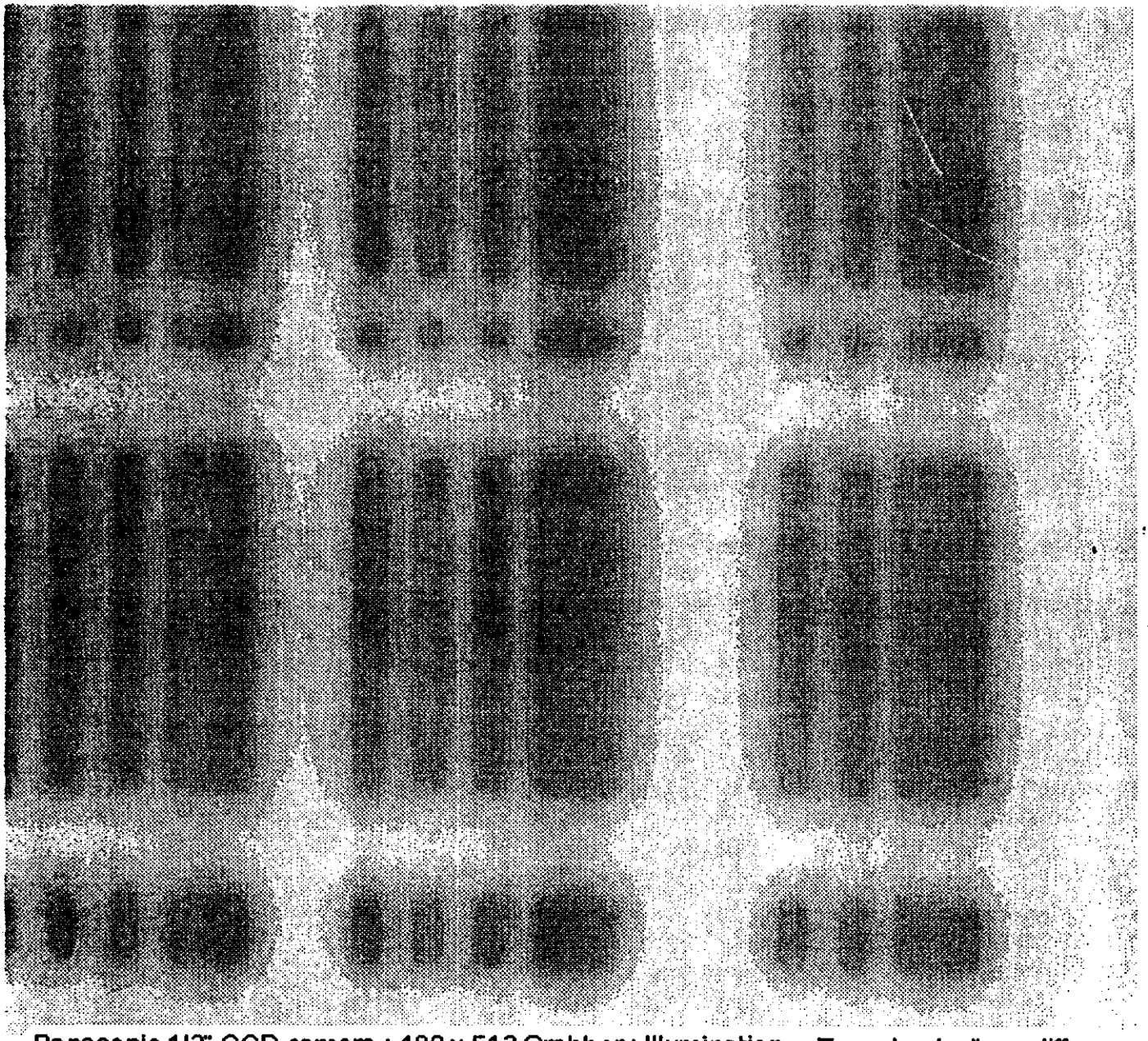

Panasonic 1/3" CCD camera : 480 x 512 Grabber : Illumination = Tungsten bulb w. diffuser
Imaged over a 9 meter path through 1.5" lens aperture

Pattern Analysis

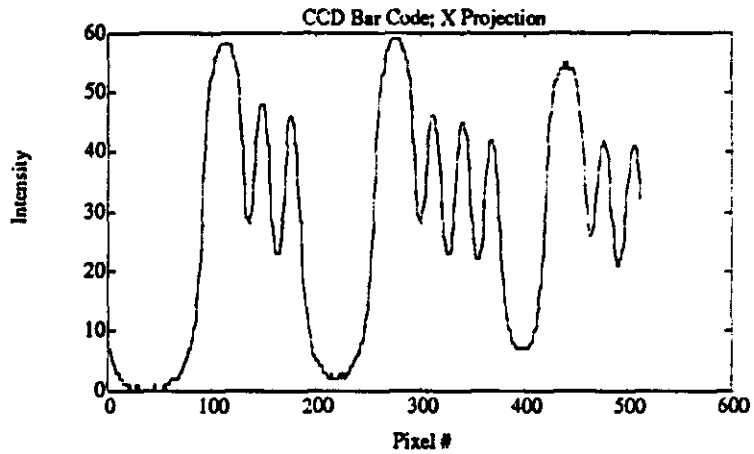

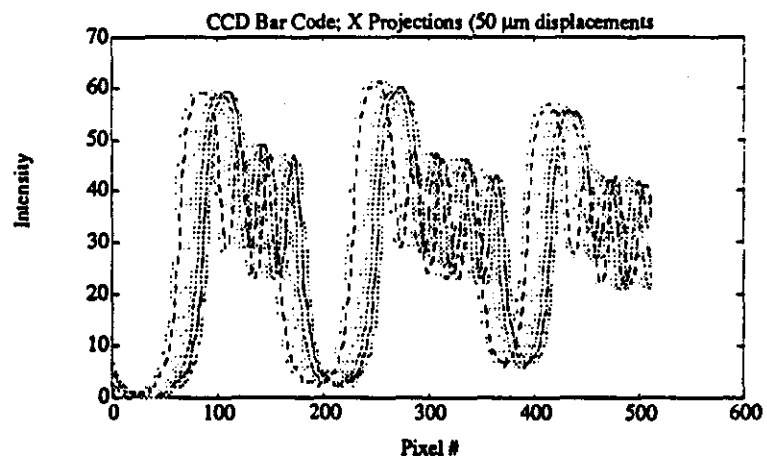

50 µm Steps

Analysis Sequence:

- Take x,y projections of averaged frames.
- Find peaks (floating threshold)
- Parse barcode (identify cluster of peaks with digit)
- Centroid all peaks (fit quadratic)
- Fit peak positions in CCD projection with their expected place in the barcode (first linear least squares to get slope, then just average over offset (CCD - Bcode)

This is quick & easy; correlation may be more precise...

GEM

X projection data (9-meter path)

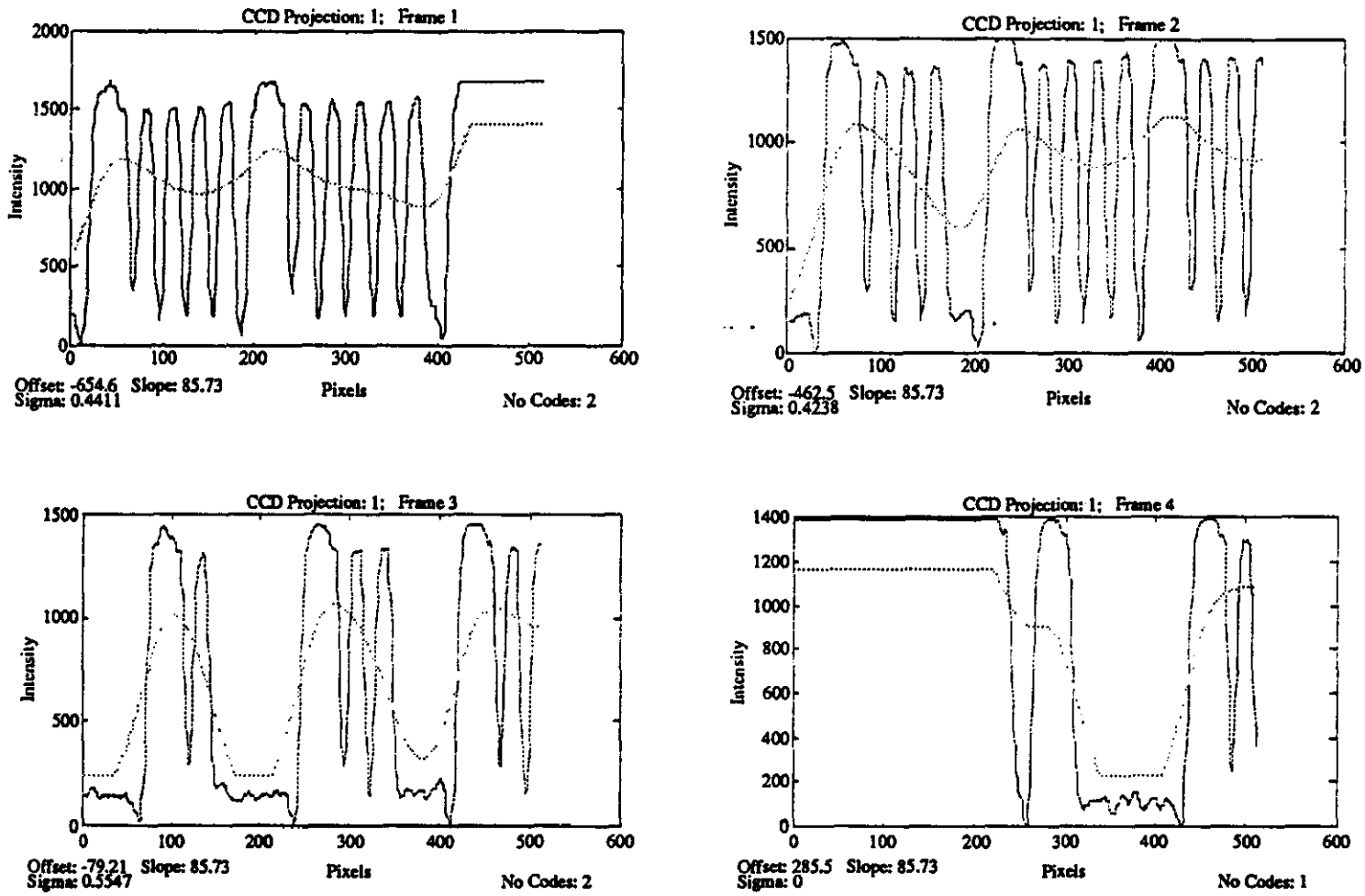

- 15 Frames averaged over 15 sec. (atmospheric dynamics at Hz-level)
- Low-pass filter serves as dynamic threshold.

GEM

Y projection data (9-meter path)

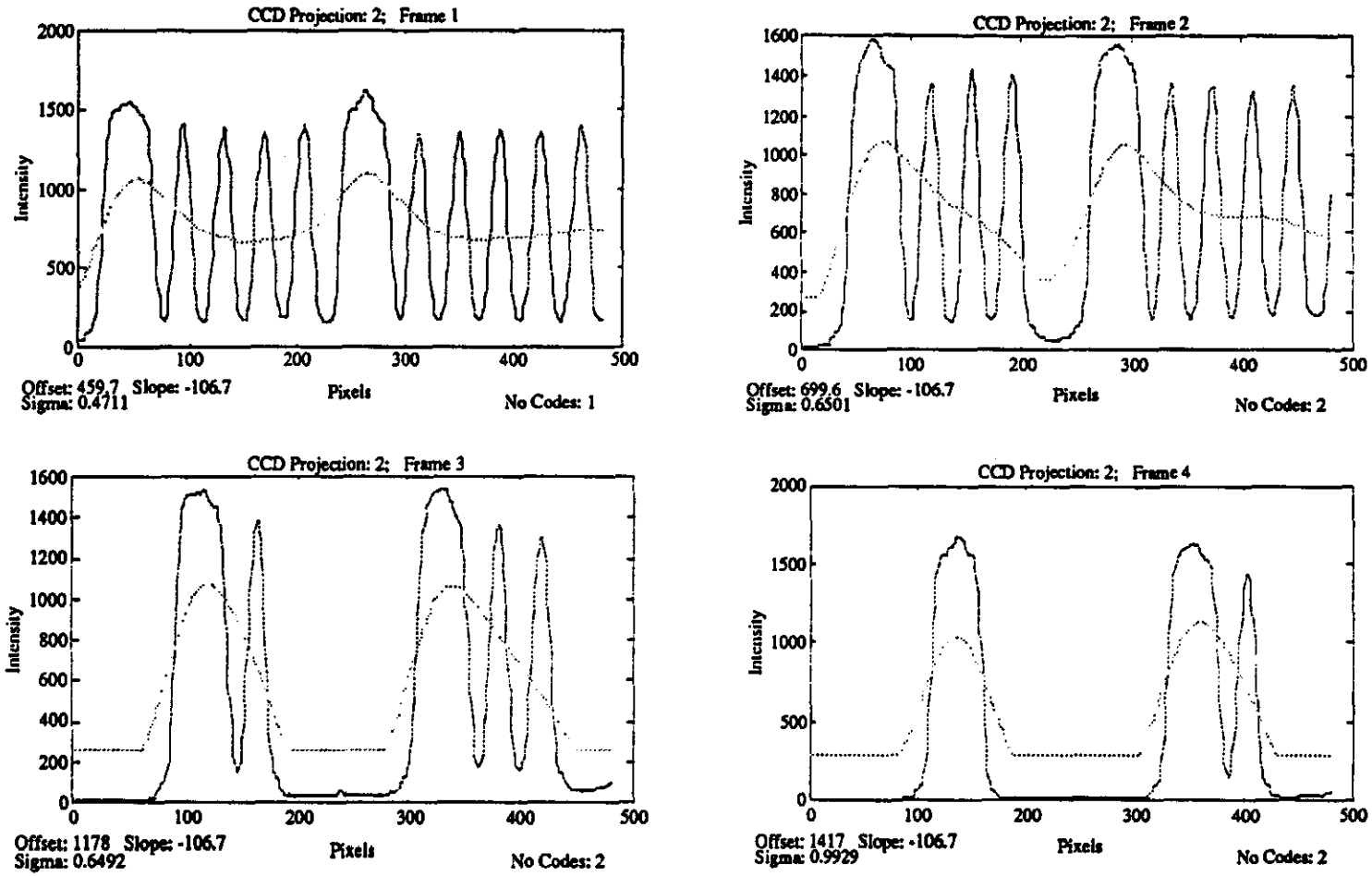

- 15 Frames averaged over 15 sec. (atmospheric dynamics at Hz-level)
- Low-pass filter serves as dynamic threshold.

GEM

Scan Test; 100 μm shifts in X

Measurement vs. Position

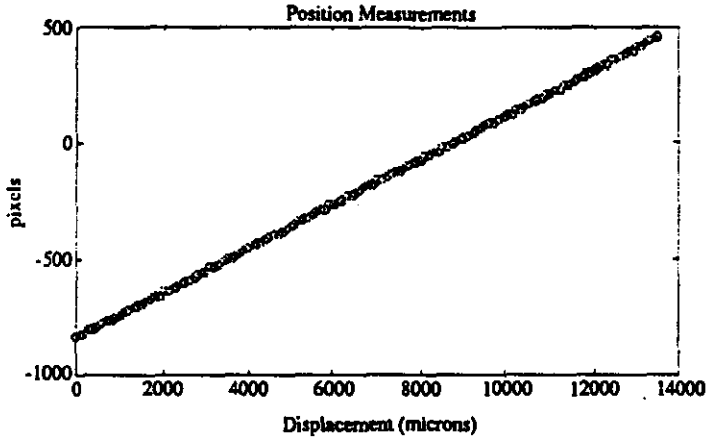

Average of Detected Bar Codes

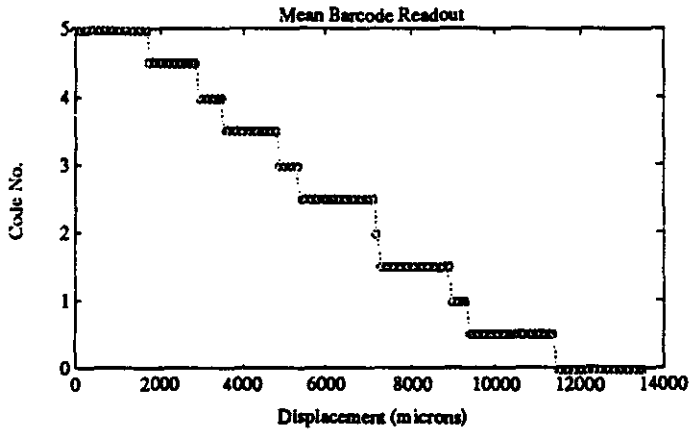

Fit Residuals to Code Template

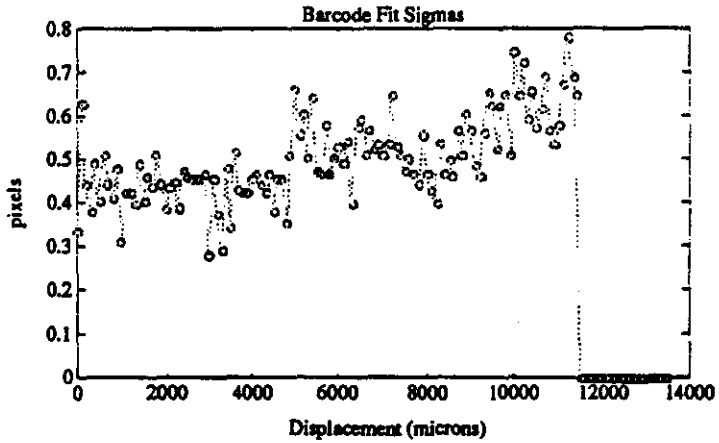

Calibration; CCD to Bar Code

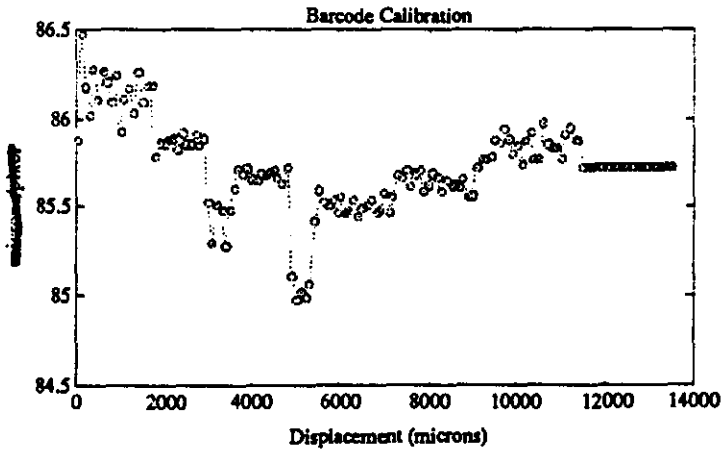

- 15 Frames averaged for 15 sec. (atmospheric dynamics @ Hz-level)
- Measurements taken over 14 mm.

GEM

Scan Test; X Residual

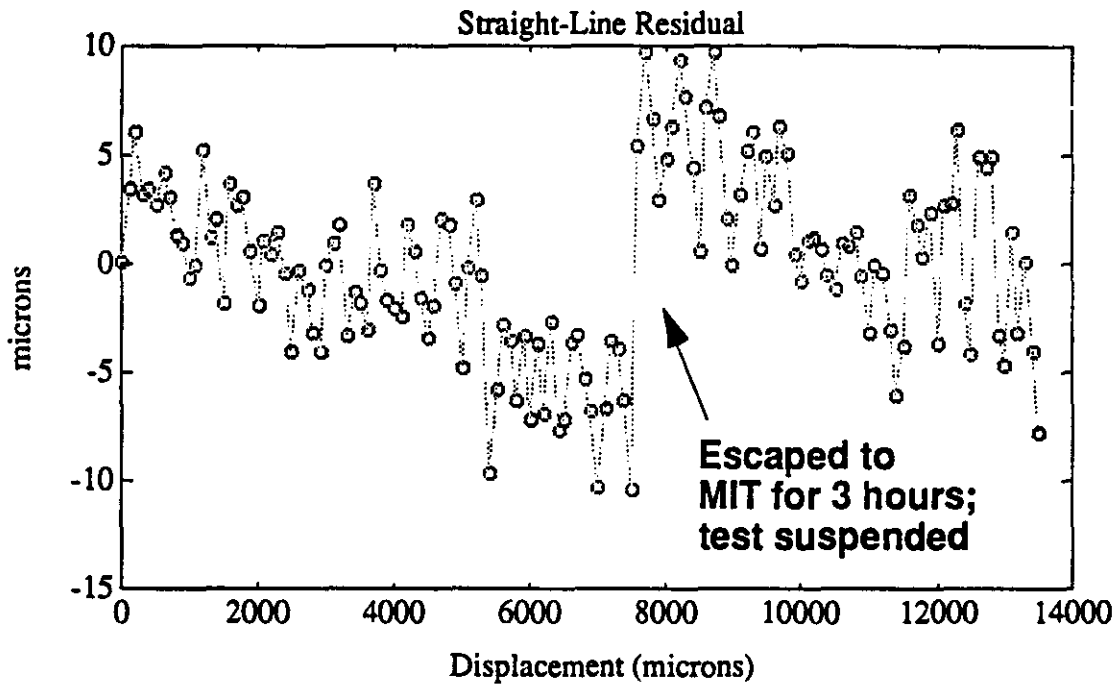

Some systematic structure within ±10 μm
(i.e. film bent, flaws in film transfer, thermal effect)
True resolution at the 5 μm level?

- **15 Frames averaged for 15 sec. (atmospheric dynamics @ Hz-level)**
- **Measurements taken over 14 mm.**

GEM

Scan Test; 100 μm shifts in Y

Measurement vs. Position

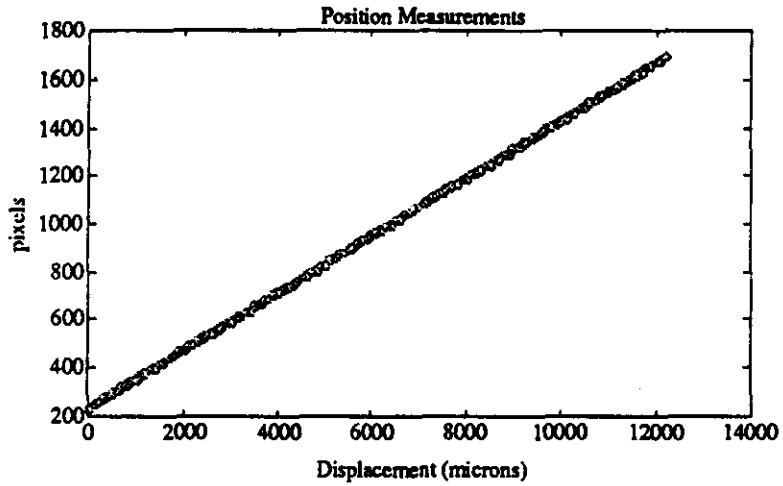

Average of Detected Bar Codes

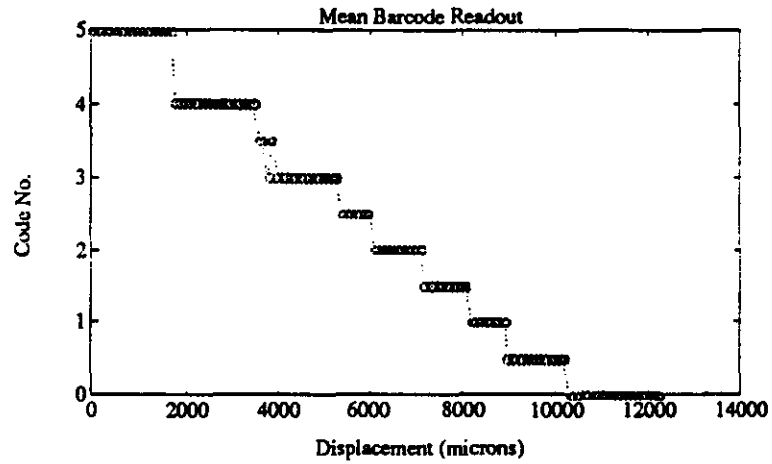

Fit Residuals to Code Template

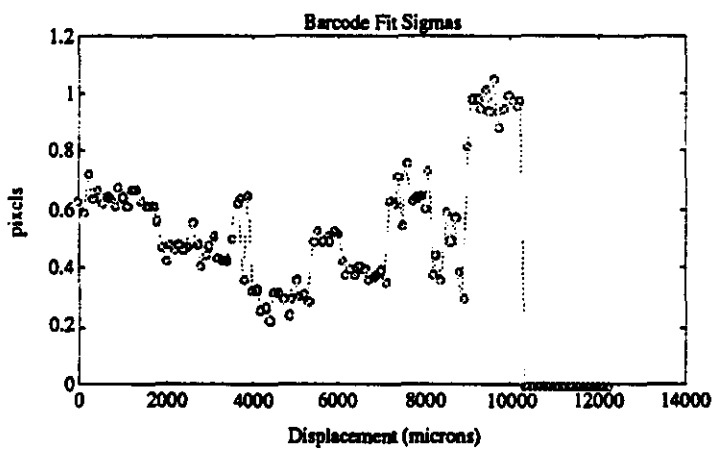

Calibration; CCD to Bar Code

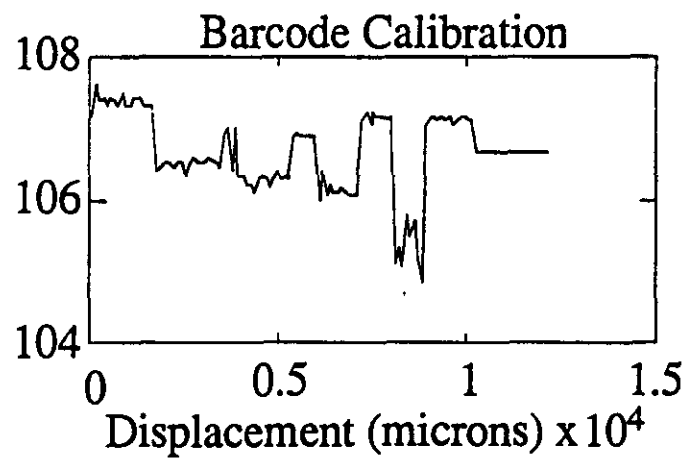

- 15 Frames averaged for 15 sec. (atmospheric dynamics @ Hz-level)
- Measurements taken over 13 mm.

GEM

Scan Test; Y Residual

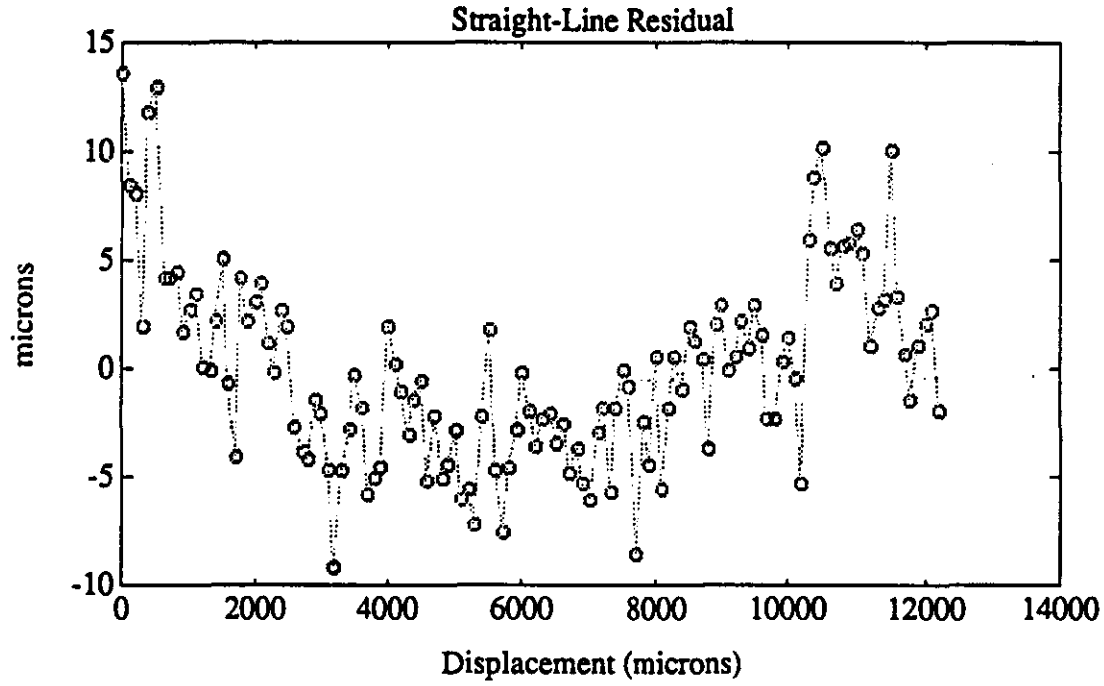

(No escape this time... ☛ test continuous over ≈2 hours)

Some systematic structure within ±10 μm
(i.e. film bent, flaws in film transfer, thermal effect)
True resolution under the 5 μm level?

- 15 Frames averaged for 15 sec. (atmospheric dynamics @ Hz-level)
- Measurements taken over 14 mm.

GEM

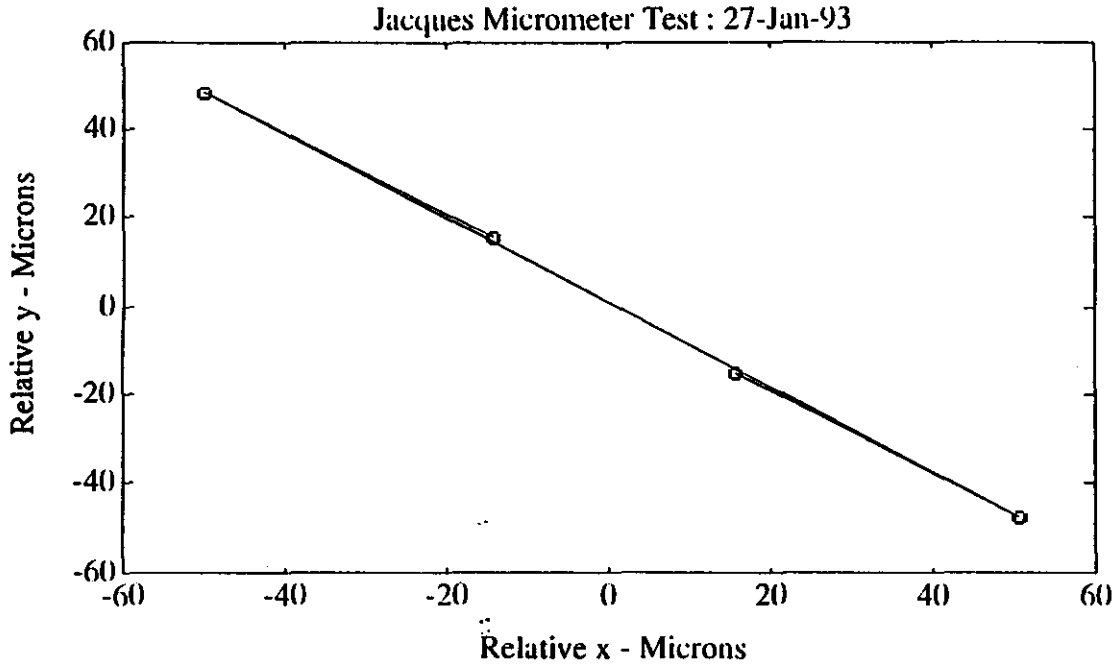

X	Y
-14.3819	15.2962
-49.8926	48.1731
50.8210	-47.6247
15.6086	-14.8726

Correct!!!!

CCD Improvements

- Cheap $170. camera arriving soon; will test.
  - Current camera has come thru hell; many image burns, defects...
- Can probably improve pattern-matching with correlation or more sophisticated algorithm (present one is quite simple)
- Much more barcode range from binary encoding and/or pairing digits!
  - Code directly in postscript to minimize nonuniformity.
  - Deposit pattern onto glass
- Will automate test scan
  - Less time (now takes 2 hours!), thermal effect limited (i.e. no MIT break).
  - More/better frame averaging.
  - Ono-Sokki computer-polled gauge arriving.
- Packaging!!!
  - Shrink distance between LED & field lens (or use other illumination).
  - Package & fiducialize CCD chip
  - Address magnetic field issues (RS-170 chip?)
  - Electronics for implementation (multiplexer, processor/DSP, etc...)

GEM

An Alternative Method

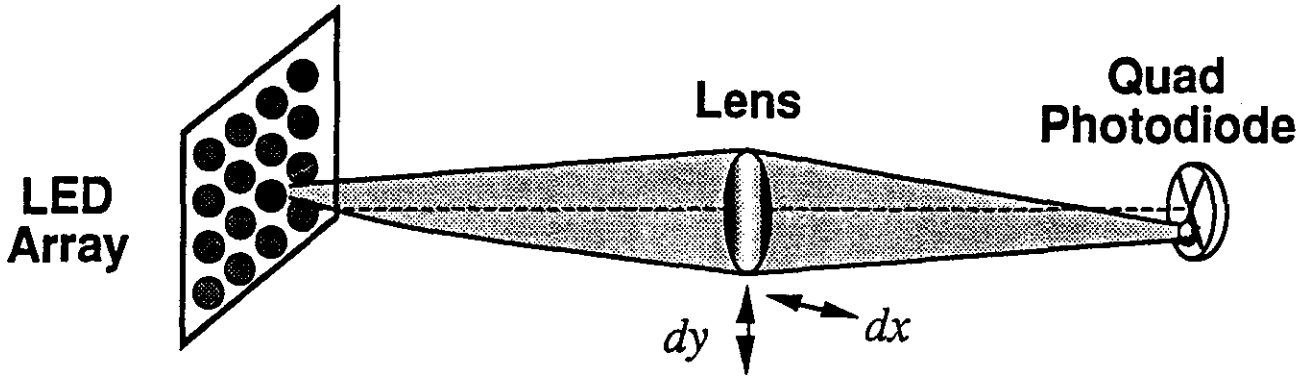

- Replace single LED with matrix of LED's.
  - Available as monolithic or moulded assemblies for displays
  - Wink LED's on/off sequentially, and interpolate between neighbors
  - Could still use quad cell if LED's are close enough
  - Issues are placement, precision, uniformity, light output.

    => Could use precision lensed LED's in machined mount...

- *Commercial LED blocks on order from Sharp and others (will test)*
- *Fiber bundle will be investigated (slip fibers into capillary spacers & bond)*

GEM

DOT MATRIX LED UNITS

Sharp has utilized the very latest optoelectronic technology to produce LED chips with unusually high light emission, suitable for either interior or outdoor use. Three colors can be displayed: red, yellow-green, and orange (by mixing red and yellow-green). The chips are unusually efficient, providing a good luminosity level at low current.

Sharp has been able to achieve a thin, light-weight design through its unique high-density design. This lets you be extremely flexible in your unit configurations, going to almost any size or shape. In addition, the fast response time can interface with the outputs of personal computers and other communication equipment.

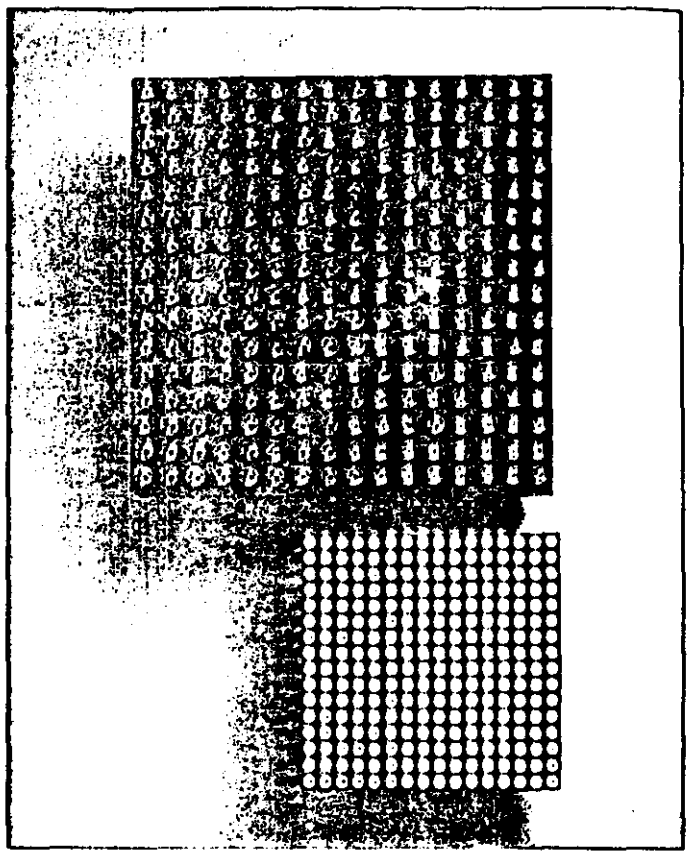

LED Units

Features:

- 16 x 16 dot matrix
- Active display sizes from 40 to 320 mm space.
- Red, yellow-green, and orange color
- Wide/narrow viewing angle
- Built-in shift registers, latch circuits, and LED driver ICs
- Clock frequency of 3 or 4 MHz (depending on model)
- Duty ratio 1/8 in LT1455M/LT1456M units, and 1/16 in LT1450ED/LT1460ED/LT1480ED units
- Static drive in LT1441M units

OUTLINE DIMENSIONS WxH (mm)	NO. OF DOTS WxH (pcs)	DOT SIZE (mm)	DOT PITCH (mm)	FOR INDOOR USE	FOR OUTDOOR USE
40x40	16x16	1.8 ø	2.5	LT1480ED	—
64x64	16x16	3 ø	4.0	LT1460ED	—
96x96	16x16	5 ø	6.0	LT1450ED	LT1455M, LT1456M
160x160	16x16	7.5 ø	10.0	—	LT1441M, LT1445M
320x320	16x16	18 ø	20.0	—	LT1470M

DOT MATRIX LED UNITS

Features

- Characters, symbols and graphics capability
- Display formats of 4 x 4, 8 x 8, or 16 x 16 dots
- Four series of radiation colors:
  - — Red (D series)
  - — Yellow-green (E series)
  - — Sunset orange (S series)
  - — Red, yellow-green, and orange (dichromatic ED series)

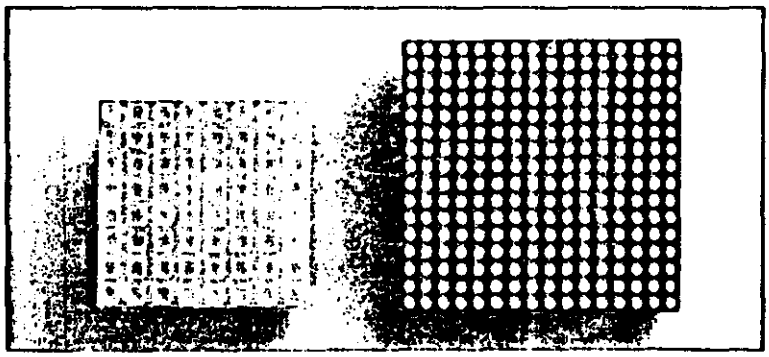

OUTLINE DIMENSIONS W X H (mm)		DOT SIZE (mm)	DOT PITCH (mm)	MODEL NO.	
8X8 DOTS	16X16 DOTS			8X8 DOTS	16X16 DOTS
16x16	32x32	1.4 ø	2	—	LT5014S
20x20	40x40	1.8 ø	2.5	LT5017ED	LT5005D LT5005E LT5005S
32x32	64x64	3 ø	4	LT5008E LT5008ED	LT5016ED
48x48	96x96	5 ø	6	—	LT5026ED

gem

γeμ

Presentation by:

P. Murat

2-cluster resolution study using TTR data (by EVENT mixing)

P. Muzat

02/03/93

→ 2-cluster resolution issue is mostly important for:
neutron background
1st superlayer (background from calorimeter)

→ It is possible to study 2-cluster resolution using EVENT mixing (MATX) (ASSUMING LINEAR RESPONCE)

⇒ Several methods OF DEFINING SINGLE CLUSTER CENTROID:
* ratio methods
* CENTROID methods (GAUSSIAN etc)
...

How do ther work FOR 2 clusters?

→ WHAT WAS DONE:

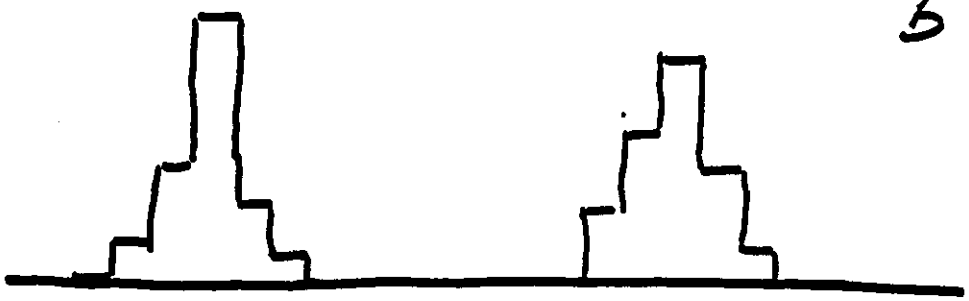

5 most SIGNIFICANT STRIPS

* CHARGE DISTRIBUTIONS FROM 2 clusters RECONSTRUCTED FROM DIFFERENT EVENTS WERE SUPERIMPOSED

* THEN POSITION OF EACH CLUSTER WAS DETERMINED FROM SUM CHARGE DISTRIBUTION

* "MOVING" CLUSTERS TO EACH OTHER WE MAY STUDY DEPENDENCE OF RESOLUTION ON DISTANCE BETWEEN CLUSTERS:

$$\Delta Y = Y_{RECONSTRUCTED} - Y_{KNOWN}$$

* BECAUSE THE REAL DATA ARE USED THE STEP, BY WHICH CLUSTERS CAN BE MOVED IS PROPORTIONAL TO STRIP PITCH

CHARGE DISTRIBUTIONS FOR DIFFERENT CLUSTER STRIPS

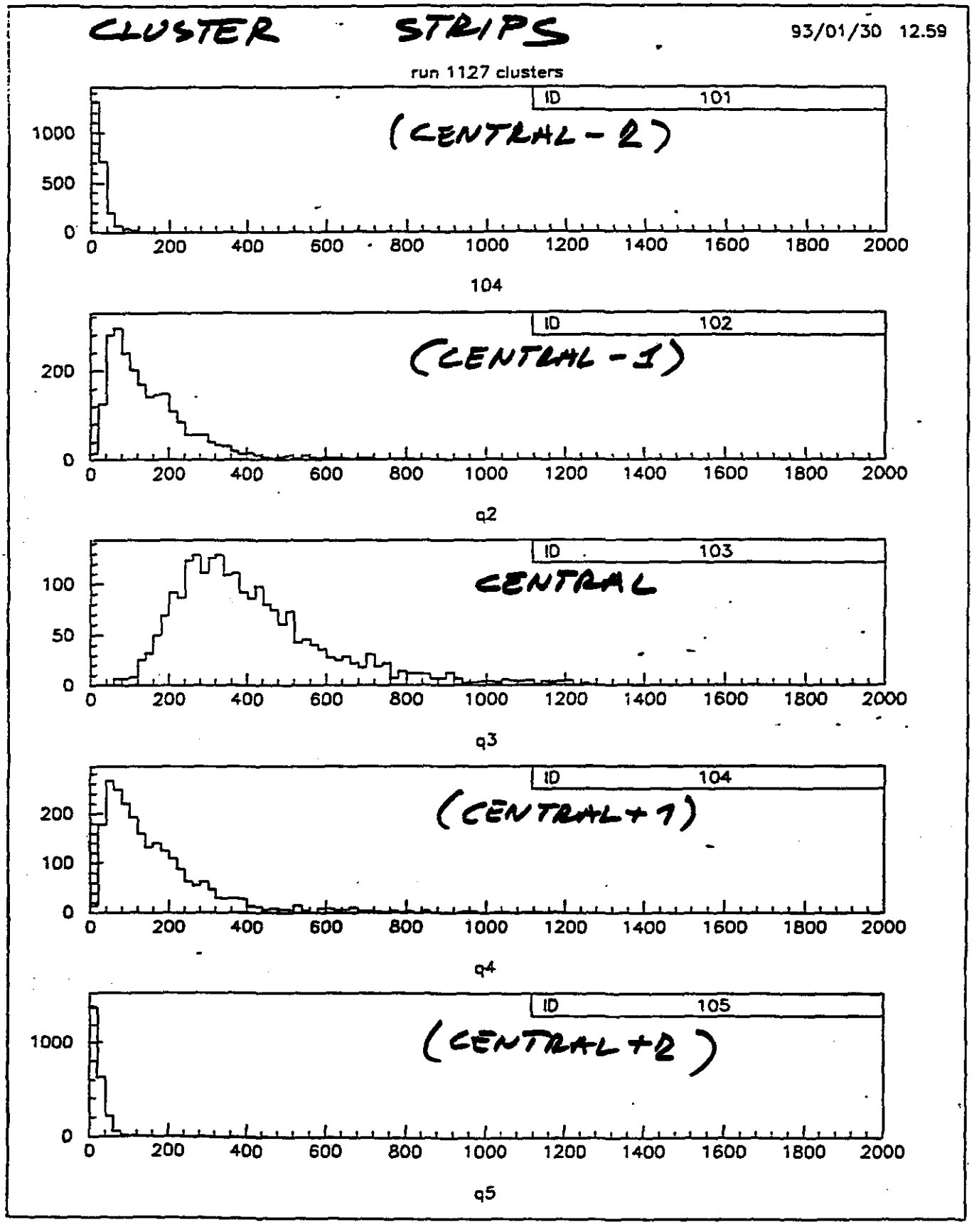

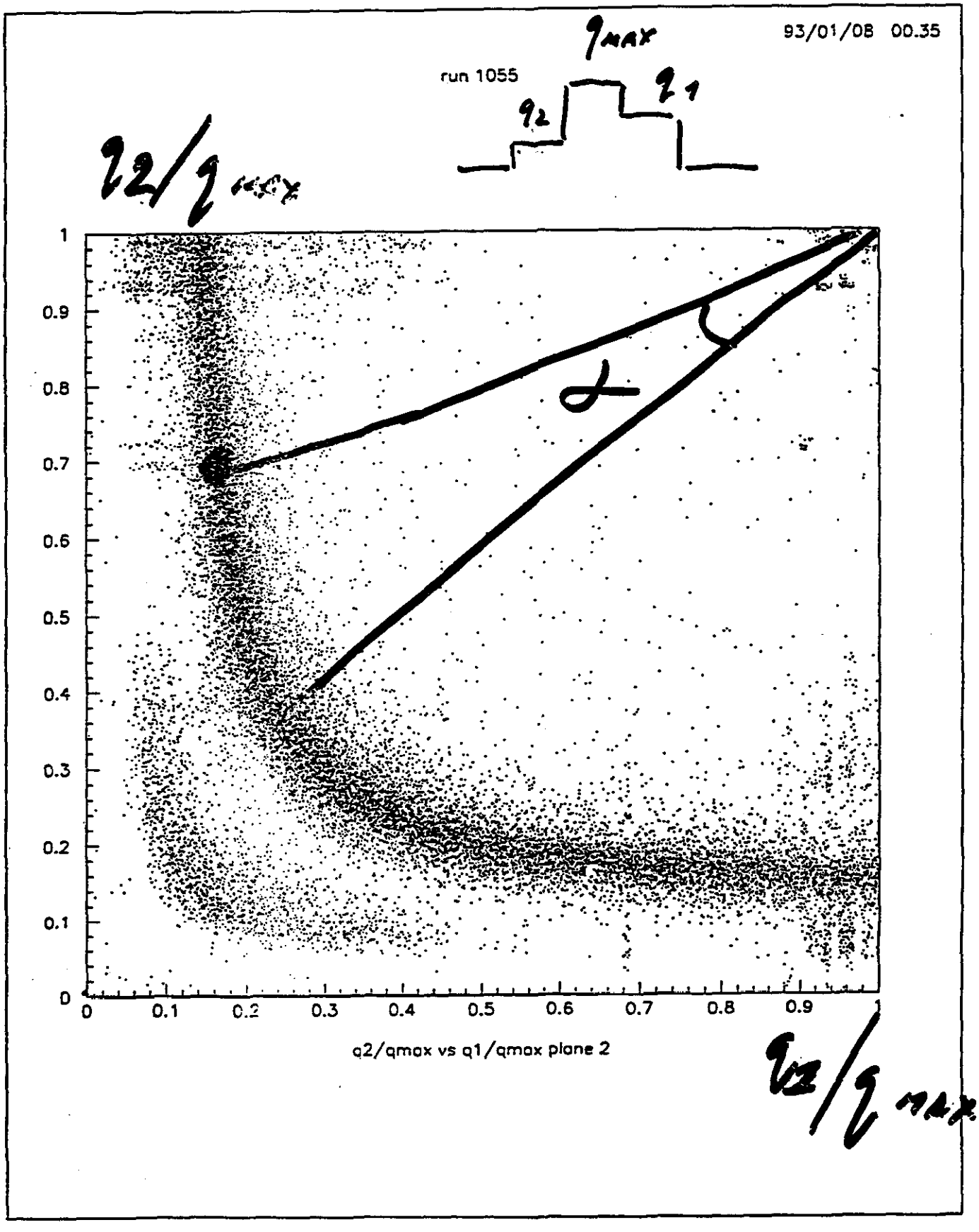
93/01/08 00.35
run 1055
q_{MAX}
q_2
q_1
q_2/q_{MAX}
α
1
0.9
0.8
0.7
0.6
0.5
0.4
0.3
0.2
0.1
0
0
0.1
0.2
0.3
0.4
0.5
0.6
0.7
0.8
0.9
1
q2/qmax vs q1/qmax plane 2
q_1/q_{MAX}

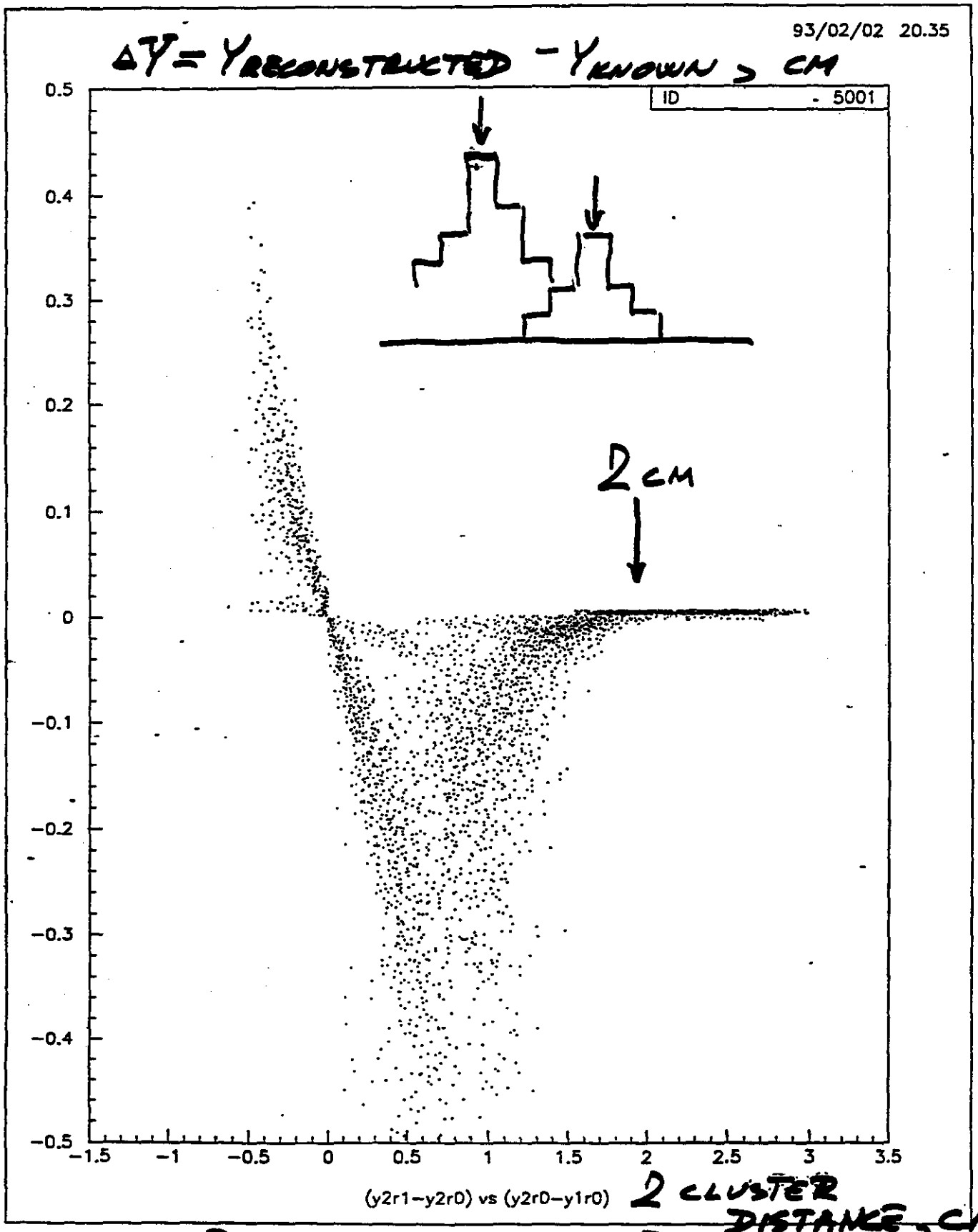

RATIO METHOD

charge ratio wrong. [illegible]

CLUSTER WIDTH VS DELTA

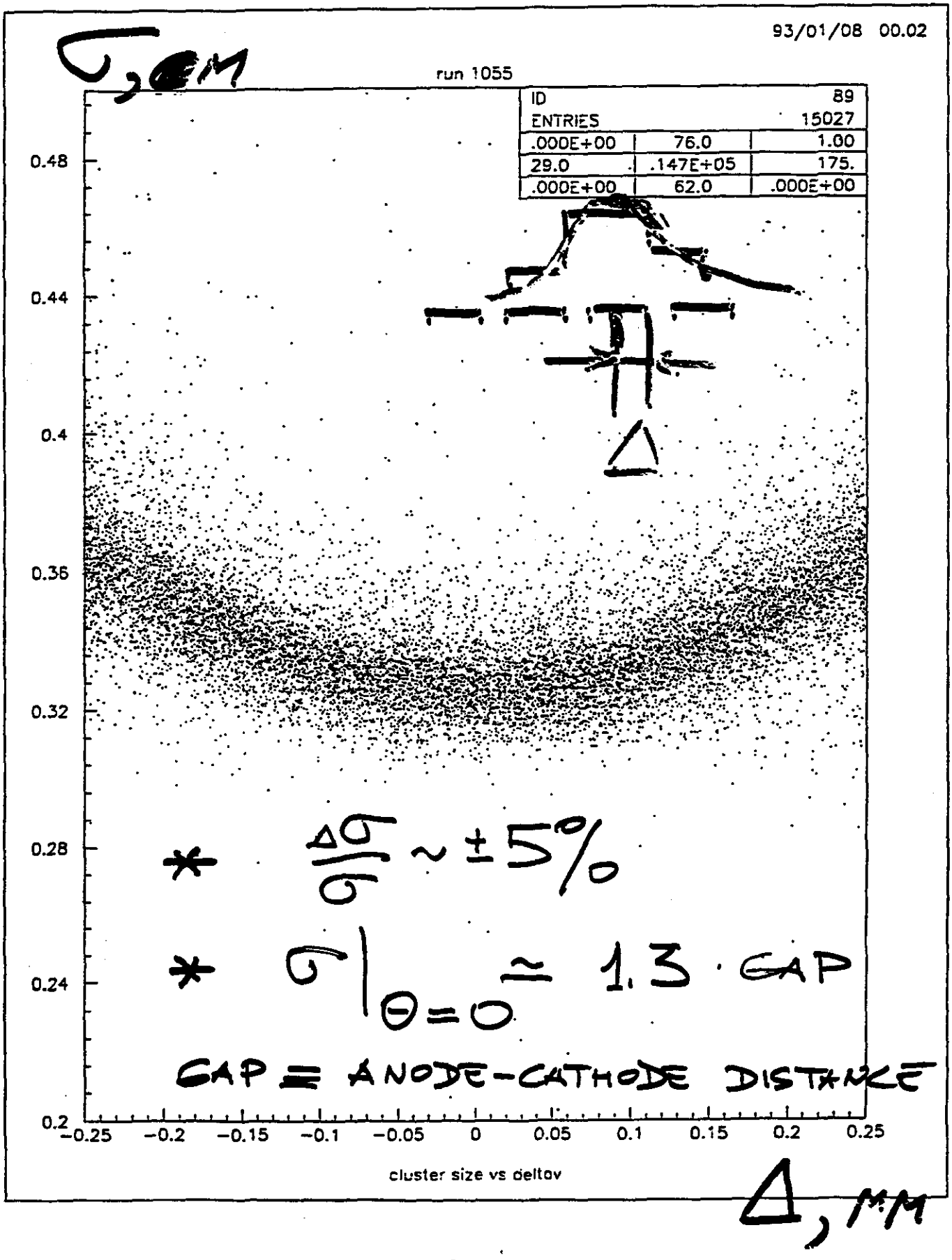

* $\frac{\Delta\sigma}{\sigma} \sim \pm 5\%$

* $\sigma\big|_{\Theta=0} \simeq 1.3 \cdot GAP$

GAP = ANODE-CATHODE DISTANCE

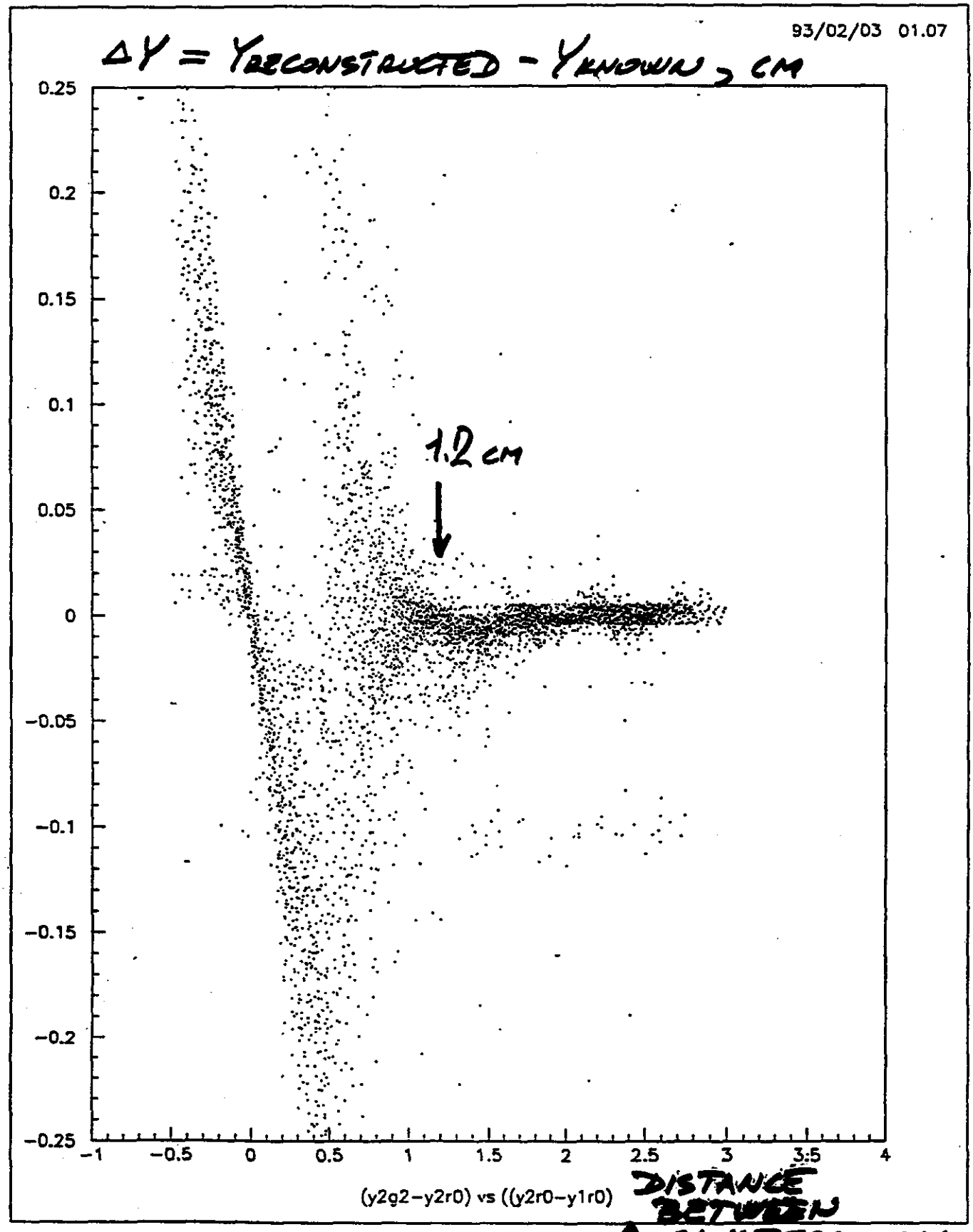

CLUSTER CENTROID FITTING BY GAUSSIAN

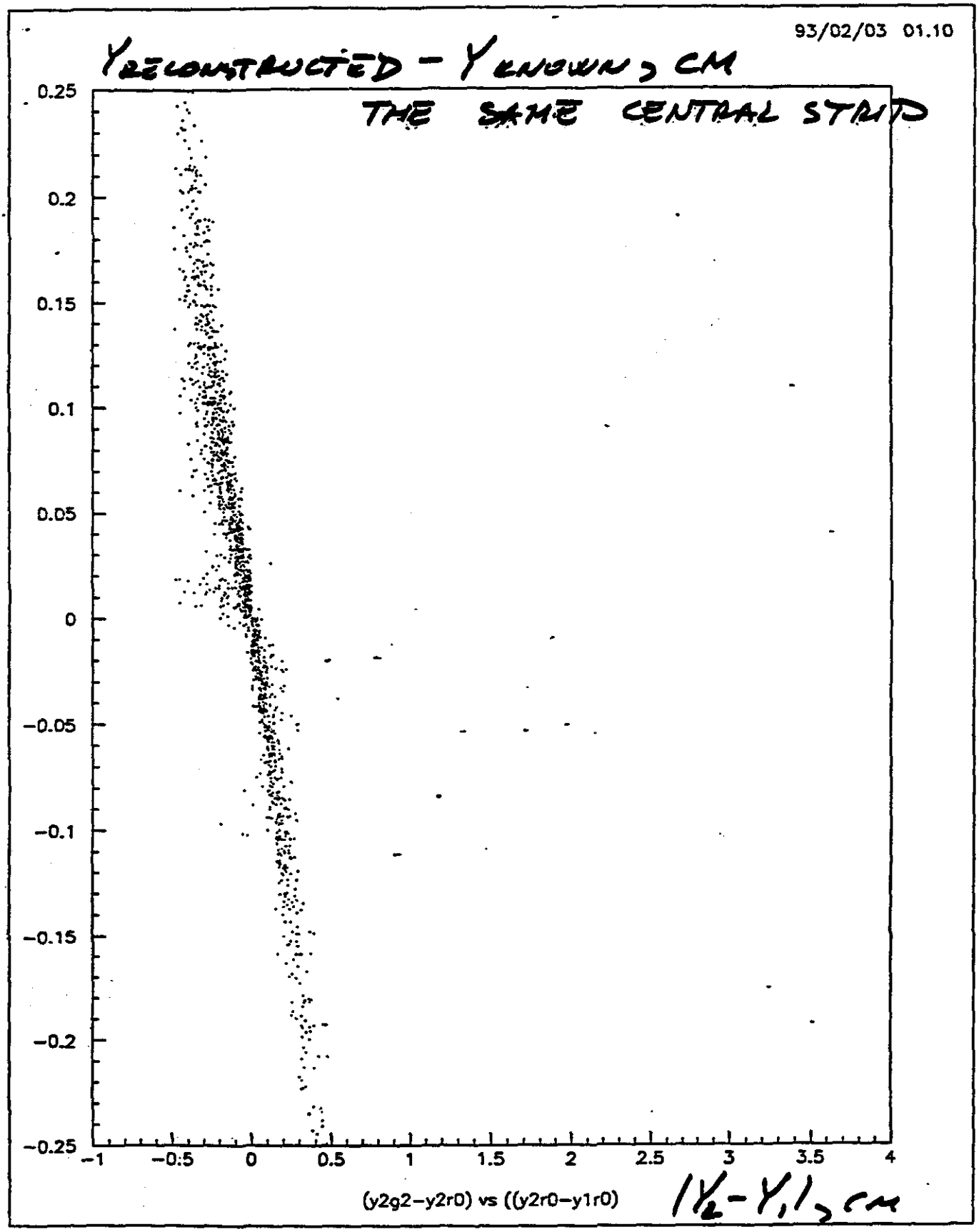
93/02/03 01.10
Y2RECONSTRUCTED - Y KNOWN, CM
THE SAME CENTRAL STRIP
0.25
0.2
0.15
0.1
0.05
0
−0.05
−0.1
−0.15
−0.2
−0.25
−1
−0.5
0
0.5
1
1.5
2
2.5
3
3.5
4
(y2g2−y2r0) vs ((y2r0−y1r0)
|Y2-Y1|, CM

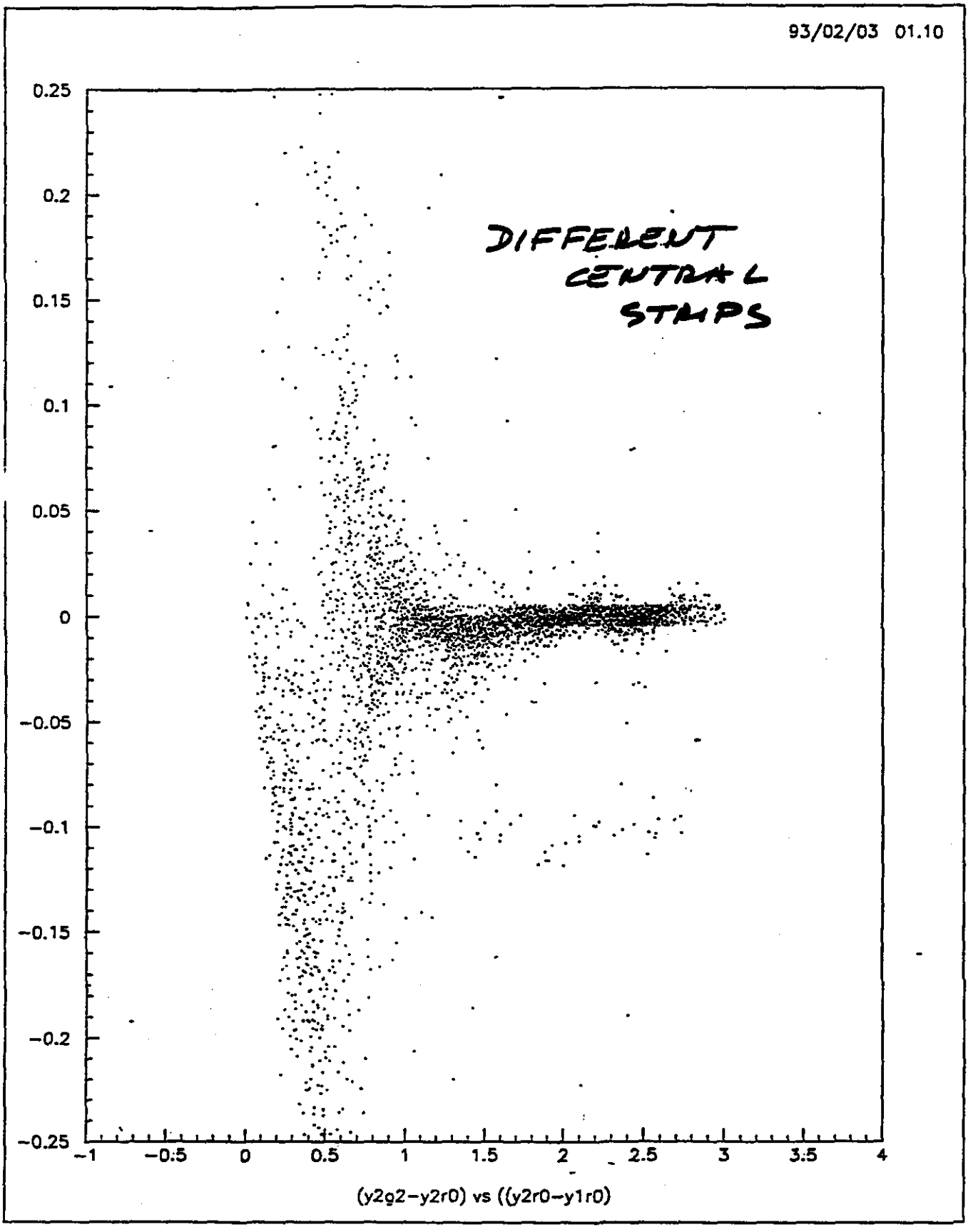
93/02/03 01.10
DIFFERENT
CENTRAL
STRIPS
0.25
0.2
0.15
0.1
0.05
0
−0.05
−0.1
−0.15
−0.2
−0.25
−1
−0.5
0
0.5
1
1.5
2
2.5
3
3.5
4
(y2g2−y2r0) vs ((y2r0−y1r0)

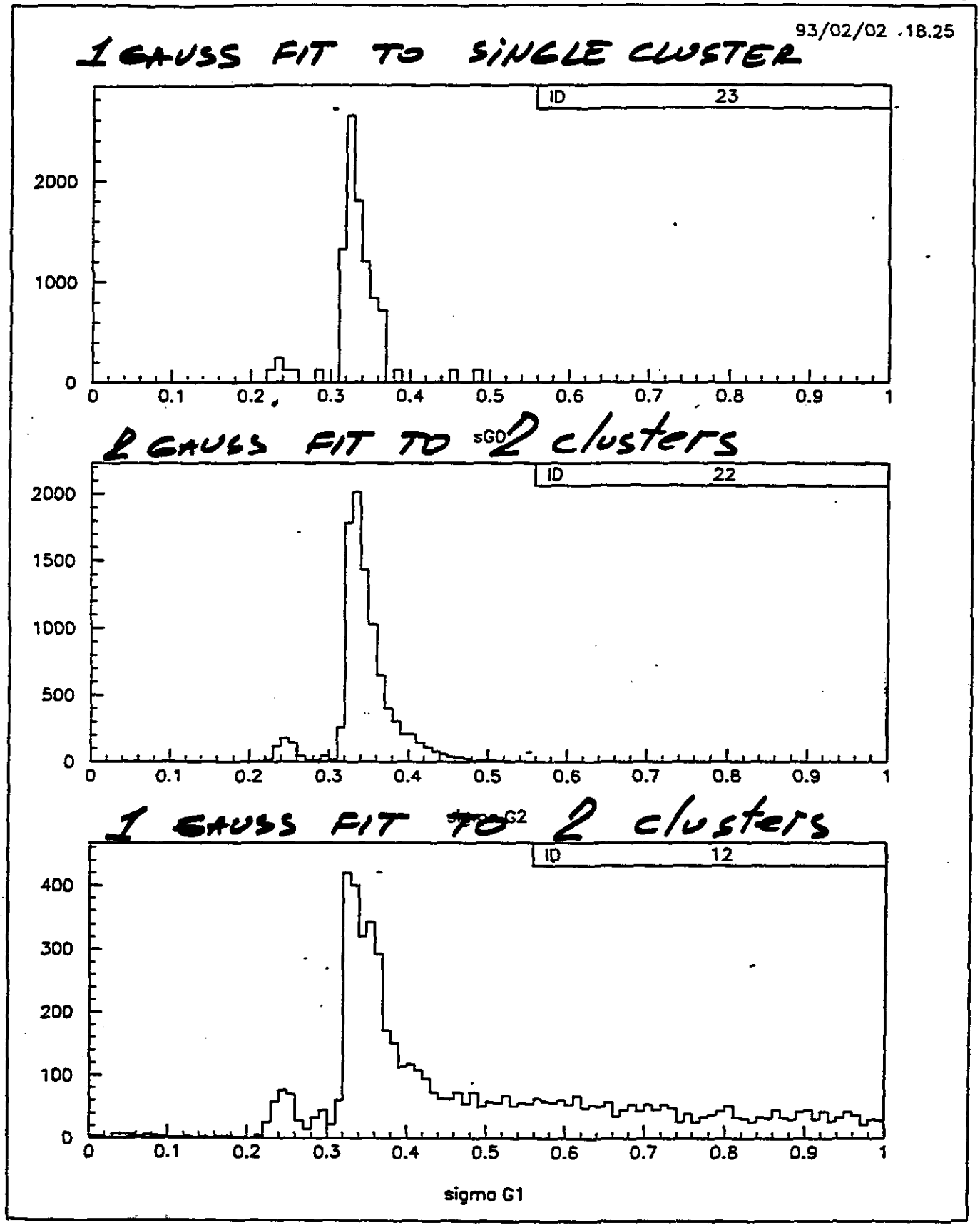

SIGMA DISTRIBUTIONS FOR DIFFERENT GAUSSIAN FITS

CLUSTER RESIDUALS FROM THE TRACK

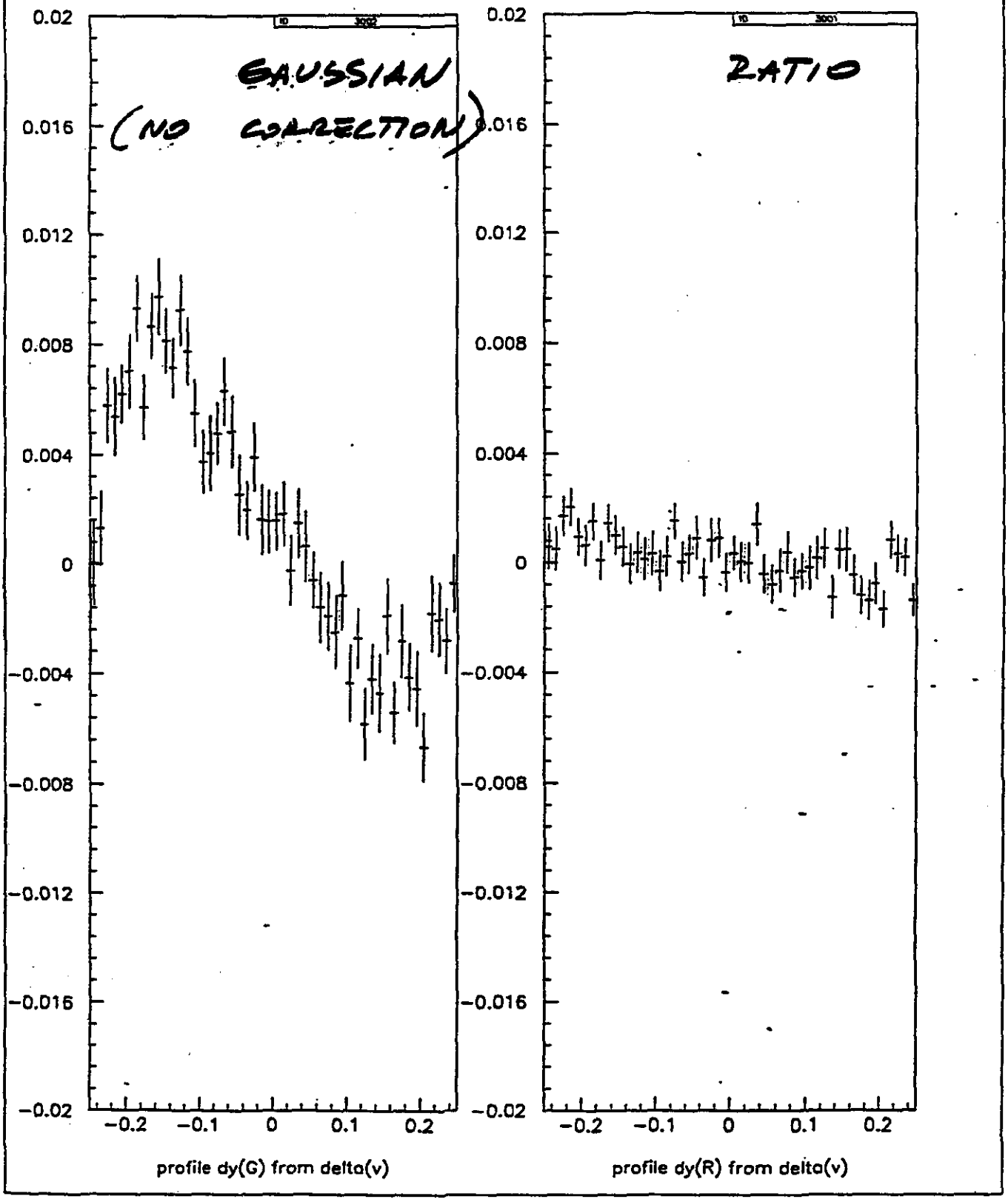

DELTA = $Y_{CLUSTER} - Y$(CENTRAL STRIP)

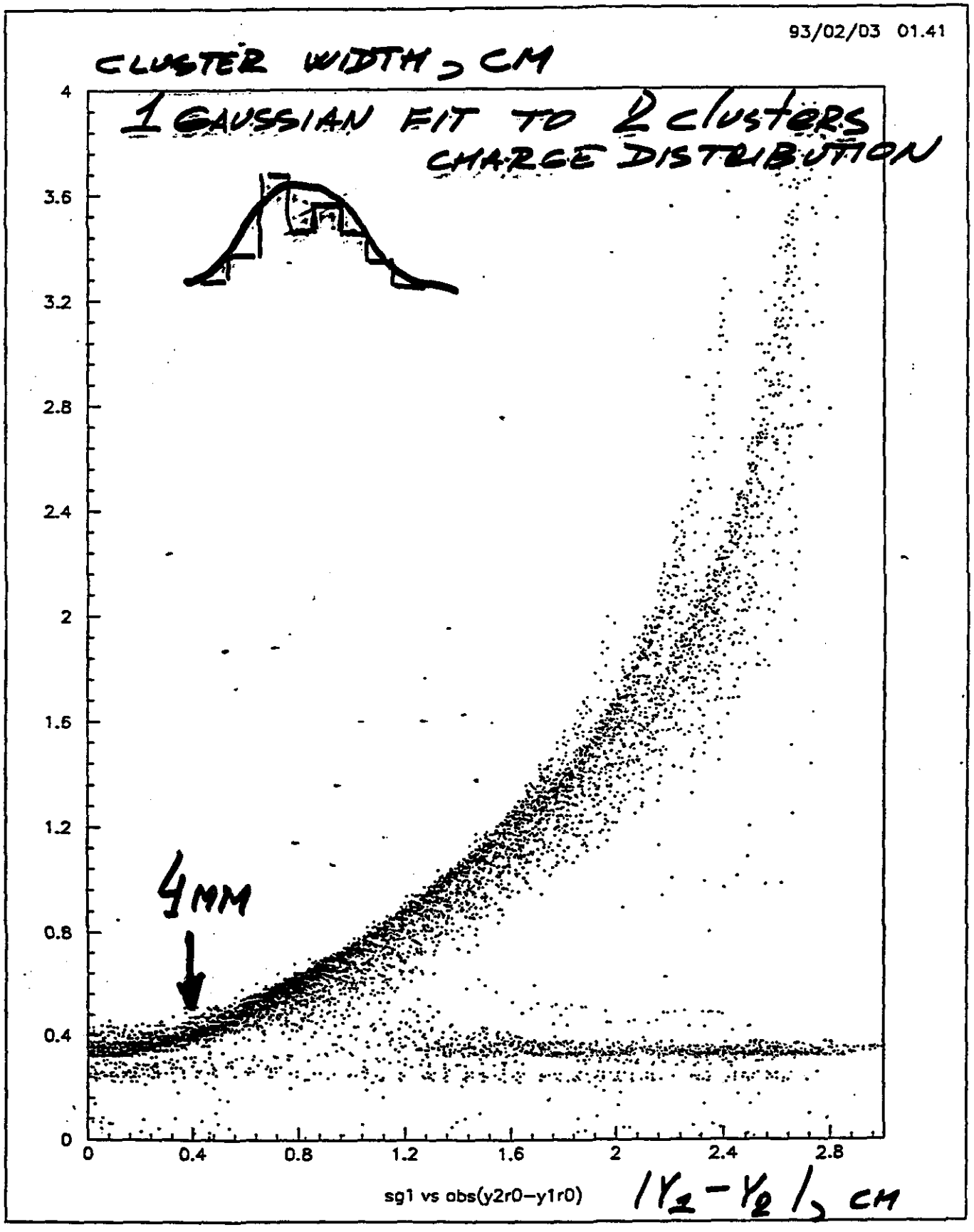
93/02/03 01.41
CLUSTER WIDTH, CM
1 GAUSSIAN FIT TO 2 CLUSTERS CHARGE DISTRIBUTION
4MM
4
3.6
3.2
2.8
2.4
2
1.6
1.2
0.8
0.4
0
0
0.4
0.8
1.2
1.6
2
2.4
2.8
sg1 vs obs(y2r0−y1r0)
|Y1 − Y2|, CM

Conclusions

* RATIO METHOD WORKS WHEN DISTANCE BETWEEN CLUSTERS IS

$\gtrsim$ 4 strips

* GAUSSIAN CENTROID FITTING WORKS DOWN TO

$\gtrsim$ 2 strips (BUT RESOLUTION IS WORSE, THEN FOR RATIO METHOD)

* IF 2 CLUSTERS ARE CLOSER THEN ~ CLUSTER WIDTH (~ 1.3 GAP).

(FOR DUBNA CSC : σ ~ 0.6 pitch)

WE CANNOT DISTINGUISH THEM FROM ONE CLUSTER

gem

γeμ

Presentation by:

R. McNeil

R. McNeil
Feb, 1993

Reconstructing Light Higgs Mass with Baseline Z Calorimeter

Consider only Calorimeter effects (perfect momentum measurement)

$$E_\nu^{OUT} = E_\nu^{IN} - E_\nu^{LOSS} + E_\nu^{CAL}$$

$$E_\nu^{CAL} = E_\nu^{MEAS}\Big|_{\substack{\text{Thru}\\ \text{Active Cal}}} + \langle E_\nu \rangle^{loss}\Big|_{\substack{\text{Thru}\\ \text{Passive Cal}}}$$

Baseline Z Calorimeter

Barrel:

	Mat'l	depth @ 90°	σ_E
EM Section	Pb/LKr	1.3 λ	$6\%\sqrt{E}$ + .04 GeV
HAD Section	Pb/LKr	4.0 λ	$20\%\sqrt{E}$ + .16 GeV
Tail Catcher	Cu/Scint (8%)	3.7 λ	$A\sqrt{E}$ + 2% E
Passive Mat'l	Al, LKr, Fe	2.0 λ	No measmt ($\langle E_{loss} \rangle$)

End Cap:

	Mat'l	depth @ η=2.5	σ_E
EM Section	Pb/LAr	1.6 λ	$6\%\sqrt{E}$ + .04 GeV
HAD Section	Cu/LAr	9.0 λ	$20\%\sqrt{E}$ + .16 GeV
Tail Catcher	Cu/Scint (8%)	3.5 λ*	$A\sqrt{E}$ + 2% E
Passive Mat'l	Al, LAr	1.0 λ	no measmt

* 4.5 λ in Baseline Z (using W as mat'l?) ~ 12 cm/λ

GEM Calorimeter

η=1.06 1.125

38° 35.06°

	Weight	Volume
Barrel Calorimeter	= 433 Mg	24135 L. LKr
2 Endcap Total	= 759 Mg	38475 L. LAr
Scint. Cal. & St. St.	= 1236 Mg	
2 Endcap PA Total	= 196 Mg	
2 FWH Total	= 30 Mg	
	2654 Mg	

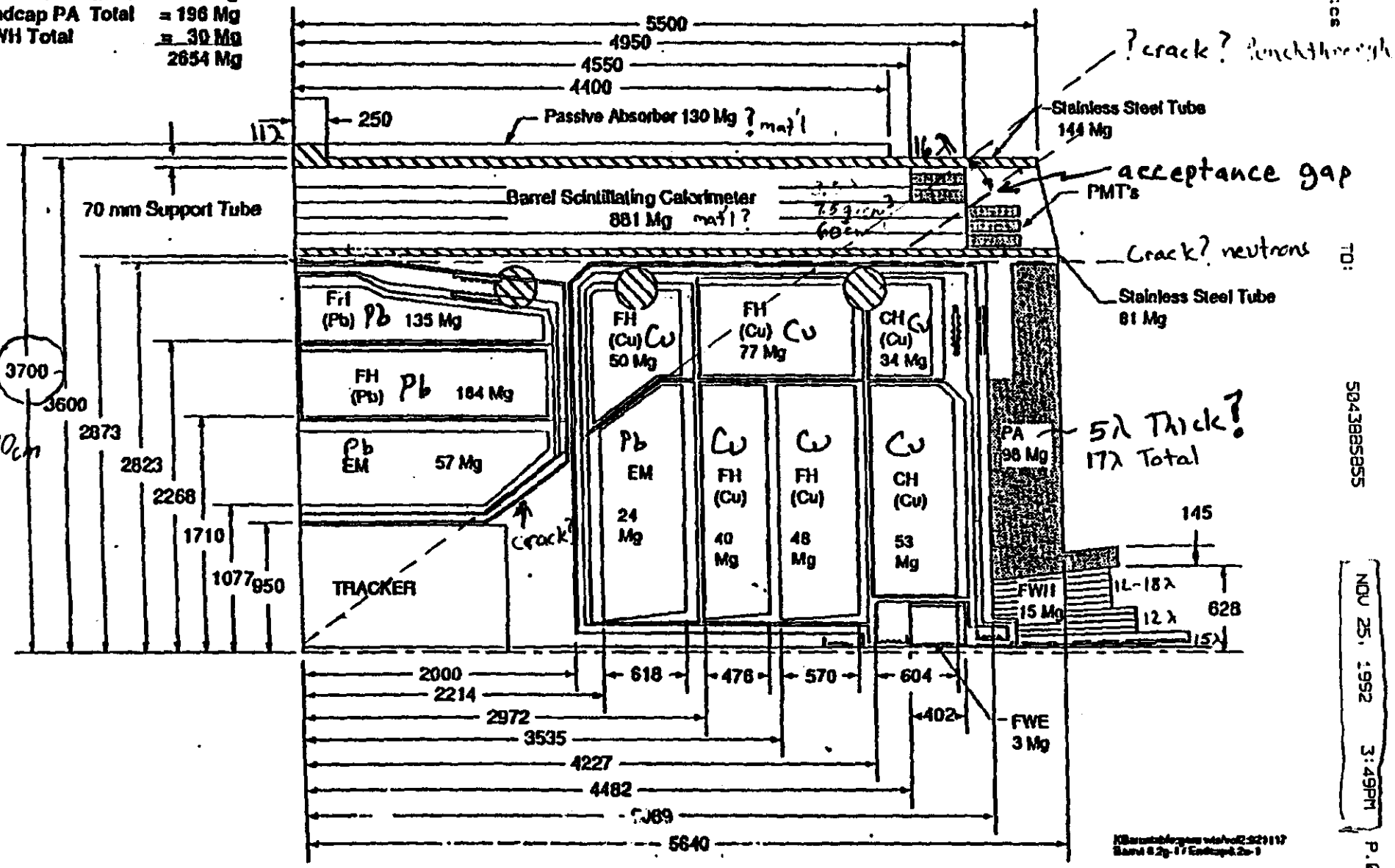

128

GEANT Geometry for simulation of Muons through Baseline 2 Calorimeter.

Boriated Polyethelene + Pb is <u>not</u> considered in the following analysis

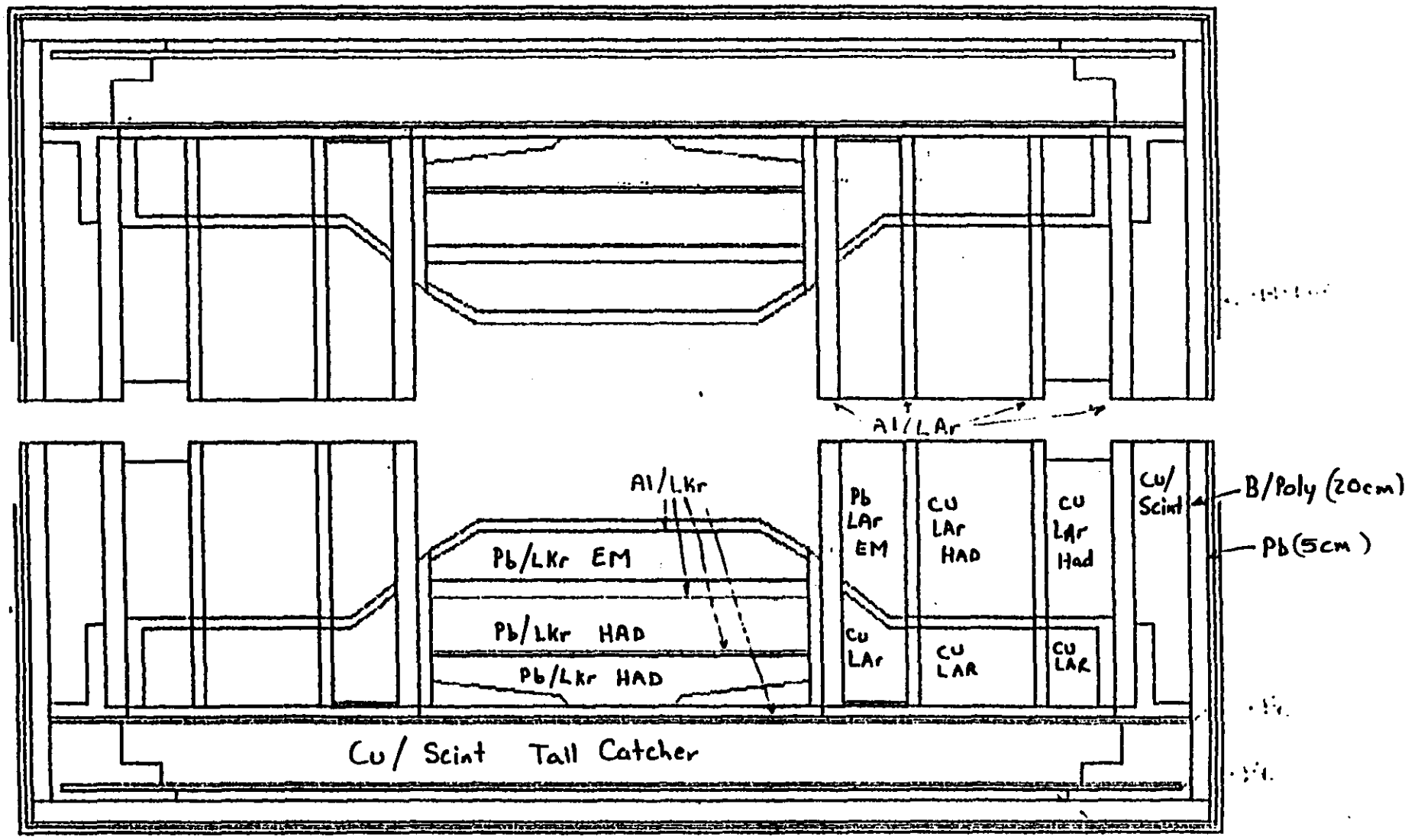

Baseline Z Calorimeter
Depth of Calorimeter vs η

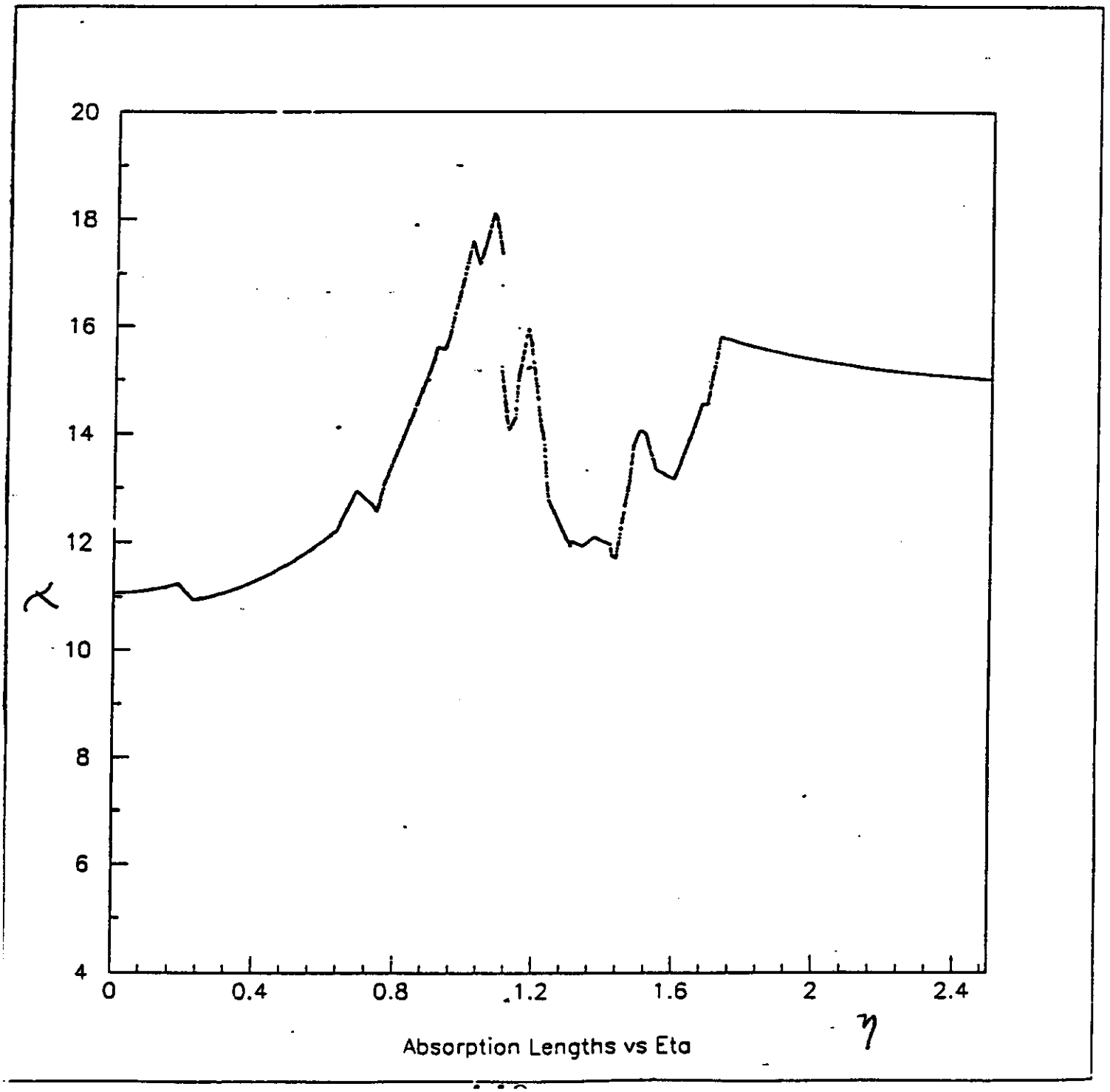

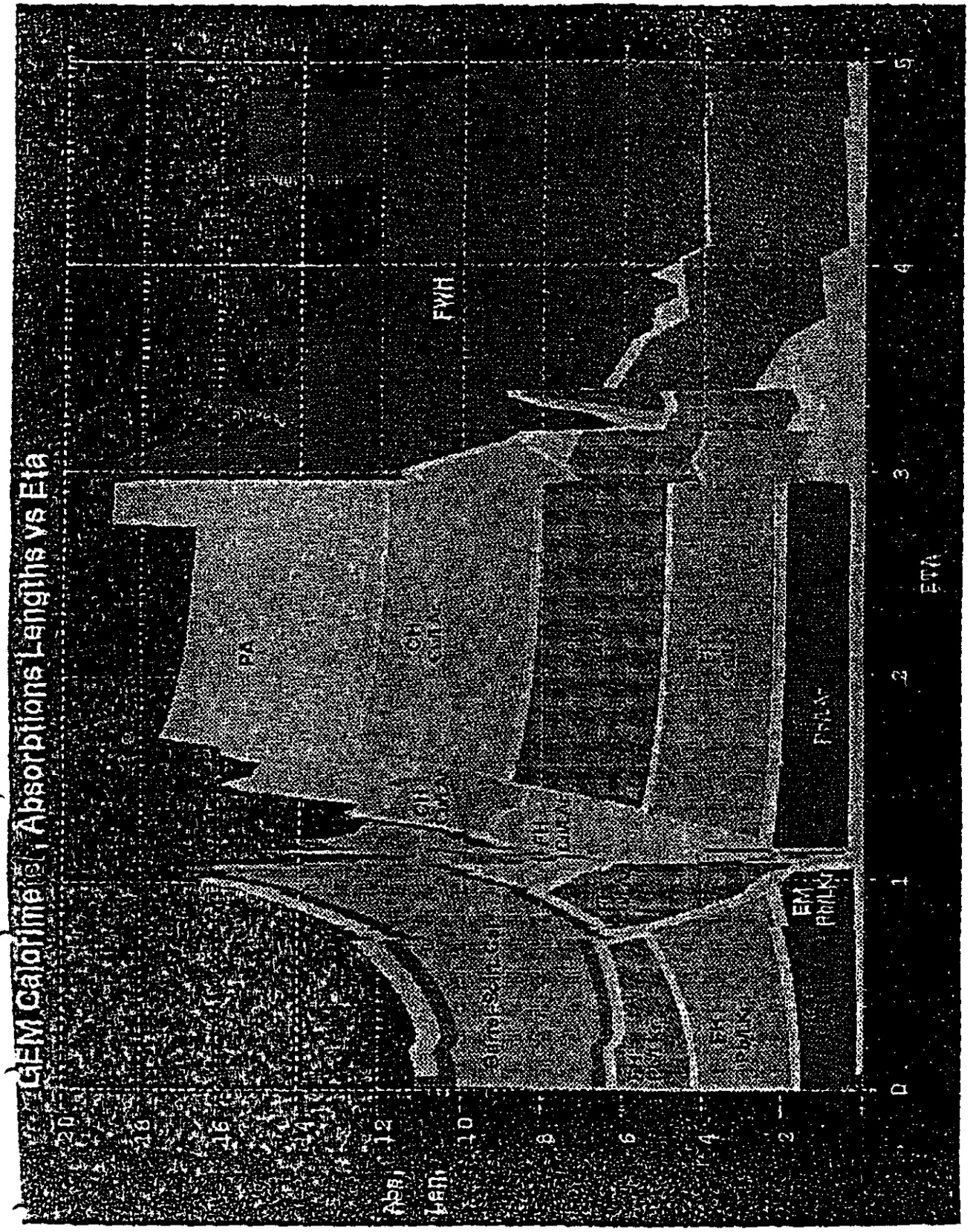
GEM Calorimeter Absorbtions Lengths vs Eta
Abs. Len.
ETA
FWH
PA
CH
EM
PHLKY
0
1
2
3
4
5
2
4
6
8
10
12
14
16
18
20

Baseline 2 Calorimeter

Depth of Active Calorimeter vs η

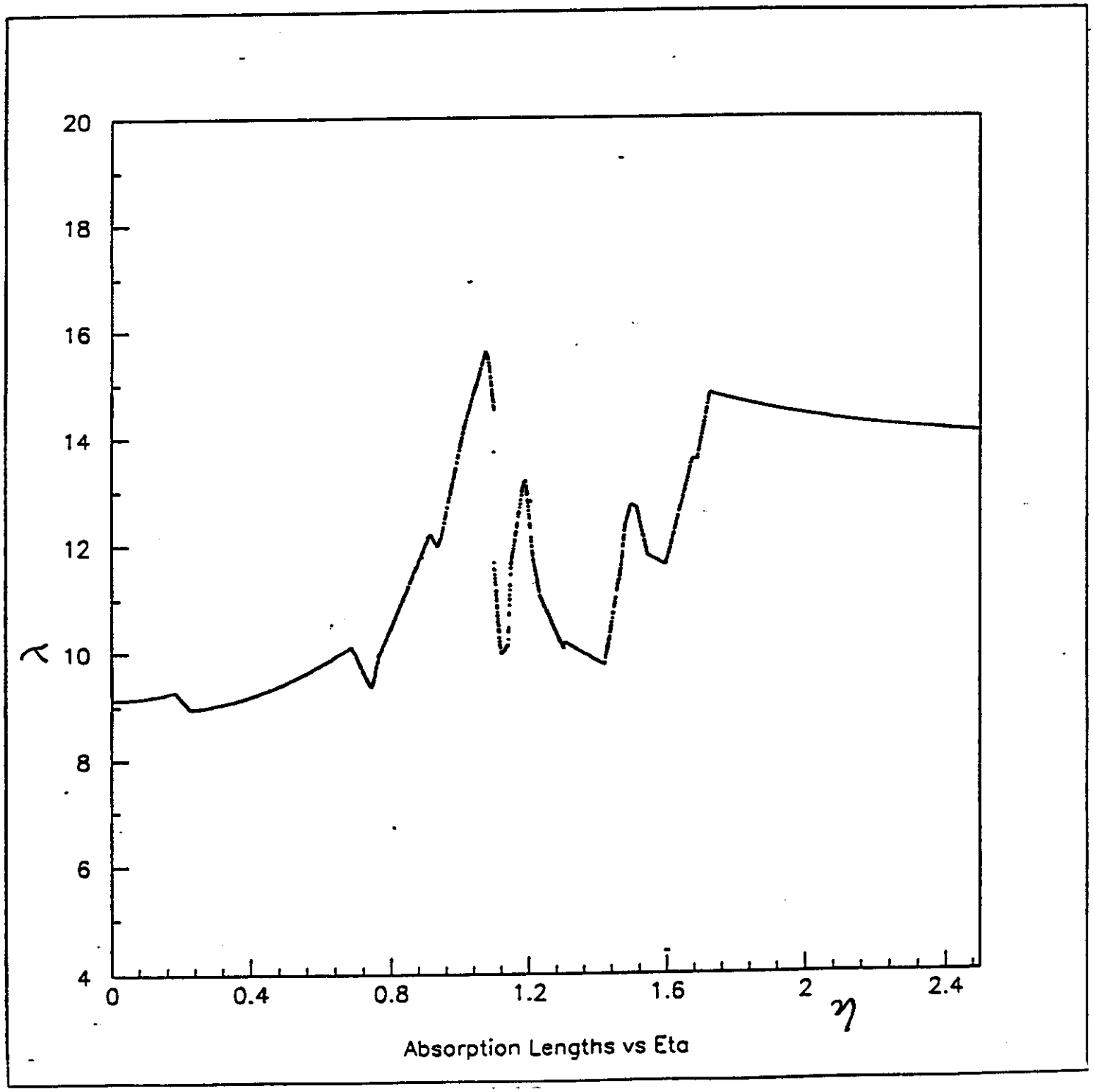

150GeV/c² Higgs → 4ν

E MC Pb/LKr Barrel
Pb/LAr End Cap

$$\frac{\sigma_E}{E} = \frac{6\%}{\sqrt{E}} \oplus \frac{40\,\mathrm{MeV}}{E}$$

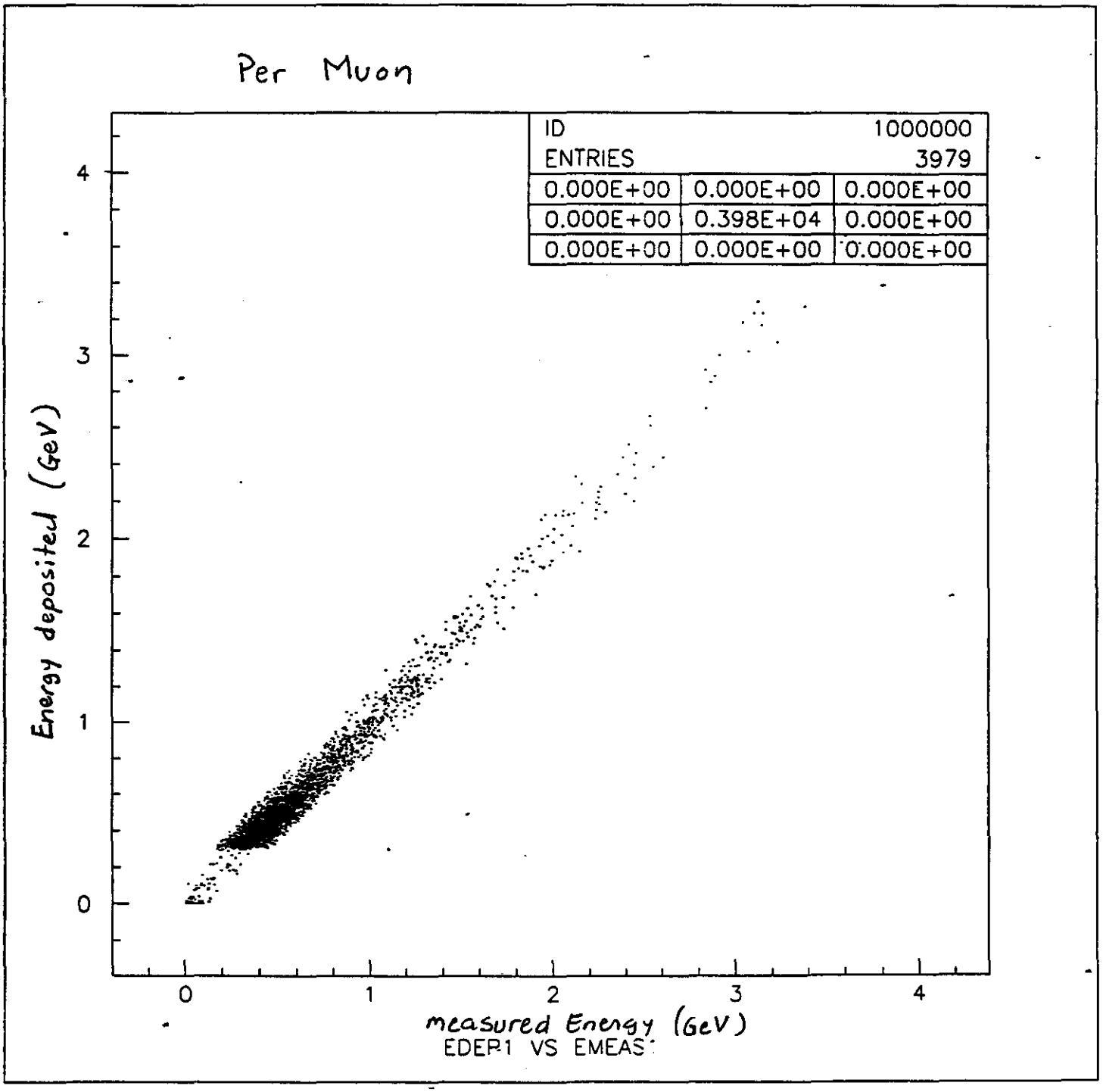

150 GeV/c² Higgs → 4ν

Liquid Hadronic Cal

Pb/LKr Barrel $\frac{\sigma_E}{E} = \frac{20\%}{\sqrt{E}} \oplus \frac{160\,\text{MeV}}{E}$

Cu/LAr EndCap

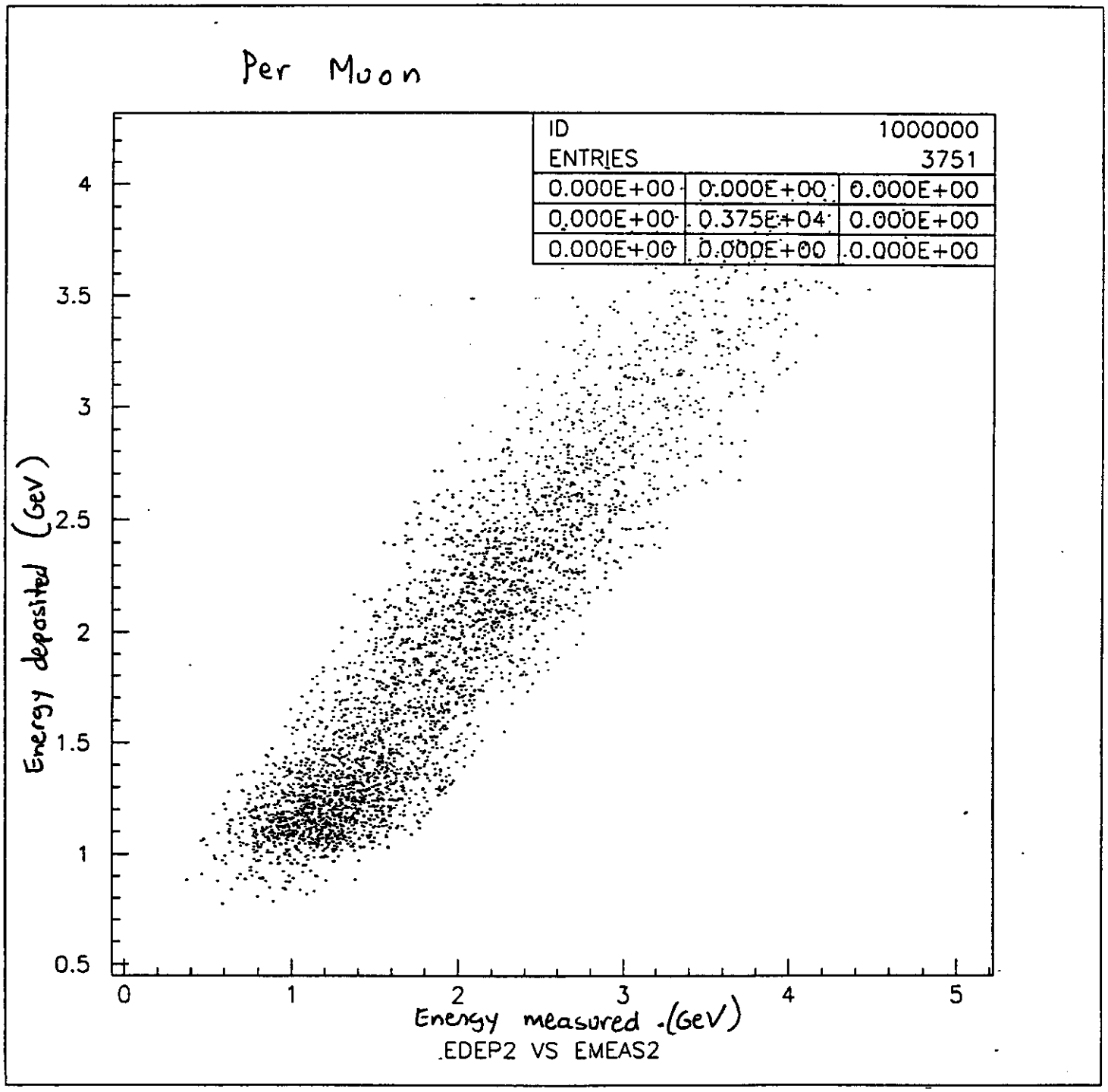

150 GeV/c² Higgs → 4ν

Tail Catcher

Cu/scint Barrel

Cu/scint EndCap

$$\frac{\sigma_E}{E} = \frac{20\%}{\sqrt{E}} \oplus 2\%$$

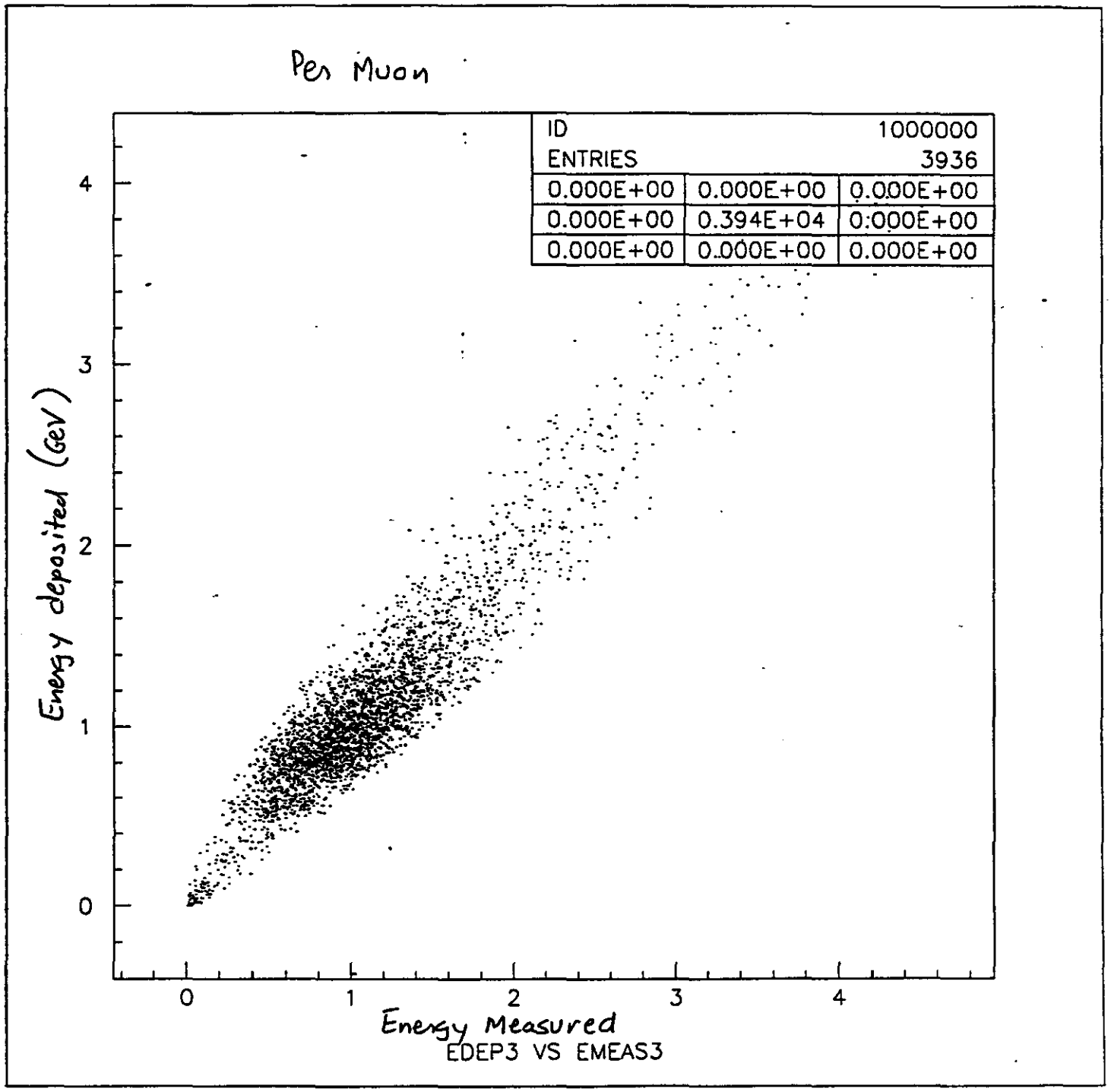

150 GeV/c^2 Higgs $\rightarrow 4\nu$

Tail Catcher

Cu/scint Barrel

Cu/scint EndCap

$$\frac{\sigma_E}{E} = \frac{90\%}{\sqrt{E}} \oplus 2\%$$

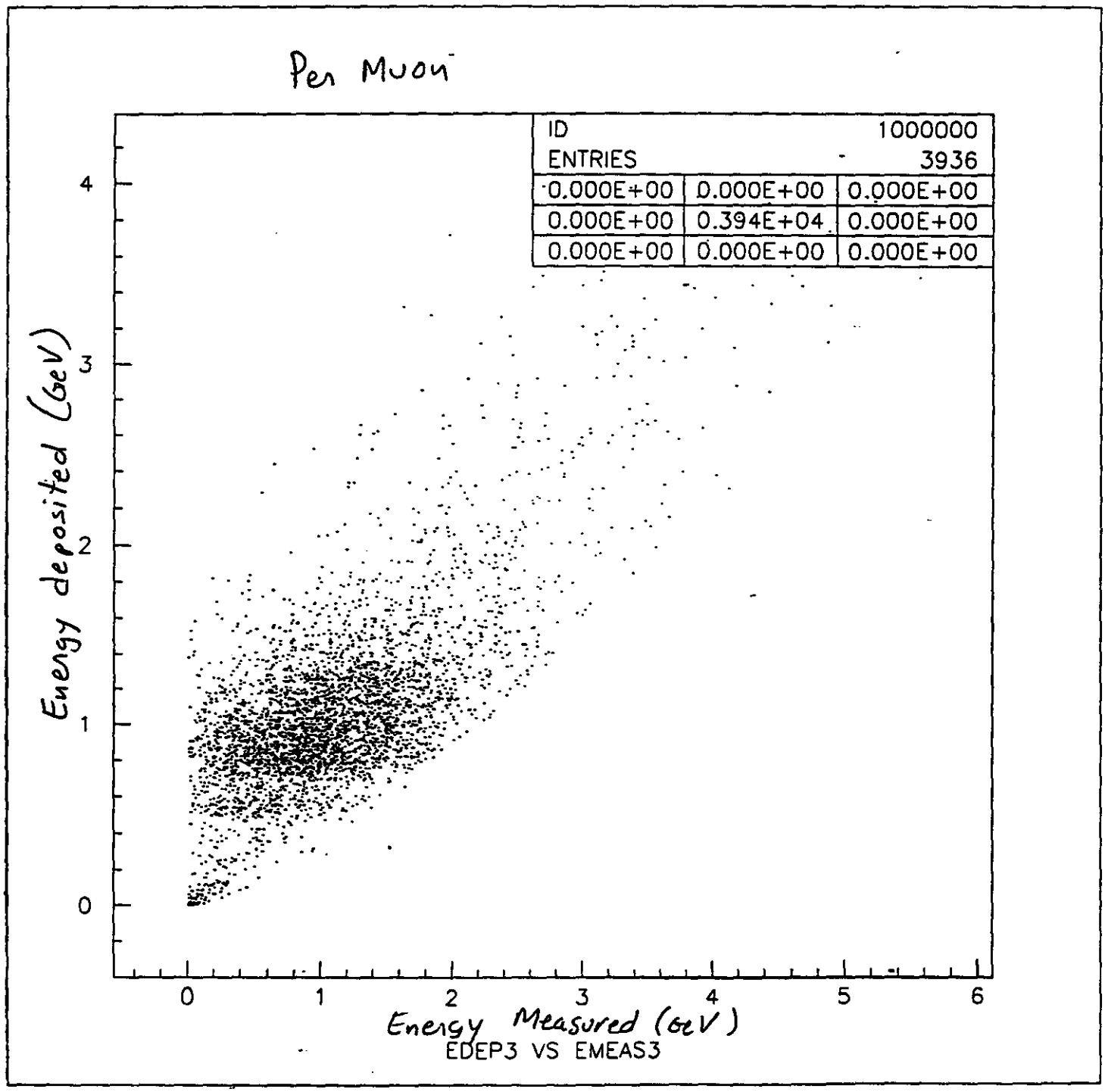

150GeV/c² Higgs → 4ν (only Muons simulated)

Baseline 2 Calorimeter

Assume Perfect Momentum reconstruction

EM resolution $\frac{6\%}{\sqrt{E}} + .040\frac{GeV}{E}$

Liquid HAD resolution $\frac{20\%}{\sqrt{E}} + \frac{.160GeV}{E}$

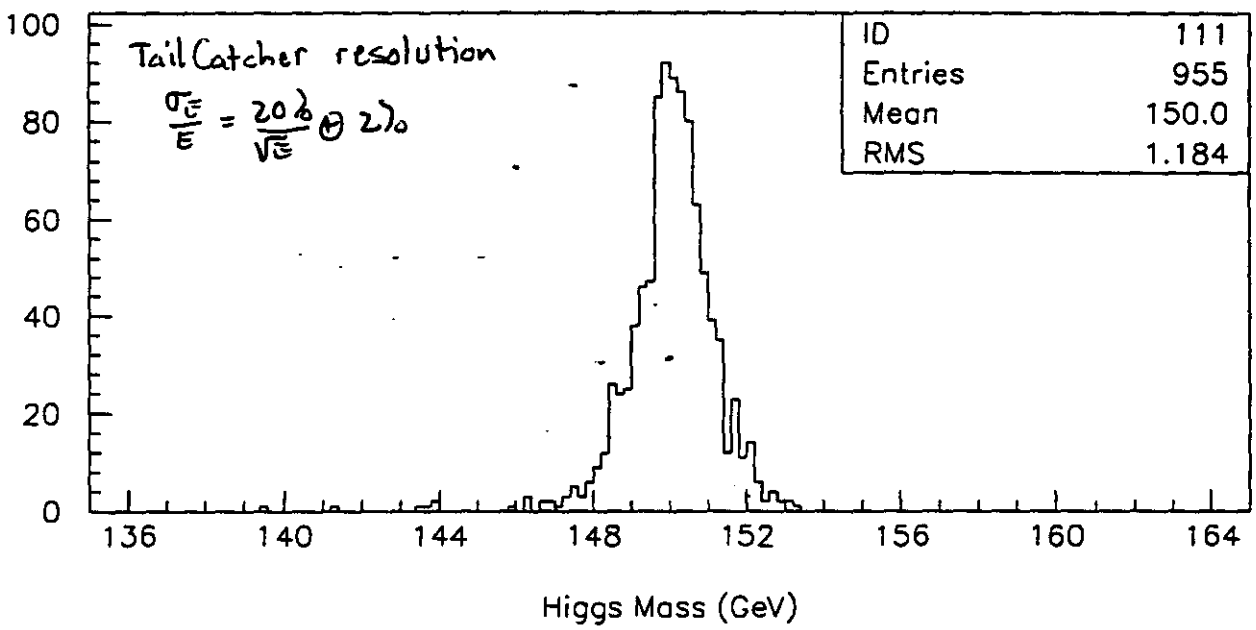

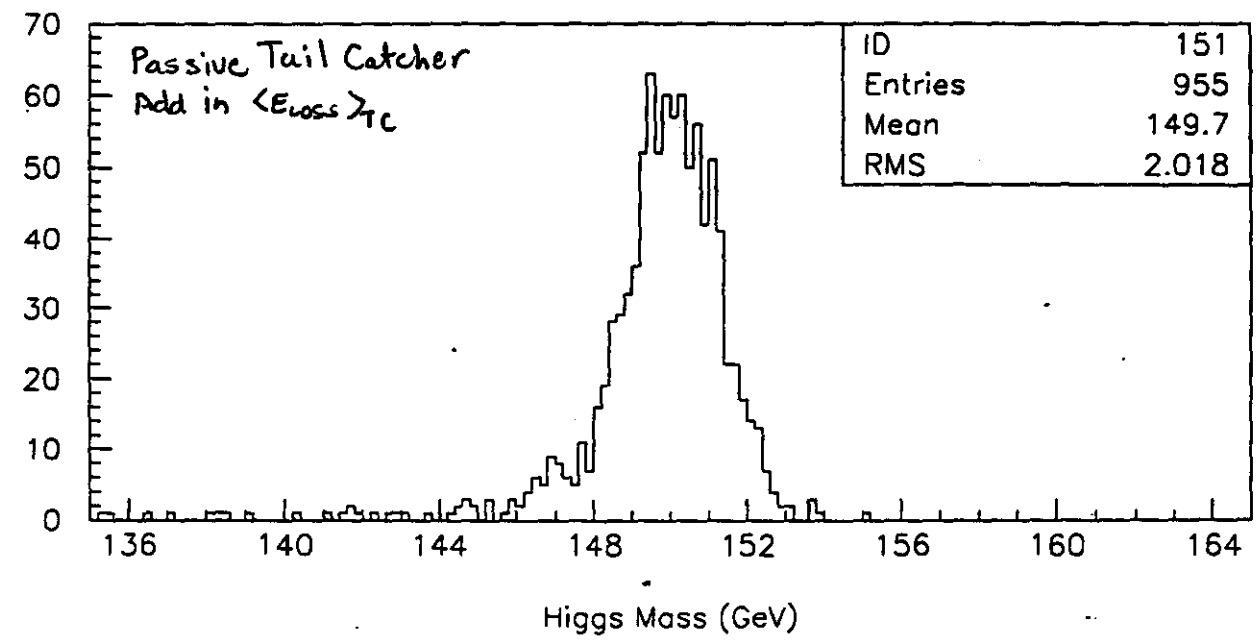

150 GeV/c² Higgs → 4μ (only Muons simulated)

Baseline 2 Calorimeter

Perfect Momentum measurement

EM resolution $\frac{6\%}{\sqrt{E}} \oplus \frac{.040\,GeV}{E}$

Liquid HAD resolution $\frac{20\%}{\sqrt{E}} \oplus \frac{.160\,GeV}{E}$

Tail Catcher resolution shown in Plots

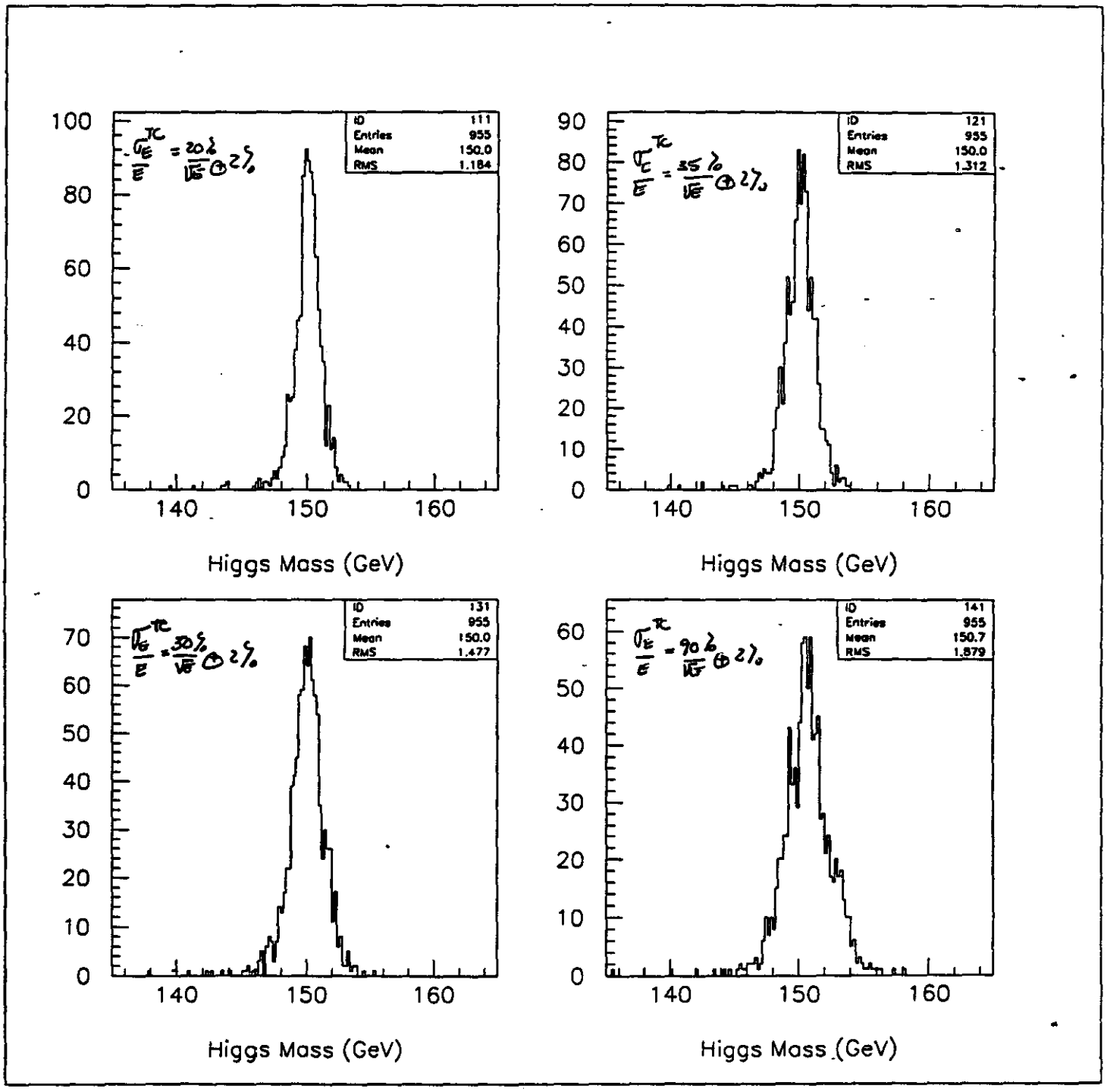

150 GeV/c² Higgs → 4μ (only Muons simulated

Baseline 2 Calorimeter

Perfect Momentum measurement

EM resolution $\frac{6\%}{\sqrt{E}} + \frac{.040\,GeV}{E}$

Liq HAD resolution $\frac{20\%}{\sqrt{E}} + \frac{.160\,GeV}{E}$

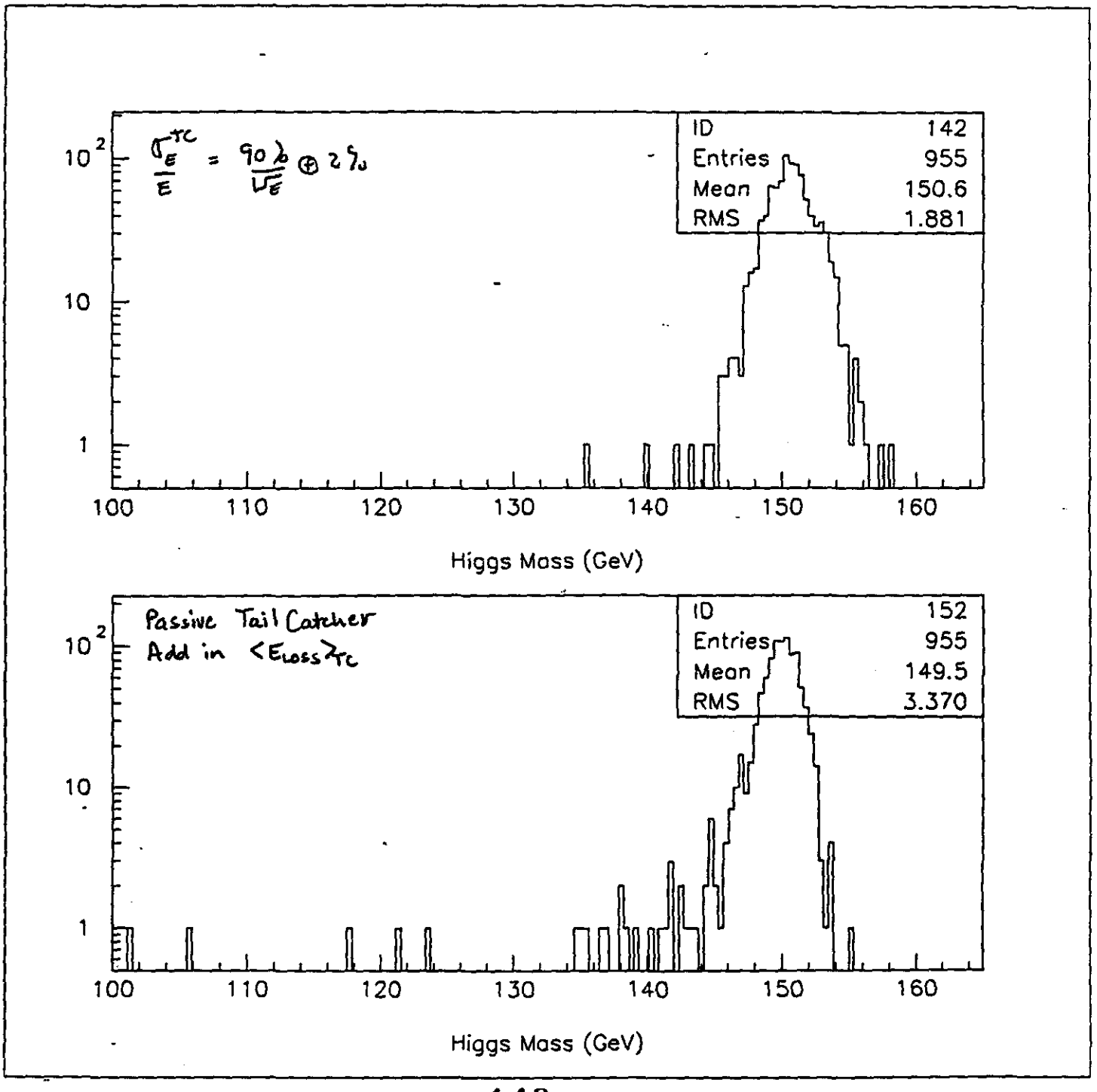

Summary

- 150 GeV/c^2 Higgs → 4μ Muons only simulated by GEANT
- Energy Loss by muon through Baseline Z Calorimeter is added back using expected energy resolution of EM/HAD section, avg. E_{Loss} through Passive mat'l, and energy resolution of Cu/Scint Tail Catcher.

Tail Catcher σ_E/E	rms $(M_H)^*$	% within * ±5 GeV/c^2	% within * ± 10 GeV/c^2
$\frac{20\%}{\sqrt{E}} \oplus 2\%$	1.18 GeV/c^2	99.3 ± .2 %	99.8 ± .1 %
$\frac{35\%}{\sqrt{E}} \oplus 2\%$	1.31 GeV/c^2	99.2 ± .2 %	99.8 ± .1 %
$\frac{50\%}{\sqrt{E}} \oplus 2\%$	1.48 GeV/c^2	99.2 ± .2 %	99.8 ± .1 %
$\frac{90\%}{\sqrt{E}} \oplus 2\%$	1.88 GeV/c^2	98.3 ± .4 %	99.8 ± .1 %
Passive TC Add $\langle E_{Loss} \rangle^{TC}$	2.02 GeV/c^2	96.4 ± .5 %	98.6 % ± .4 %

Note: This is only the effects of Calorimeter measurement of ISOLATED muons. Not included is momentum resolution, Acceptance Losses.